INFORMATION TO USERS

This manuscript has been reproduced from the microfilm master. UMI films the text directly from the original or copy submitted. Thus, some thesis and dissertation copies are in typewriter face, while others may be from any type of computer printer.

The quality of this reproduction is dependent upon the quality of the copy submitted. Broken or indistinct print, colored or poor quality illustrations and photographs, print bleedthrough, substandard margins, and improper alignment can adversely affect reproduction.

In the unlikely event that the author did not send UMI a complete manuscript and there are missing pages, these will be noted. Also, if unauthorized copyright material had to be removed, a note will indicate the deletion.

Oversize materials (e.g., maps, drawings, charts) are reproduced by sectioning the original, beginning at the upper left-hand corner and continuing from left to right in equal sections with small overlaps. Each original is also photographed in one exposure and is included in reduced form at the back of the book.

Photographs included in the original manuscript have been reproduced xerographically in this copy. Higher quality 6" x 9" black and white photographic prints are available for any photographs or illustrations appearing in this copy for an additional charge. Contact UMI directly to order.

UMI

A Bell & Howell Information Company
300 North Zeeb Road, Ann Arbor MI 48106-1346 USA
313/761-4700 800/521-0600

Université d'Ottawa · University of Ottawa

ERROR CONTROL CODING IN ADSL DMT SYSTEM

by

Liang Zhang

A thesis submitted to the
School of Graduate Studies and Research in
Partial fulfillment of the requirements for the degree of

Master of Applied Science

Ottawa-Carleton Institute for Electrical Engineering
School of Information Technology and Engineering
Faculty of Engineering
University of Ottawa
Ottawa, Ontario

Sept., 1998

Copyright © 1998, Liang Zhang

National Library of Canada

Acquisitions and Bibliographic Services

395 Wellington Street
Ottawa ON K1A 0N4
Canada

Bibliothèque nationale du Canada

Acquisitions et services bibliographiques

395, rue Wellington
Ottawa ON K1A 0N4
Canada

Your file Votre référence

Our file Notre référence

The author has granted a non-exclusive licence allowing the National Library of Canada to reproduce, loan, distribute or sell copies of this thesis in microform, paper or electronic formats.

The author retains ownership of the copyright in this thesis. Neither the thesis nor substantial extracts from it may be printed or otherwise reproduced without the author's permission.

L'auteur a accordé une licence non exclusive permettant à la Bibliothèque nationale du Canada de reproduire, prêter, distribuer ou vendre des copies de cette thèse sous la forme de microfiche/film, de reproduction sur papier ou sur format électronique.

L'auteur conserve la propriété du droit d'auteur qui protège cette thèse. Ni la thèse ni des extraits substantiels de celle-ci ne doivent être imprimés ou autrement reproduits sans son autorisation.

0-612-36760-6

Canada

Abstract

Asymmetric Digital Subscriber Line (ADSL) is an access technology intended to provide up to *8 Mbps* downstream digital transmission from the central office to customers and up to *640 kbps* upstream transmission over the existing nonloaded copper loop plant. The transfer characteristics of twisted pairs make high-speed data transmission very difficult. Sharply increasing attenuation with the increase of frequency makes the higher frequency band unavailable for transmission and also gives very severe inter-symbol-interference (ISI). In ADSL, instead of using conventional single carrier transmission the preferred approach is to employ discrete multitone (DMT) transmission. The main idea of DMT is to change a high-rate transmit data sequence into some frequency-division multiplexed low-rate data sequences. With narrow-band subchannels, DMT systems can make much better use of the bandwidth and furthermore, it can solve the ISI problem in a simple way.

In this thesis, a performance evaluation structure of RS codes in ADSL DMT systems against stationary noises (including additive-white-Gaussian noise (AWGN) and crosstalk noise) is designed. With this structure, we found through simulations that in ADSL DMT systems, for stationary noises, an optimal value of the RS code redundancy exists. In designing the system, the redundancy of the RS code should be chosen close to the optimal value to achieve good performance. Besides AWGN and crosstalk, impulse noise is another performance limiting impairment for data transmissions in subscriber loops. To evaluate the performance of RS codes in ADSL DMT systems in an impulse noise environment, an extensive survey of impulse noise in subscriber loops is conducted. Based on the survey, three performance evaluation approaches are proposed in this thesis. Results obtained with one of these evaluation approaches show that using only RS codes without interleaving, satisfactory performance of ADSL DMT systems can not be achieved. With interleaving, good coding gain could be achieved with the price of system latency introduced by the interleaving/deinterleaving operations. If the system latency can not be large, then some coding gain against stationary noises of the RS codes must be sacrificed to guarantee the satisfactory performance against impulse noise.

Erasure decoding technique is proposed in this thesis to improve the system performance because of its capability to combat burst errors, which often occur in ADSL DMT systems as a result of the impulse noise. Simulation results in this thesis show that, with erasure decoding technique, either we can save some RS coding gain against stationary noises for ADSL services that require small system latency, or we can reduce the system latency greatly with the same system performance.

Acknowledgements

First of all, I would like to express my sincere appreciation to my thesis supervisor, Dr. Abbas Yongacoglu, for his constant guidance, support and encouragement throughout the course of this project. New ideas in this thesis came from him, and his patience and rich knowledge make it a pleasure to have discussion with him.

The work in this thesis has a lot of contribution from Alberto Ginesi and Christian Bourget in NORTEL who were always ready to discuss any problems in this project with me. Also I gained a lot of working experience while working with them.

I would also like to thank Yunjun Zhang, who is a Ph.D. candidate in University of Ottawa. He has been a very patient and enthusiastic consultant in my thesis work.

I am also grateful for the help of Yang Xu, Gurkan Kurtoglu and all other students and researchers in the Communications and Signal Processing Research Laboratory (CASP).

TABLE OF CONTENTS

Abbreviations

A/D	Analog-to-Digital Converter
ADSL	Asymmetric Digital Subscriber Line
AFE	Analog Front End
AWGN	Additive White Gaussian Noise
BER	Bit-Error-Rate
CAP	Carrierless AM/PM
CIR	Channel Impulse Response
CP	Cyclic Prefix
CSA	Carrier Serving Area
D/A	Digital-to-Analog Converter
DFE	Decision-Feedback Equalizer
DFT	Discrete Fourier Transform
DMT	Discrete-Multitone
DSP	Digital Signal Processing
DWMT	Discrete Wavelet Multitone
EC	Echo Canceller
FEC	Forward-Error-Correction
FEXT	Far-End-Crosstalk
FIR	Finite-Impulse-Response
FTTN	Fiber-To-The-Neighborhood
HDSL	High Rate Digital Subscriber Line

ICI	Inter-Channel-Interference
ISDN	Integrated Services Digital Network
ISI	Inter-Symbol-Interference
LE	Linear Equalizer
MDS	Maximum-Distance-Separable
MLSE	Maximum-Likelihood Sequence Estimator
MSE	Mean Square Error
NEXT	Near-End-Crosstalk
NSNR	Normalized Signal-to-Noise Ratio
OFDM	Orthogonal Frequency Division Multiplexing
PAPR	Peak-to-Average Power Ratio
POTS	Plain Ordinary Telephone Service
PSD	Power Spectral Density
RS	Reed-Solomon
SER	Symbol-Error-Rate
SNR	Signal-to-Noise Ratio
SQAM	Staggered Quadrature Amplitude Modulation
TEQ	Time-Domain Equalizer
TIR	Target Impulse Response
UTP	Unshielded Twisted Pairs

List of Symbols

b	Number of bits in one DMT symbol
B	Channel bit rate
d	Minimum distance of RS codes
d_{min}	Minimum distance of QAM constellations
D	Interleave depth
E	Energy
G	RS Coding Gain
k	Number of bits per QAM symbol
K	Number of information bytes in one RS code word
l	Radius of the bounded distance RS decoder
L	QAM constellation size
N	Number of subcarriers in the ADSL DMT systems
N_0	Variance of AWGN
P	Probability
r	Number of redundancy symbols in one RS code word
R	Termination resistance
S	Power

t	Error correction capability of RS codes
U	Duration of one multicarrier symbol
v	Redundancy in percentage of RS codes
w	Bandwidth of subchannels of the ADSL DMT system
W	Total bandwidth of the ADSL DMT system
Γ	Power spectral density margin
Λ_c	PSD of the DMT symbols in *dBm/Hz*

List of Figures

List of Tables

Chapter 1

Introduction

1.1 ADSL DMT System

There is a never-ending demand for higher data rate transmission between service providers and customers. Telephone companies use various digital subscriber line (DSL) techniques (abbreviated as xDSL where x represents different configurations) to provide high rate data transmission through telephone lines, usually Unshielded Twisted Pairs (UTP). Cable-TV companies are also using new techniques in cable modems to make two-way transmission possible. Another technique to increase the data rate is Fiber-To-The-Neighborhood (FTTN).

While FTTN can provide the largest usable bandwidth, the cost of building the infrastructure makes it an unsuitable choice for the next decade. Coaxial cable has much larger usable bandwidth than UTP, but the one-way amplifiers in the current cable network must be changed to enable two-way transmissions. Also, the penetration of coaxial cable to residence is much less than that of telephone lines. The frequency characteristics of UTP make it not preferable for high rate data transmission. However, with sufficiently powerful digital signal processing (DSP) techniques, xDSL techniques make high-speed data transmission possible over UTP without significant additional cost in reconstructing the infrastructure.

DSL technique became the basis for the ISDN (Integrated Service Digital Network) Basic Rate Access standard that provides over *128 kbps* data rate for almost all of the nonloaded subscriber loops. High-Rate DSL (HDSL) was proposed after the DSL to provide about *1.5 Mbps* full duplex data transmission over two wire-pairs for CSA (Carrier Serving Area) loops. However, the need for two pairs and the CSA range limitation may be prohibitive in certain areas where a significant portion of customers are out of CSA or where the number of pairs per living unit are less than two. Therefore, ADSL is proposed.

Asymmetric Digital Subscriber Line (ADSL) is an access technology intended to provide up to *8 Mbps* downstream digital transmission from the central office to customers and up to *640 kbps* upstream transmission over the existing nonloaded copper loop plant [80]. While not fully duplex, ADSL has potential usage in services as advanced videotext, compressed TV quality video and education applications, where most of the information goes from providers to the customers. The main performance limiting impairment in HDSL and DSL transmission, Near-End-Crosstalk (NEXT), is no longer a big deal in ADSL systems because of the almost unidirectional transmission. Therefore transmission capacity is greatly improved compared with DSL and HDSL systems [5]. Furthermore, unlike current voice band modems, in ADSL systems, Plain Ordinary Telephone Service (POTS), down-stream data transmission and up-stream transmission can be implemented by using frequency division multiplexing techniques which will also further mitigate NEXT problem.

There are mainly two modulation/demodulation techniques that can be used to implement ADSL transmissions, the single carrier QAM and the multicarrier QAM. A "carrierless" implementation of QAM, referred to as Carrierless AM/PM (CAP), can reduce hardware complexity while preserving the flexibility of placing the signal in a desired portion of the spectrum.

Multicarrier is another solution in which the channel is divided up into subchannels. In a multicarrier system, each subchannel is individually optimized for maximum throughput. The 'bad' frequency subchannels can be intentionally nulled, that is, the ADSL systems will place no energy on a selected frequency. Given sufficient hardware precision and enough subchannels, this scheme makes optimal use of the available bandwidth.

Discrete-Multitone (DMT) is a kind of multicarrier transmission techniques, which makes use of Fast Fourier Transform (FFT) techniques to perform modulation and demodulation at the transceivers. DMT is also widely used in wireless systems, frequently referred to as OFDM: Orthogonal Frequency Division Multiplexing, ADSL transmission system using DMT modulation technique is the basic system studied in this thesis.

1.2 Forward-Error-Correction-Coding in ADSL DMT Systems

Forward-Error-Correction (FEC) code is used in both single carrier and multicarrier systems to improve the transmission quality and possibly the achievable highest transmission rate. Using FEC will result in some additional complexity to the transceivers caused by the encoder/decoder, and this is the price for the above mentioned improvement.

In this thesis, we concentrate on the FEC techniques used in ADSL DMT transmission systems. In ADSL DMT systems, the main impairments are crosstalk noise and impulse noise. Crosstalk is usually modeled as colored Gaussian noise, which in turn is modeled as narrowband Additive-White-Gaussian noises (AWGN) with different variances in different sub-channels, provided that the bandwidth of each subchannel is small enough. Trellis code is known to give excellent performance for bandlimited transmission in stationary noise environment, such as Gaussian noise [86]. For impulse noise, Reed-Solomon (RS) code is well known for its burst error correction capability [34]. Therefore, both of RS codes and trellis codes can be employed in error correction in ADSL DMT systems.

Concatenated code with multi-dimensional trellis code as inner code and RS code as outer code was proposed in order to benefit from these two powerful FEC techniques, and this coding structure is recommended in the ADSL DMT Standard [2]. Previous performance test results [10,32] show that more than *5 dB* coding gain could be achieved by the proposed concatenated code and about *3 dB* coding gain could be achieved by using RS code alone in an AWGN channel. However, two facts make the concatenated code not very attractive. The first one is the very complex decoder structure due to the Viterbi decoder at the receiver. The other fact is that the coding gain penalty of not using trellis code in ADSL transmission will not be so significant. The performance of trellis code in a burst error environment is not so good as that can be achieved in a Gaussian noise environment. From [10,32], we can see about *2 dB* coding penalty for not using trellis code in AWGN channels. It is reasonable to expect that in a channel with impulse noise as one of the critical impairments, such as subscriber loops, the coding penalty will be less than *2 dB*. These two facts justify the usage of only RS codes in ADSL DMT systems.

Instead of the hard-decision decoding technique, an erasure-decoding technique can be used to improve the performance. The advantage of using erasure decoding technique lies in the fact that in ADSL DMT system, impulse noise is one of the performance-limiting impairments.

1.3 Organization

In *Chapter 2*, an overview of ADSL DMT transmission system is given and several important aspects of it are presented. The channel model and impairments are discussed in *Chapter 3*. Some background information on RS codes, erasures decoding of RS codes and techniques of interleaving are introduced in *Chapter 4*. *Chapter 5* gives an RS code performance evaluation simulation structure and shows the coding gain results obtained using this structure. Next, in *Chapter 6*, a survey of impulse noise in subscriber loops is presented; and from the survey, an evaluation method of RS code performance against impulse noise in combination with AWGN and crosstalk noise are proposed. Some simulation results are also presented in *Chapter 6*. *Chapter 7* gives the conclusions and suggestions for future work. Two other evaluation methods of RS code performance against impulse noise in ADSL DMT systems are presented in the *Appendix*.

1.4 Contributions

In this thesis, a performance evaluation structure of RS code in ADSL DMT systems against random errors is designed and the performance results are presented. The criterion of choosing correct code parameters is shown. Three methods of evaluating RS code performance in ADSL DMT system against impulse noise are given, and the simulation results corresponding to using one of them are presented.

This work also tests the performance improvement by using erasure-decoding technique in the ADSL DMT systems instead of using hard-decision decoding technique.

Chapter 2

Overview of ADSL DMT Transmission Systems

This chapter gives a brief overview of the ADSL DMT systems. The main features of the ADSL DMT systems, the cyclic-prefix (CP) and the bit-allocation algorithm are introduced. Some other techniques used in the transceivers, such as time-domain equalization and echo cancellation, are also briefly described.

2.1 Multicarrier and Discrete-Multitone (DMT) Systems

Multicarrier transmission technique has been of interest for a long time in the literature. Some main attractive properties of this technique are: [5,10]

- With relatively narrow-band subchannels, the problem of bandwidth optimization is greatly simplified, which in turn increases the channel capacity.
- In a single carrier system using linear equalization, the equalizer will cause noise and/or interference enhancement at null (or nearly null) points of the channel frequency response. A multicarrier system can avoid this problem by not using those subchannels containing null points.
- In the multicarrier systems, each subcarrier has a much longer symbol duration than that of a single carrier system. The longer symbol duration gives a much greater immunity to impulse noise and fast fades.

The earliest multicarrier system made use of conventional Frequency-Division-Multiplexing (FDM) technology and employed filters to completely separate the sub-channels [5]. However, it is very difficult to implement filters with very sharp edges. Therefore, in this method, a bandwidth wider than the minimum Nyquist bandwidth has to be used. As a result of using some bandwidth for guard band, the spectral efficiency is reduced. Using Staggered Quadrature Amplitude Modulation (SQAM) achieved a frequency efficiency of *1* [5]. For SQAM, the individual transmit spectrum of the modulated signal also used an excess bandwidth, while the composite spectrum is flat. The orthogonality of the sub-bands is achieved by setting a phase difference of half a symbol period between the in-phase and quadrature components. In this method, the requirement for filters is decreased. However, it is still considerably high. A basic multicarrier transmitter structure is shown in Figure 1.

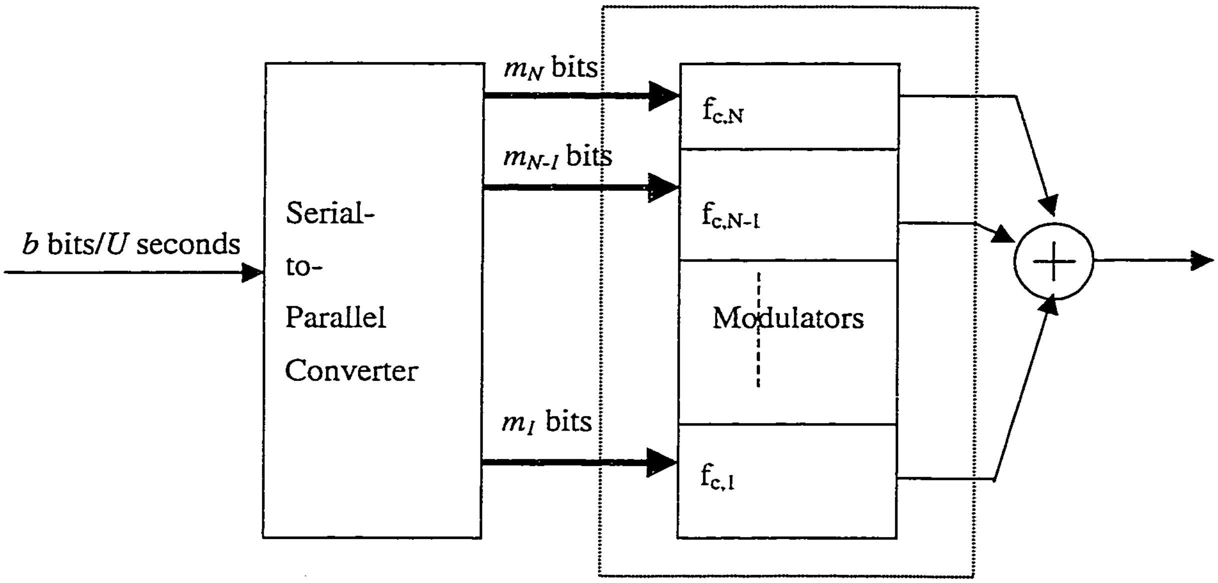

Figure 1 Basic multicarrier transmitter

where U is one multicarrier symbol duration in which totally b bits are transmitted, m_k is the number of bits transmitted by the k^{th} subcarrier $f_{c,k}$ in one symbol duration.

In [9], Weinstein and Ebert used discrete Fourier transform (DFT) to perform baseband modulation and demodulation. The focus was then concentrated on efficient signal processing techniques, which eliminate the filter banks requirement of the traditional multicarrier techniques. In [9], a guard space between adjacent symbols and a raised-cosine windowing in time domain is used to eliminate the inter-symbol-interference (ISI) and reduce the inter-channel-interference (ICI), which is caused because the sub-channels are on longer orthogonal to each other after they go through a nonideal channel. Peled and Ruiz solved the orthogonality problem in [13] by introducing a cyclic prefix (CP) instead of using a vacant time domain guard space. Current DMT system is such a multicarrier system making use of FFT technique, in which, the carriers are 'keyed' by the QAM data in each sub-channel. In this case, the signal spectrum is a *sinc* function, and is no longer bandlimited. However, the signals in

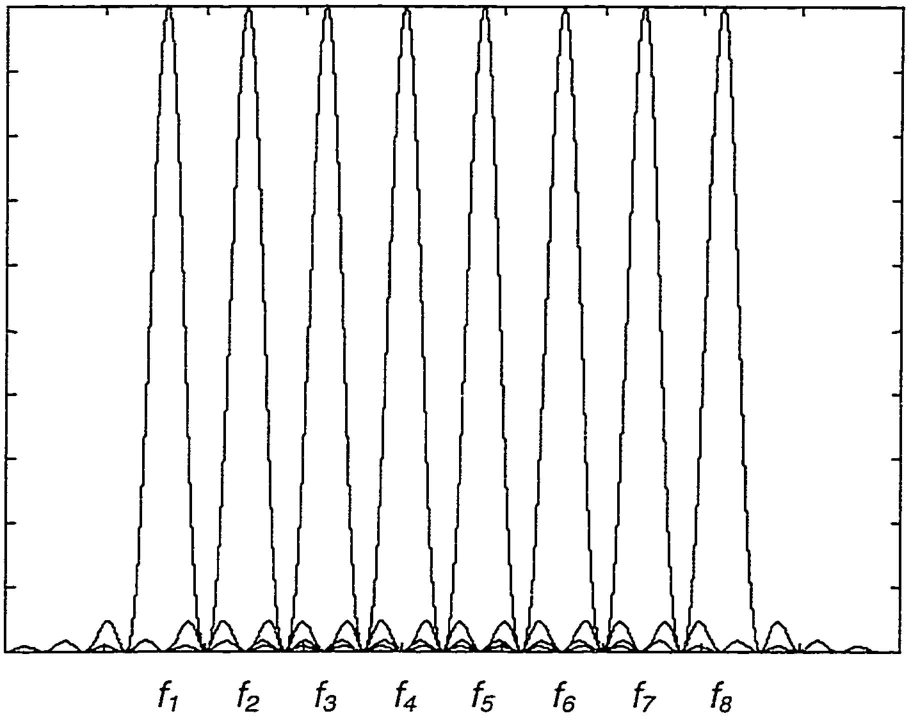

Figure 2 Power spectral density of *8* subchannels of a DMT system

different sub-channels can be separated in the receiver by baseband signal processing. The main advantage of this approach is that the transceivers can be implemented using FFT techniques, thus the computational load is greatly reduced. Power spectral density (PSD) of the subchannels for a DMT system with *8* subchannels is shown in Figure 2.

The *sinc* function signal spectrum will give relatively large sidelobes in an FFT-DMT system. Therefore, Discrete Wavelet Multitone (DWMT) technique is proposed in [70]. In DWMT, a wavelet transform instead of Fourier transform is used to greatly reduce the level of the sidelobes [71].

2.2 ADSL DMT Transmission System Model

A simplified ADSL DMT transmission system model is shown in Figure 3. It is assumed that the signal from each sub-channel is sampled at more than the sampling rate.

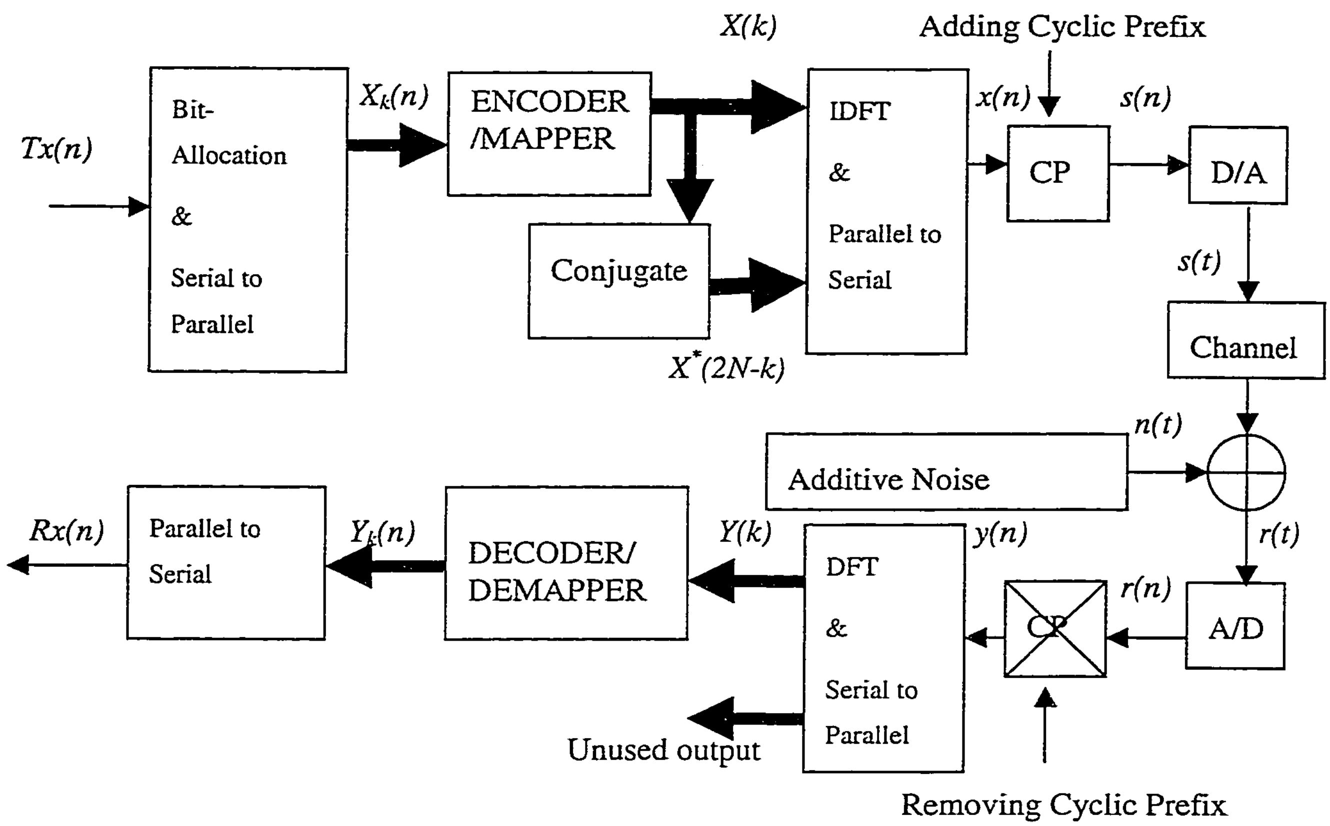

Figure 3 ADSL DMT system model

Block processing is one of the main characteristics of DMT systems. The information bits are divided into blocks, and each time, a block of bits is processed at the transceiver. Let's assume that there are b bits in each block. These b bits are allocated to the sub-channels by a bit-allocation algorithm, which decides the optimal power and bit distribution among all the subchannels based on the signal-to-noise ratio (SNR) distribution. $X_k(n)$ in Figure 3 is the bit group assigned to the k^{th} sub-channel. The ENCODER/MAPPER translates these bit groups into the corresponding complex QAM signals, $X(k)$. In order to guarantee the output of the IDFT operator is real, a conjugate-symmetric complex sequence $\overline{X}(k)$ is formed as follows:

$$\overline{X}(k)=\begin{cases} X(k) & 0\le k\le N-1 \\ X^{*}(2N-k) & N\le k\le 2N-1 \end{cases} \tag{1}$$

with $\overline{X}(0)$ and $\overline{X}(N)$ real. $\overline{X}(k)$ is input into the IFFT operator and the output sequence, $x(n)$, is

$$x(n)=\frac{1}{N}\sum_{k=0}^{2N-1}X(k)\cdot e^{j\frac{2\pi nk}{2N}} \qquad (0\le n\le 2N-1) \tag{2}$$

Another sequence, $s(n)$, is then generated by adding a cyclic prefix of length v to $x(n)$.

$$s(n)=\begin{cases} x(2N+n) & -v\le n\le -1 \\ x(n) & 0\le n\le 2N-1 \end{cases} \tag{3}$$

This digital signal, $s(n)$, is converted into the analog signal, $s(t)$, by the Digital-to-Analog converter (D/A), and $s(t)$ is transmitted into the channel.

$$s(t)=\sum_{n=-v}^{2N-1}s(n)\cdot g(t-nT) \tag{4}$$

where, $g(t)$ is the low-pass filter at the transmitter, and T is the sampling interval. Such a signal block is called a DMT symbol. Here, we can see that using the IFFT technique in the transmitter to perform modulation is equivalent to QAM modulation in each sub-channel in which the fundamental baseband pulse shape is a rectangle; thus the spectra of the signal in each sub-channel has the form of a *sinc* function.

It is shown in [15] that the power spectral density (PSD) of the transmitted signal $s(t)$ can be expressed as:

$$S(f)=\frac{T}{2N}\cdot\left(\sum_{k=0}^{2N-1}\sigma_k^2\cdot Sinc^2\left[2NT\left(f-\frac{2\pi k}{2NT}\right)\right]\right) \tag{5}$$

where σ_k^2 is the variance of the QAM signals transmitted in the k^{th} subchannel. Equation (5) doesn't consider the effect of the cyclic prefix. However, since cyclic prefix usually takes only a few percent of a DMT symbol, its effect is ignored here for simplicity.

The received signal *r(t)* contains the channel attenuated and distorted signal and the additive noises, including AWGN, crosstalk and impulse noise.

$$r(t) = s(t) * h(t) + n(t) \tag{6}$$

where $h(t)$ is the channel impulse response (CIR), $n(t)$ is the sum of the additive noises.

By an Analog-to-Digital converter (A/D), the *r(t)* is converted into a digital form *r(n)*, which can be expressed in a discrete form as:

$$r(n) = s(n) * h(n) + n(n) \tag{7}$$

After stripping off the CP from *r(n)*, we obtain *y(n)*. This signal is input into the FFT operator for demodulation.

$$Y(k) = \sum_{n=0}^{2N-1} y(n) \cdot e^{-j\frac{2\pi nk}{2N}} \tag{8}$$

As we know from the transmitter structure, only the first half of the output, $Y(k)$ $0 \le k \le N-1$, is useful data, because the second half is only the conjugate of the first half. Also because the second half always experiences much higher attenuation than the first half due to the channel attenuation characteristics of the subscriber loops, the first half is chosen to recover the information. After DECODER/DEMAPPER, these complex symbols are translated back to bit groups, and by a parallel-to-serial converter, the information bit sequence is recovered.

It is convenient to think of DMT system as consisting of *N* quadrature amplitude modulation (QAM) channels under certain conditions. For ideal channels, it is proved in [5] that using IFFT/FFT as modulation/demodulation in transceivers will keep the orthogonality among the sub-channels. However, the orthogonality is lost when the channel is nonideal. In practice, the modulation is done digitally and no explicit use of any carrier modulation frequencies or modulators is required.

For an ADSL DMT system, the bit-allocation and the settings for time-domain equalizer and echo canceller as well as the synchronization patterns must be decided before it can operate properly. Here, we describe a process as follows: [72]

a) When receiving a request for transmission, some loopback and test patterns are exchanged, followed by timing and synchronization patterns.

b) A predefined sequence is sent from the transmitter to the receiver for channel estimation.

c) Based on the result of the above channel estimation, the optimum settings of the time domain equalizer is calculated and the bit-allocation is achieved.

d) The bit assignments are sent to the transmitter in a reliable fashion.

e) The above steps are repeated for both upstream and downstream transmissions.

f) After frame synchronization and start commands are exchanged, the DMT transceiver is ready for actual data transmission.

In the following sections, some details of ADSL DMT transmission systems will be discussed.

2.3 Cyclic Prefix

The two most important aspects of a DMT system are the cyclic prefix (CP) and bit-allocation. In this section, we discuss the significance of the CP to the system.

As said above, when the channel is nonideal, the orthogonality among sub-channels is lost. As a consequence, signal received in one subchannel will contain contributions from some other subchannels, which is termed inter-channel-interference (ICI). In addition, ISI between adjacent DMT symbols will also distort the received signals. In a DMT system, ISI and ICI are eliminated by adding a CP to each DMT symbol.

With a discrete channel-impulse response (CIR) of length $\nu+1$ samples, each received sample block is the convolution of the $2N$ samples of one DMT symbol and the CIR. The result has a length of $2N+\nu$, which means this received DMT symbol will overlap with the adjacent received DMT symbols in ν samples. This will cause ISI to the other received DMT symbols. In [9], this problem is solved by adding a guard space of at least ν sample intervals. The ISI from this DMT symbol will fall into the guard space, therefore, it will not have any effect over other DMT symbols.

However, adding a guard space will not solve the orthogonality problem, because some information falls into the guard space and is thus abandoned at the receiver end, which means that the discrete convolution theorem doesn't hold in this case. In [13], the CP is first introduced to solve the orthogonality problem in DMT systems. Before the $2N$ samples of each DMT symbol is transmitted, the last M samples are prefixed to the sample vector to give a length-$(2N+M)$ DMT symbol, as shown in Figure 4. At the receiver, the prefix part is abandoned. As we see, when $M \geq \nu$, no ISI will occur. At the

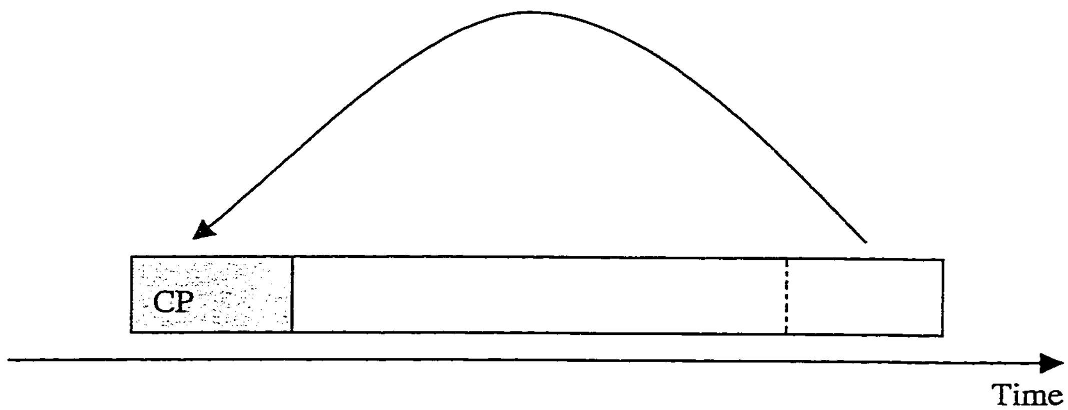

Figure 4 Cyclic prefix

same time, adding the last M samples instead of leave them zero causes the transmitted sample sequence to appear periodic to the channel with length $\nu+1$. Therefore, the linear convolution of the transmitted samples and the CIR will appear to be a cyclic convolution. Under this condition, the discrete convolution theorem holds, which makes the following equation correct:

$$Y(k) = H(k) \cdot X(k) + n_k \tag{9}$$

where $H(k)$ is the channel frequency response at the k^{th} sub-carrier. If equation (9) holds, then the received signal in the k^{th} sub-channel, $Y(k)$, only has the contribution of the k^{th} input, $X(k)$, and the additive noise. Therefore, the orthogonality between the sub-channels is kept. A one-tap frequency equalizer will make up for the attenuation and phase shift caused by the channel response, $H(k)$, for each sub-channel. Details of the above issues have been discussed in [3,13,72].

However, adding CP will increase the bandwidth of the subchannels, or will reduce the transmission rate by $M/2N$, refer to M -sample cyclic prefix and $2N$ -sample DMT symbols as assumed above. When M is large, the transmission rate lost will be too large to tolerate. Note that until now, time-domain equalizer (TEQ), which is used in single carrier transmission system to combat the ISI has not found its position in this DMT system because the ISI problem is solved by the CP. When the CIR is too long, TEQ will be used in a DMT system, not to try to equalize the nonideal channel into an ideal one, but to shorten the length of the combined CIR and equalizer to some value we can tolerate.

In [14], analysis and simulation show that a comprise between transmission rate and the length of channel impulse response exists and sometimes, with a CIR a little longer than the cyclic prefix it will still give satisfactory performance with higher transmission rate. However, in most cases, the reduction of the length of the CP can only be small. This will be of some use for wireless systems who has a long CIR with very small probability, but not for our ADSL systems.

2.4 Bit-Allocation

Bit-allocation is the most important technique used in a DMT system operating on stationary, or slowly changing channels. For slowly changing channels, adaptive allocation must be carried out. However, in our case, the subscriber loops change very little with time, therefore, bit-allocation only needs to be performed in the initialization process.

Bit-allocation is an optimization process of DMT system's transmission performance by allocating different number of bits and power, which in turn means QAM signals from different-size constellations, to the sub-channels. Data rate, transmit energy or error probability can all be chosen as the criterion for the optimization problem. Typically, two of these three parameters are fixed and the other one is optimized. Common case is that given the maximum bit-error-rate (BER) and the maximum transmit power, bit-allocation process tries to find the optimal bit allocation to achieve the maximum transmission rate. In this case, we have a performance upper bound, the capacity of the channel, and what we want is to approach this capacity as closely as possible. The capacity of a frequency selective channel can only be achieved by assigning different power to different frequency components [18]. This also suggests that with good bit-allocation, DMT systems can achieve much better frequency efficiency than single carrier systems.

There are several different algorithms for bit-allocation in DMT systems. Given a certain data rate and an energy constraint, the Hughes-Hartogs algorithm provides the bit-loading factors that yield minimal bit-error rate [5]. The idea is to assign one bit at a time to the sub-channels. The sub-channel with the smallest energy cost is then assigned this bit. The procedure is repeated until a desired bit rate is obtained. In [11], the optimization problem of bit-allocation is solved to find the maximal transmission rate of the DMT system. A practical bit-allocation procedure is given in [33]. The optimization methods in [11,33] are used in our simulation to test the RS code performance. It is shown in these references that the optimal power distribution over the entire frequency band is always approximately flat with several *dB* fluctuations in each subband, which is in agreement with the water-pouring solution with high signal-to-noise ratio (SNR) in information theory. An example bit-allocation results for a subscriber loop transmission with narrowband AM interference and near-end-crosstalk (NEXT) is shown in Figure 5.

Now, we discuss the bit-allocation algorithm in some details.

In ADSL DMT systems, QAM signals are transmitted in different sub-channels. Now we assume that rectangular constellation $L_k - QAM$ is used in the k^{th} subchannel, which means that each symbol carries $b_k = \log_2 L_k$ bits. For even values of b_k, and for the case of high SNR with constellation of size L_k, the probability of symbol error for QAM signaling is given by: [11,73-Ch. IV]

$$P_e = 4\left(1 - \frac{1}{\sqrt{2^{b_k}}}\right) Q\left[a\sqrt{\frac{2}{N_0}}\right] \cong 4Q\left[a\sqrt{\frac{2}{N_0}}\right] \qquad (10)$$

where $2a$ is the minimum distance between points in the constellation at the receiver end, N_0 is the variance of the AWGN.

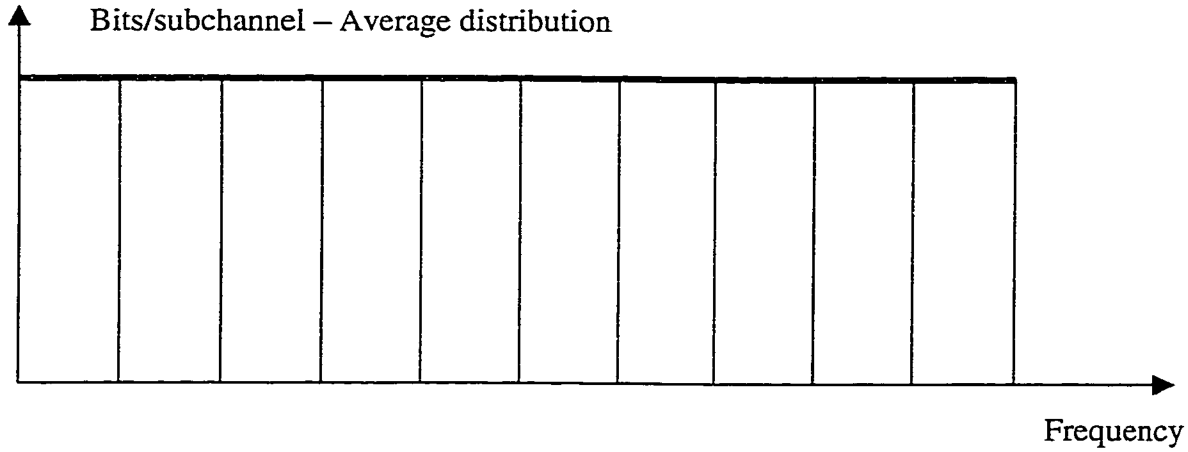

(a) Uniform bit distribution in a DMT system

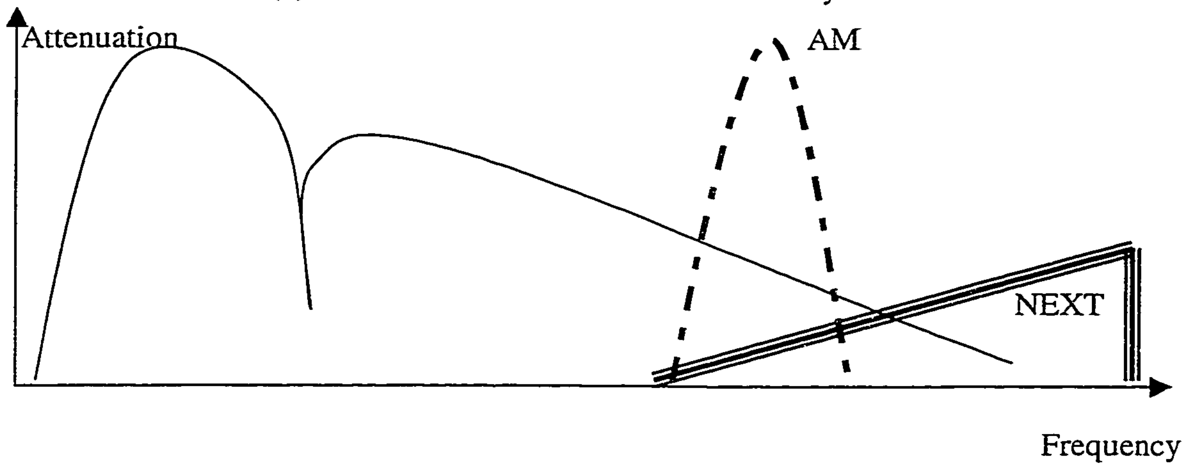

(b) Loop attenuation and noise environment

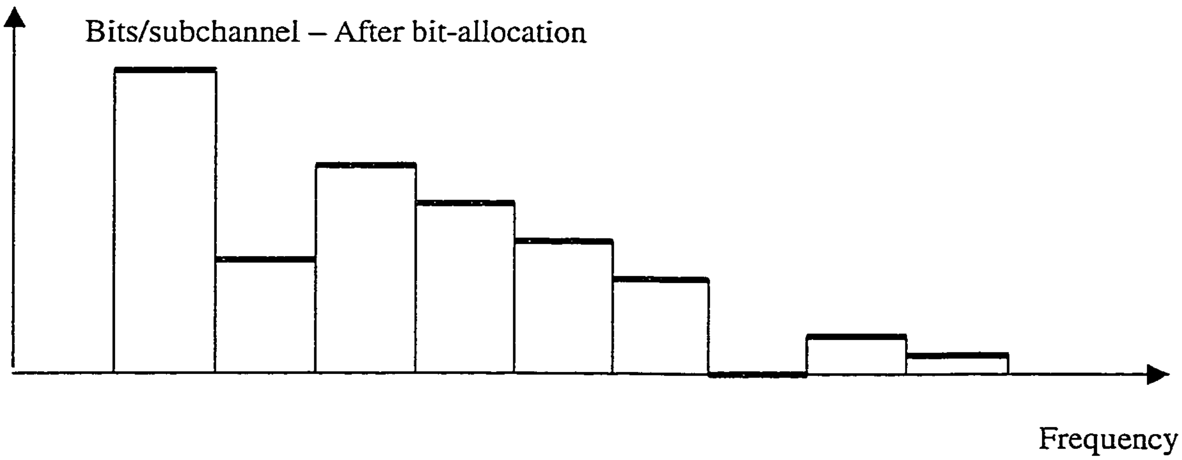

(c) Bit-allocation results in a practical DMT system according to (b)

Figure 5 Bit-allocation in loop channels in the presence of: channel null point, AM narrowband interference and near-end crosstalk noise

The value of a is related to the average symbol energy E for even b_k by the equation below: [74]

$$a^2 = \frac{3E}{2} \Big/ (2^{b_k} - 1) \tag{11}$$

For odd values of b_k, the probability of symbol error and the average symbol energy can be closely approximated by (10) and (11).

The aggregate number of bits per symbol, b, is:

$$b = \sum_{k=1}^{N} b_k = \sum_{k=1}^{N} \log_2(L_k) \tag{12}$$

where N is the number of tones we used. Therefore, the channel bit rate is:

$$B = b / U \tag{13}$$

where U is the duration of one DMT symbol.

Let d_{TX} be the minimum distance in the transmitted constellation, then the received constellation minimum distance d_{RX} is:

$$d_{RX}^k \approx |H(f_k)| \cdot d_{TX}^k \tag{14}$$

where $H(f)$ is the loop channel response, and f_k for $k=1,2,\ldots,N$, is the center frequency of the tones. Then the symbol error rate for a given tone can be calculated from equation (10) with $2a = d_{RX}$.

For an ADSL-DMT system, it is required that all the tones have the same symbol error rate P_e, then for each subchannel we must have

$$\gamma = \left(\frac{d_{RX}}{2\sigma_k} \right)^2 \tag{15}$$

as a constant, which is equal to approximately 14.73 dB for a symbol error rate (SER) of 10^{-7}.

The transmitted power on the k^{th} subchannel, S_k, (normalized to the characteristic impedance of the line) is defined as:

$$S_k = \frac{1}{6}(L_k - 1)d_{TX}^2 \tag{16}$$

Then the normalized aggregate power is:

$$S_{TX} = \sum_{k=1}^{N} S_k \tag{17}$$

From (14) - (16), we can solve for L_k to obtain:

$$L_k = 1 + \frac{3S_k \mid H(f_k) \mid^2}{2\sigma_k{}^2 \gamma} \tag{18}$$

where σ_k^2 is the variance of the stationary noise, including AWGN and crosstalk, in the k^{th} subchannel.

Now our problem is to minimize the transmit power with the data payload constraint. We can formulate a Lagrange optimization problem with Lagrangian:

$$L(S_k) = \sum_{k=1}^{N} \log_2\left(1 + \frac{3S_k \mid H(f_k) \mid^2}{2\sigma_k^2 \gamma}\right) - \lambda \sum_{k=1}^{N} S_k \tag{19}$$

with the constraint that:

$$\sum_{k=1}^{N} b_k = b \tag{20}$$

Solving this Lagrangian optimization problem, the optimal values of S_k are given by:

$$S_k = S_0 - \frac{2\sigma_k^2 \gamma}{3 \mid H(f_k) \mid^2} \tag{21}$$

where S_0 is a constant.

According to the ANSI T1E1.4 Standard, the number of bits b_k in the k^{th} sub-channel is constrained to be an integer between 2 and 15. This integer constraint will cause the optimal power distribution to have some kind of saw shape, instead of a flat one.

An example of this bit-allocation algorithm result is shown in Figure 6, and Figure 7 shows the corresponding power allocation.

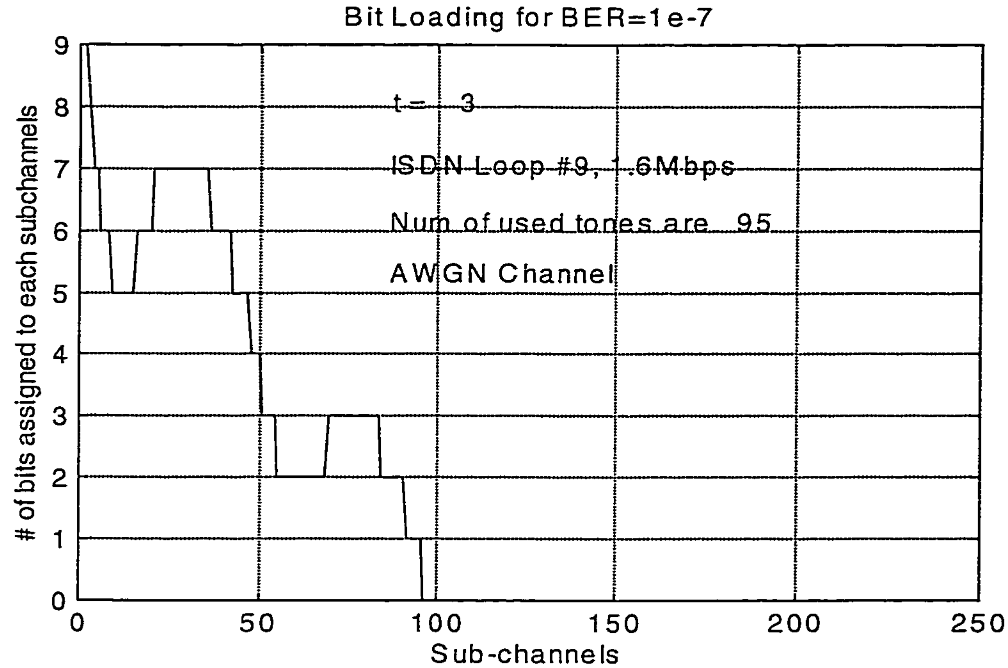

Figure 6 Example of bit allocation in DMT systems

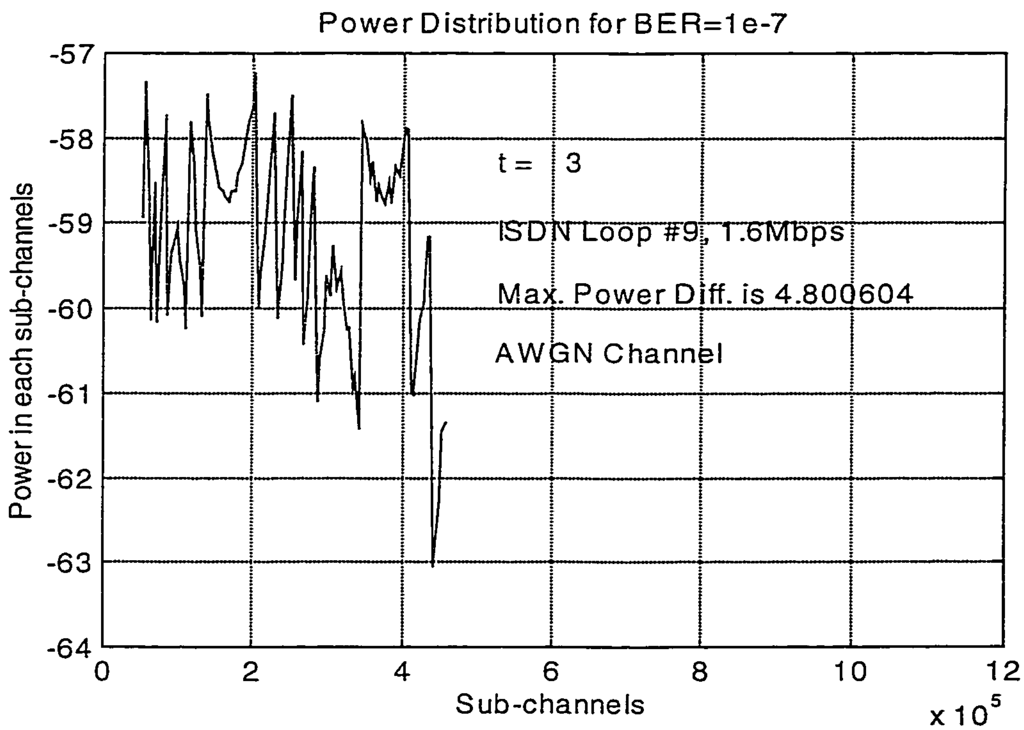

Figure 7 Example of power allocation in DMT systems

A sub-optimal bit allocation algorithm given in [33] will be described in *Chapter 5*, which is the main algorithm we used to evaluate the performance.

2.5 ADSL DMT Transmission Capacity

Capacity is the maximal achievable information rate in a channel with given transmit power and required BER. The capacity of an ideal bandlimited channel of bandwidth W Hz with AWGN of power spectral density σ^2 in nats per second for an input signal power level S is given by [18] as:

$$C = \frac{W}{2} \cdot \ln\left(1 + \frac{S}{W \cdot \sigma^2}\right) \tag{22}$$

For capacity calculations in nonideal channels, we divide the power transfer characteristic of a single wire-pair into N parallel independent sub-channels, where each sub-channel occupies a flat narrow pass-band centered at frequencies equally distributed across the Nyquist band used, as shown in Figure 8. This suggests that DMT system can achieve more potential transmission capacity than any single carrier system over non-ideal loops like subscriber loops. With a careful allocation of bits and transmit power into all of the subchannels, it is shown in [11,15,72] that the DMT system can operate at the highest theoretical limits and no other system can exceed its performance

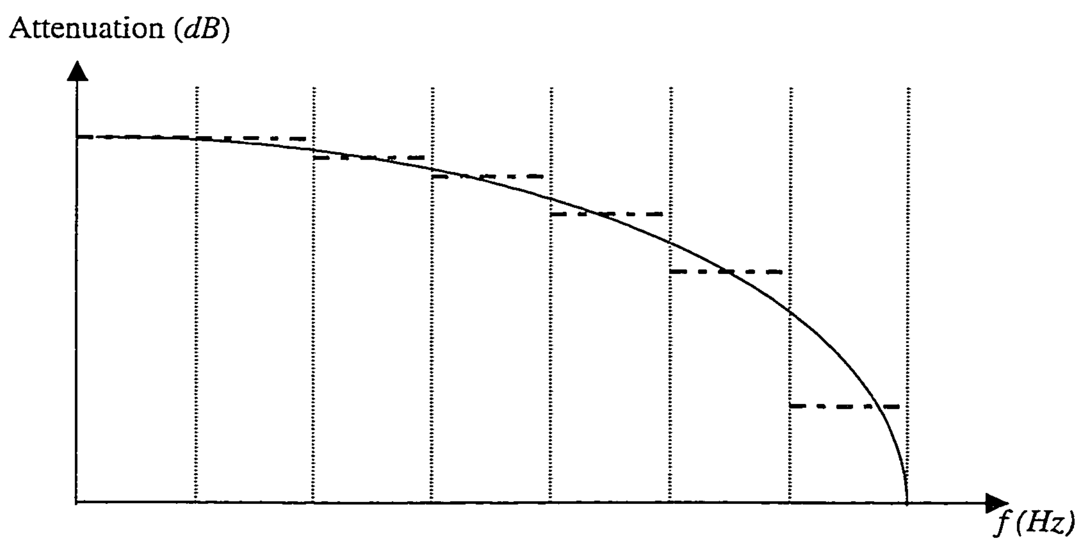

Figure 8 Subchannel representation of the subscriber loop's attenuation

Commonly, increasing the transmitting power will increase the capacity. However, for transmission in subscriber loops, because of the crosstalk, increasing the power to a certain range will result in the capacity saturation because the power of the crosstalk will increase proportionally to the transmit power by a coupling factor of a constant K. Therefore, in subscriber loops, crosstalk is one of the performance-limiting impairments. The capacity of the channel can then be expressed as: [18]

$$C = \sum_{k=1}^{N} \frac{W}{2N} \log\left(1 + \frac{S_k H_k^2}{\sigma_k^2}\right) \tag{23}$$

where

$$\sigma_k^2 = w_k + K f_k^{1.5} S_k \tag{24}$$

is the total additive Gaussian noise variance in the k^{th} subchannel, w_k is the AWGN variance in this subchannel, $K f_k^{1.5} S_k$ is the variance of the coupled NEXT noise in this subchannel, and the total bandwidth is divided into N subchannels.

We can see from the capacity equation (23, 24) that the smaller the coupling factor K, the higher is the capacity. In ADSL, because there is much less NEXT from other ADSL services, and the power of the FEXT noise is much smaller than that of NEXT noise because it goes through the attenuation of the loops, the channel capacity is much higher than that of full-duplex transmission systems like HDSL and T1 systems.

Equations (23, 24) also suggest that an optimal power distribution exists for S_n with which we can achieve the highest capacity.

2.6 Time-Domain Equalization, Echo-Cancellation and Peak-to-Average Power Ratio Reduction

2.6.1 Time-Domain Equalization

In ADSL DMT transmission systems, a cyclic prefix is added to the output sample block from the IDFT at the transmitter to avoid the ISI and ICI. For satisfactory performance, the cyclic prefix should have a length longer than that of the channel-impulse response (CIR). However, a long CP would result in a high reduction in the effective data rate.

Therefore, a time-domain equalizer (TEQ) must be used, not to fully equalize the CIR to an ideal channel, but to partially equalize the CIR to a target impulse response (TIR) of much shorter length.

The structure of a typical TEQ is shown in Figure 9, which is based on minimum square error criterion proposed by Falconer and Magee [23]. The coefficients of the equalizer, $w(k)$, and the TIR, $b(k)$, are optimized at the same time to minimize the variance of the error signal $e(k)$.

Since TEQ is not one of the main issues of this thesis, we will not give more details on this. Anyone who is interested in this can refer to reference [19 - 25].

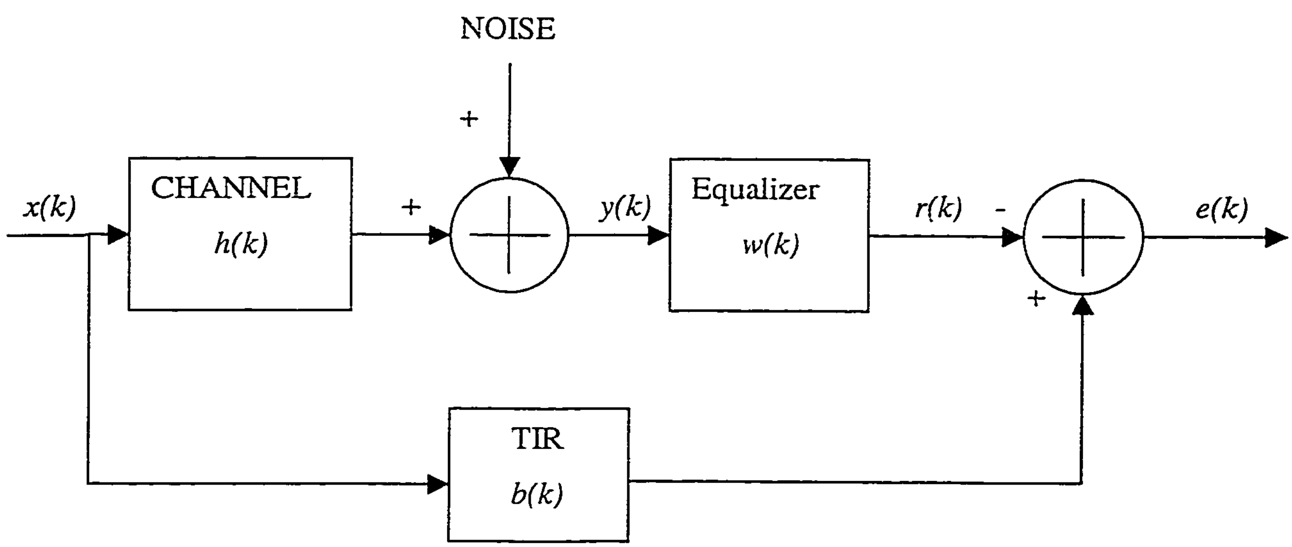

Figure 9 Time-domain equalizer in ADSL DMT system

2.6.2 Echo-Cancellation

Echo signal in subscriber loop transmissions is mainly generated by the four-wire to two-wire conversion hybrid, which enables the simultaneous transmission in both directions on the two-wire pair [26], see Figure 10. In most cases, the hybrid is an imperfectly matched electrical bridge, thus part of the transmit signal will appear at the receiving circuit as echo. Therefore, an echo-canceller (EC) is required to cancel this interfering signal. The main aim of an EC is to estimate the echo path transfer function with a FIR filter. Like the transfer functions of the subscriber loops, the transfer functions of echo paths are also different from one to another. This suggests that an adaptive algorithm must be used in the EC.

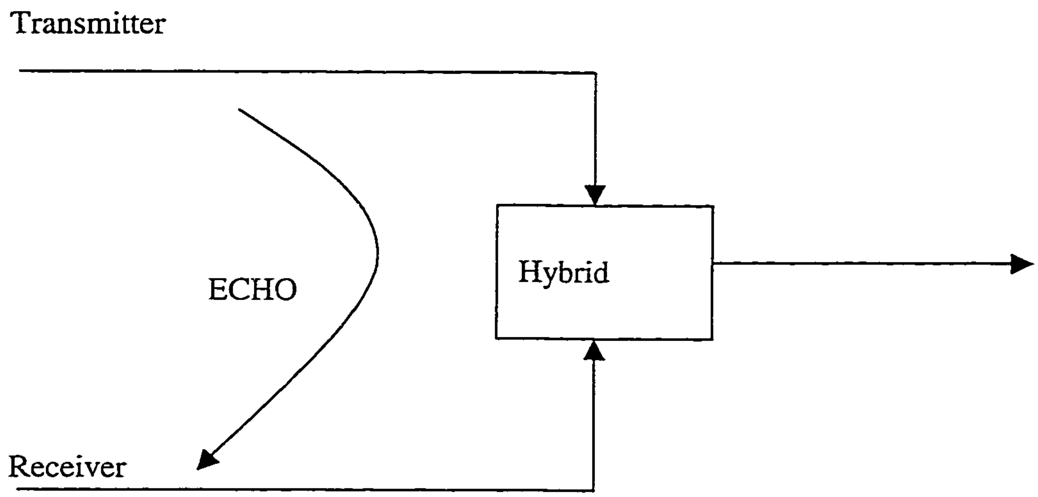

Figure 10 Echo generation

Echo cancellation is required in the half-duplex ADSL DMT transmission systems as well as in the full duplex HDSL transmission systems. It is usually a very difficult part of the system design because it always requires very high digital processing power. New ideas of echo canceller (EC) designs are presented in the last few years for multicarrier systems, specifically for DMT systems. The main objective is to decrease computational load requirement of the echo cancellation process to a range tolerable by current microprocessors.

Like TEQ, this is also not a main issue in this thesis either, details can be found in reference [26 ~ 30].

2.6.3 Peak-to-Average-Power Ratio Reduction

In a DMT system, each sample in a DMT symbol is the weighted summation of the QAM signals modulated to different tones. The QAM signals on different tones are independent random complex symbols. Summing these independent random symbols leads to a transmit signal whose probability density function is close to Gaussian (central limit theorem) and has a much higher peak to average power ratio (PAPR) than most single-carrier modulated signals. The Gaussian approximation is accurate for DMT systems with more than *100* subchannels. To tolerate the high peak of this signal, the D/A must be of significantly high resolution to prevent distortion of the signal peaks and the analog front end (AFE) must have a large dynamic range. This is a significant disadvantage of DMT systems compared with single-carrier systems, because the D/A and AFE can be a significant percentage of the cost of the overall system as well as the greatest power consuming elements. To reduce the AFE complexity and power consumption, DMT transmitters are often designed to support lower PAPR values.

Since high peak of the DMT samples is expected to arise very rarely (statistical averaging), it is advantageous to accept some clipping in the DMT-symbol and to trade-off the resulting SNR loss against the A/D-D/A and line driver dynamic ranges. It is shown in [76] that even without loss of the SNR, proper clipping can reduce the required number of bits of the A/D-D/A converters.

More details about the clipping issue can be found in reference [75 ~ 84].

Chapter 3

Channel Model and Impairments in ADSL DMT Systems

This chapter gives some detailed explanations of the transmission model and main impairments in ADSL DMT transmission systems.

3.1 UTP Loop Model

Among all the subscriber loops, about *25-30%* is "loaded", which contains loading coils to equalize the *3 kHz* voice frequency band. However, only "nonloaded" subscriber loops can be used in high data rate transmission. Among these "nonloaded" loops, previous surveys showed that about *20~30%* of all the "nonloaded" loops have length more than *12 kft* and about *2%* have length more than *18 kft* [6].

It is worth mentioning a popular group of subscriber loops, Carrier Serving Area (CSA) loops. CSA loops are those "nonloaded" loops that are not longer than *12 kft* with *24-gauge* wires and *9 kft* with *26-gauge* wires. About *70-80%* of "nonloaded" loops belong to CSA loops. Previous xDSL techniques such as HDSL aimed at mainly providing service over CSA loops. However, ADSL will provide services to almost all the "nonloaded" loops.

Some key characteristics of the ADSL environment have been identified as: [8]

- All loops are nonloaded
- All loops consist of *26 gauge* or coarser cables, either used alone or in combination with other gauge cables.
- The maximum allowable loop length, including bridged taps, is *18 kft.*

To model the transfer characteristics of the loop channel is to find its transfer function. For a DMT system, the channel is divided into a lot of narrow band subchannels, and each subchannel is assumed to have a flat frequency response. Although it was stated in [4] that the non-zero slope in one subchannel would cause significant interference, when the bandwidth of the each subchannel is small enough, the flat approximation is valid.

In this case, the characteristics are just the attenuation and phase shift in each sub-channel. The most important one is the attenuation, which is also called the propagation loss.

A loop is said to be perfectly terminated if it is terminated with its characteristic impedance. For a perfectly terminated loop with length l, the attenuation at frequency f can be approximately given by [6]:

$$L_{dB}(l,f) \approx 8.686 \cdot l \cdot \alpha(f) \qquad (dB) \tag{25}$$

where $\alpha(f)$ is roughly proportional to $\sqrt{f}$. (This is a good approximation with f less than 20 kHz or more than 200 kHz.)

Figure 11 shows the propagation loss models of five CSA test loops, which will be used to test the system performance together with two ISDN test loops in our work. Some more information about these loops can be found in *Chapter 5*.

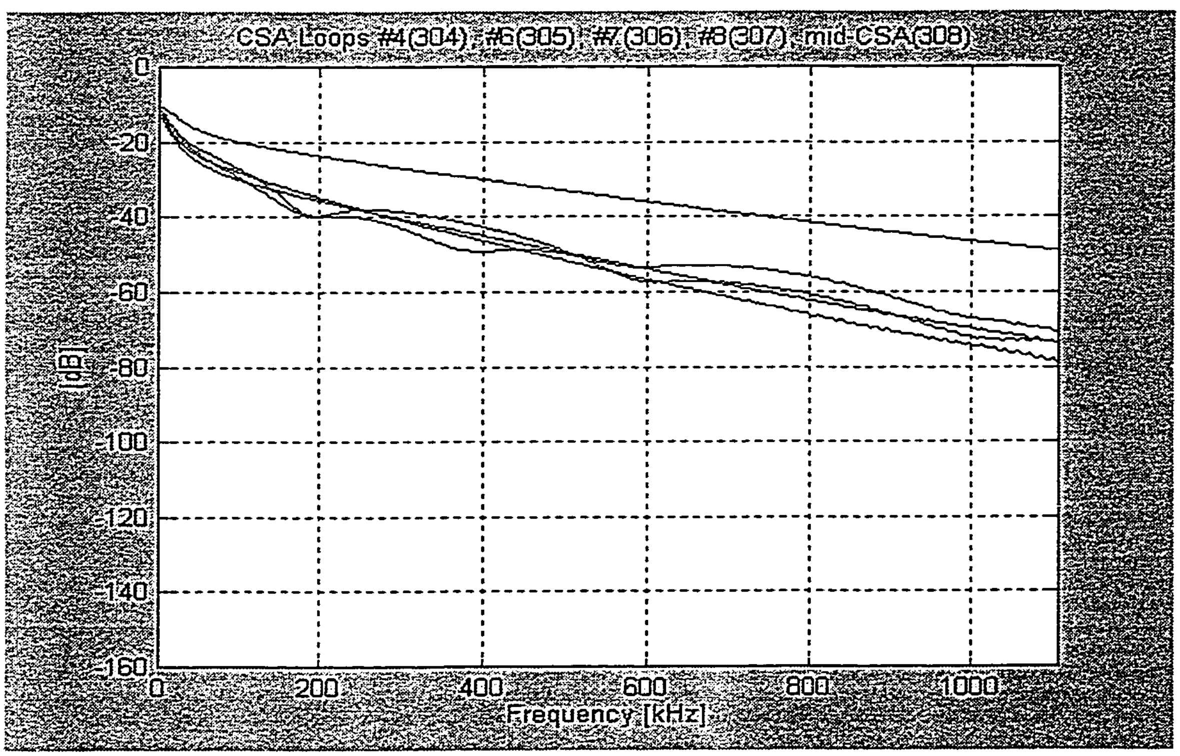

Figure 11 Propagation loss of 5 CSA test loops

3.2 Additive-White-Gaussian Noise (AWGN)

Electronic noise, including quantization noise from the A/D converter, and thermal noise in the analog portion of the receiver, can be modeled as additive white Gaussian noise (AWGN). Residual noise from the echo canceller will also contribute to the AWGN noise.

Because of the very low power-spectral-density (PSD) of the AWGN, *-140 dBm/Hz* in [2], it is not one of the limiting impairments in ADSL DMT systems.

3.3 Crosstalks –FEXT and NEXT

Crosstalk generally refers to the interference that enters a communication channel, such as an unshielded twisted-pair channel, through some coupling path. In Figure 12, wire pair *1* and *2* are two twisted pairs in one pair bundle; NEXT and FEXT from wire pair *1* to wire pair *2* are as shown.

We can see that NEXT will be much more damaging than FEXT because it doesn't experience the attenuation of the loop, which will greatly decrease the power of the FEXT noise.

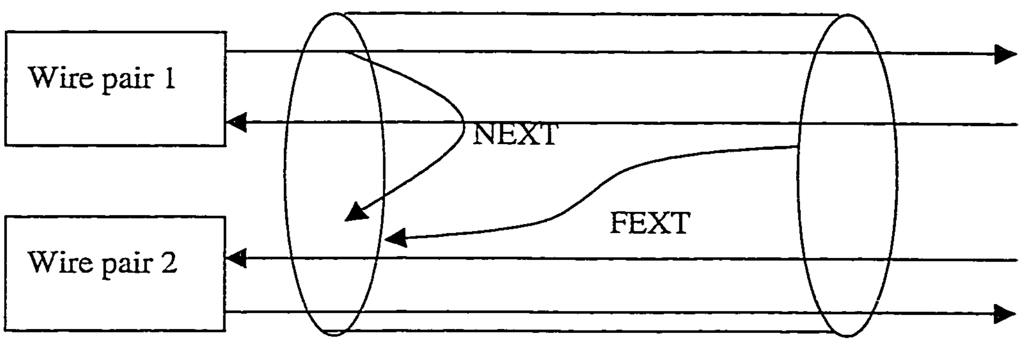

Figure 12 NEXT & FEXT

Empirical studies show that crosstalk is one of the limiting impairments for the transmissions over UTP [8]. Crosstalk usually has much higher power spectral density (PSD) than background AWGN noise. In [18], NEXT is found to limit the capacity of the

HDSL transmission because of the full duplex transmission. However, in ADSL systems, data is transmitted almost unidirectionally. Therefore, there will be nearly no NEXT term in the frequencies of interest due to other ADSL services in the same wire bundle. However, there will still be a significant amount of spillover NEXT from bi-directional baseband services in the same wire bundle due to non-ideal filtering.

The NEXT term can be modeled by a coupling function of the form:

$$\left|H_{NEXT}(f)\right|^2 = K_{NEXT} \cdot f^{3/2} \tag{26}$$

where f is frequency in *Hz* and K_{NEXT} is determined through empirical measurements.

In addition to spillover NEXT, FEXT also exists in the ADSL environment, and it can be modeled with a coupling transfer function of the form:

$$\left|H_{FEXT}(d,f)\right|^2 = K_{FEXT} \cdot d \cdot \left|C(f)\right|^2 \cdot f^2 \tag{27}$$

where $C(f)$ is the channel transfer function, d is the length of the cable in *kft*, f is frequency in *Hz*, and K_{FEXT} is determined through empirical measurements.

3.4 Impulse Noise

Impulse noise in ADSL DMT systems is one of the major topics in this thesis. A detailed description of impulse noise will be given in *Chapter 6* of this thesis.

Chapter 4

Error-Correction-Coding in ADSL DMT Transmission Systems

This chapter focuses on the Forward-Error-Correction (FEC) code used in ADSL DMT transmission systems. First, the properties of RS codes are briefly described. Next, some simulation approaches of the RS coded systems are discussed. Finally, three different types of periodic interleavers are compared. The background given in this chapter is important because in *Chapter 5*, the overall simulation structure is based on the analysis presented here.

4.1 Structure of FEC in ADSL DMT Systems

The coding scheme applied to the ADSL DMT systems is desirable to have a good coding gain, a reasonable implementation complexity, flexibility for different data rates, and some burst error immunity. Concatenated code with RS code as the outer code and trellis code as the optional inner code is recommended in [2] for ADSL DMT systems. The basic idea is to take advantage of the excellent performance of trellis code in AWGN channel, while at the same time, making use of the outer RS code to combat burst errors caused by both impulse noise and Viterbi decoder. It is well known that, the errors at the Viterbi decoder output occur in bursts. Also, the independence of the memoryless subchannels makes trellis codes very easily concatenated to the modulation structure, see Figure 13, because every subchannel can use its own trellis encoder/decoder without any interference from other subchannels.

Reed-Solomon (RS) code in Galois Field of *256* (GF(256)) is recommended in [2] for ADSL DMT transmission systems. Therefore, the input to the RS encoder is assumed to be divided into groups of 8-bits, or one byte. The output is then input to an interleaver, which also works on byte basis. An optimal bit-allocation is operated on the output bit sequence from the interleaver, as shown in Figure 13. Next, the trellis encoder operates on the bits at the output of the bit allocation unit, producing a set of complex symbols that serves as the input to the IFFT block. Note that the subchannels can share one trellis encoder/decoder pair, which operates across them [10]. The convolution encoder and coset selector remain the same, just the signal selector component must select points from different size constellations as the encoder operates across the tones. In the receiver, a Viterbi decoder operates across the subchannels at the output of the FFT block. The validity of using this receiver structure is based on the fact that the subchannels are independent and memoryless in the DMT systems. However, using the above structure, while only one pair of trellis encoder/decoder is used, results in very large latency and memory requirement.

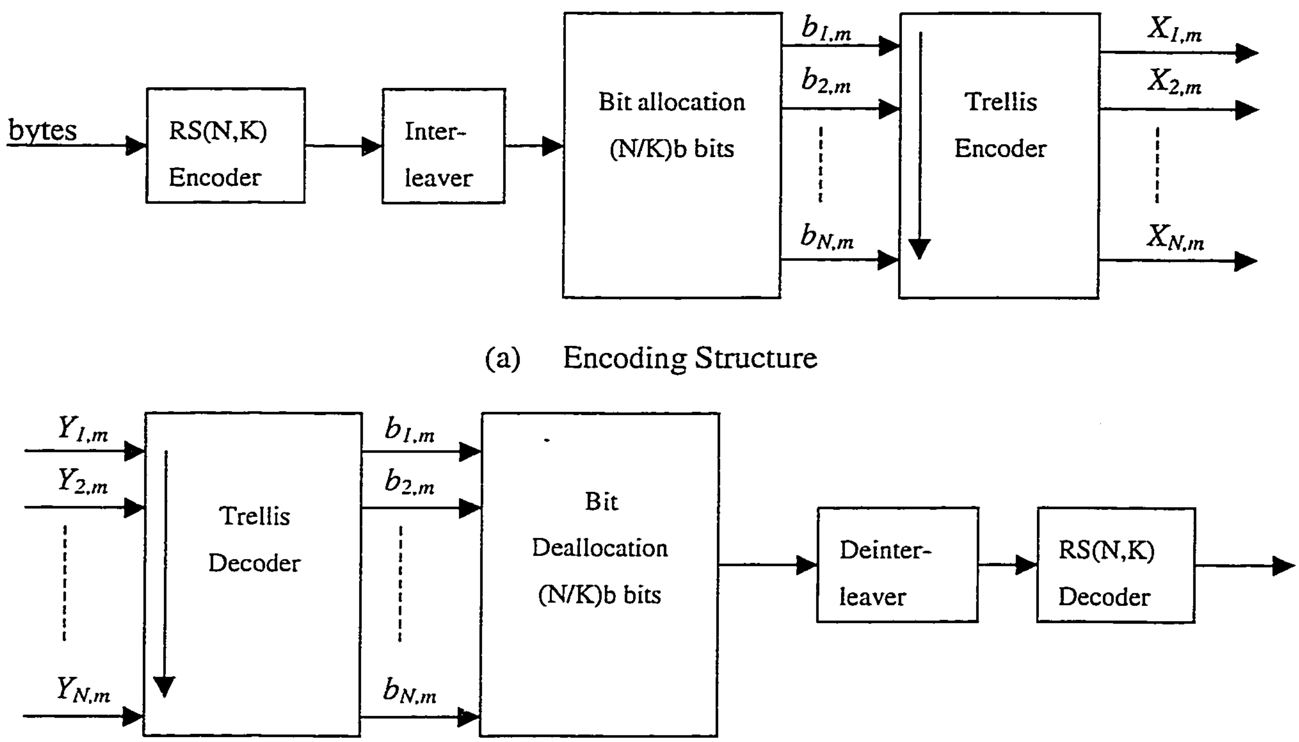

(a) Encoding Structure

(b) Decoding Structure

Figure 13 Coding and decoding structure in a concatenated system

Wei's 4-dimensional Trellis code is optional in the coding scheme in ADSL DMT systems to further increase the system margin. An effective average fractional bit granularity among the subchannels can be achieved in an ADSL DMT system by using many different size multidimensional QAM constellations. It is known that the integer constraint is a factor that results in some potential capacity loss of the DMT systems. Smaller bit granularity in the subchannels will give bit-allocation results closer to the optimal solution. While these multidimensional constellations can be accomplished by various algorithms given in [16] and some other methods, the complexity will be more than what we can afford.

4.2 Introduction to RS and Erasure RS code

Reed-Solomon code (RS code) is a special kind of nonbinary BCH codes. An RS code $RS(N,K)$ on $GF(q)$ has the code word length $N=q-1$ and the minimum distance $d=N-K+1$, with each character in the code word standing for $\log_2 q$ bits.

4.2.1 Properties of Reed-Solomon Code

RS code has some very good properties, which make it one of the most popular codes used in practical communication and storage systems. We are going to discuss these properties in the following.

1. RS code is Maximum-Distance-Separable (MDS) code

As stated above, an RS code $RS(N,K)$ has minimum distance

$$d = N - K + 1 = r + 1 \tag{28}$$

where $r = N - K$ is the number of redundancy characters.

2. Error and Erasure correcting capability

$RS(N,K)$ code can correct up to t character errors where

$$t = \left\lfloor \frac{N-K}{2} \right\rfloor = \left\lfloor \frac{r}{2} \right\rfloor \tag{29}$$

and it can correct any pattern of t character errors and s character erasures for which

$$2t + s < d = r + 1 \tag{30}$$

The property of erasure correction capability makes it the most popular code to combat burst errors. It is apparent now that if we have some means to decide the reliability of the incoming characters, making use of erasure decoding with RS code will give us almost twice the error correction capability.

3. Any K positions in a N-character length RS code word can be used as an information character set

The simplest case is the systematic RS code, in which the first K characters in the N length code word are the information characters. In this way, we can have an approximate estimate of the error output when the number of error characters in one code word exceeds its error- correction capability and a decoding failure occurs. This will be explained in details later.

4. Shortened RS code

RS code $RS(N\text{-}l,\ K\text{-}l)$ is called a shortened RS code of $RS(N,K)$ code, where l is an integer less than K. Shortened RS code has the following properties:

- Shortened RS code is still MDS code.
- Shortened RS code is not cyclic code, but it can use a cyclic encoder and decoder with minimal modifications.
- For RS code, shortening is always done in the most convenient manner, setting the string of highest order consecutive information characters equal to zero.

Shortened RS codes are used in most of the practical systems instead of the standard RS codes.

4.2.2 Decoding Failure and Decoding Error

In a practical communication system that makes use of some kind of block code with minimum distance d, usually a bounded-distance decoder is used. The bounded-distance decoding is defined as a decoding procedure that corrects all error patterns of weight l or less and no others, where $l \leq t$ and t is the largest integer equal to or less than $(d\text{-}1)/2$. All practical bounded-distance decoders use some form of syndrome decoding, in which the syndrome computed from the received word is interpreted as an indicator of either some specific error pattern of weight l or less, or the occurrence of some unidentifiable error patterns that have caused the received word to lie outside any sphere of radius l centered on a code word.

At the receiver of the coded transmission system which makes use of a bounded-distance decoder, three possible outcomes may occur at the output of the decoder.

- Decoding correct: The correct information characters are recovered from the received code word. This happens when the received word is within the decision sphere of the transmitted word with radius l.
- Decoding error: The received code word is recovered into an information word different from the input information word to the encoder. This happens when a received word is within the decision sphere of a code word other than the transmitted code word.
- Decoding failure: The bounded-distance decoder can not recover the received code word. This happens when a received word falls outside of all decision spheres of the code words.

We know that only 'perfect codes' have the entire received words lie inside the surrounding spheres with radius $d_{min}/2$, which means that the bounded-distance decoder with $l=d_{min}/2$ can only be a complete decoder for 'perfect codes'. RS code is definitely not 'perfect'; it can be shown later that most of the received error words will lie outside of the decision regions. When this condition occurs, no attempt is made to correct this word and a decoding failure signal is declared. With this decoding failure signal, different backup strategies will be carried out in different communication systems.

There are only the first two situations in complete decoders, one of which is the maximum likelihood decoder. The maximum likelihood decoder will compare the code word that it can't decode with every valid code word and chooses the one with minimum Hamming distance. However, it is impractical when the number of valid code word is very large because comparing the received word with every valid code word will cost too much time and computation.

It is shown in [34] that the probability of the decoder error is much smaller than the probability of decoder failure for RS codes. We can lower the decoder error probability by refusing to accept some noise patterns which the decoder thinks it has 'decoded' with a penalty of decreasing the probability of correct decoding. However, RS codes provide an uncommon exception to this rule, because many error patterns which are "corrected" by the common decoding algorithm are quite unlikely to be caused by multiple bursts of 'natural' errors. This is because most patterns of t or fewer character errors consist of bursts of length slightly less than $\log_2 q$ bits, and these bursts rarely cross over the boundaries between characters of the code, whereas most "natural" error bursts occur at phases uncorrelated with the code's character boundaries. In this way, the error decoding probability will be further decreased.

In the following section, we will see that the low decoding error probability of RS code will give us a very simple way to estimate the coding performance of RS codes in a communication system.

4.2.3 RS Code Simulation in ADSL DMT Transmission Systems

1. Simulation in random error environment

Random errors are caused by the stationary noises in ADSL DMT transmission systems. The stationary noises include mainly Additive-White-Gaussian-Noise (AWGN) and crosstalk (FEXT/NEXT), while the crosstalk is also modeled as narrow-band AWGN in each sub-channel.

Assume that an RS code $RS(N,K)$ in $GF(256)$ is used and the error-correction capability is t. Now we divide the time axis into a lot of periods, where each period lasts for U seconds, which is the length of one RS code word. These periods can be divided into three groups, let's call them 'good' periods, 'bad' periods and 'terrible' periods. The definitions of these three different periods are based on the number of error bytes in one period, which is the same thing as in one RS code word. When the noise causes t or less byte errors in one period, this period is a 'good' one; when more than t but less than $2t+1$ byte errors occur, it is called a 'bad' one; finally, when there are more than $2t+1$ error bytes, we call it a 'terrible' period.

Assume that the average bit-error-rate (BER) of the transmission with a fixed signal-to-noise ratio (SNR) is p_{bit}. Then we have the average byte error rate of the system expressed as:

$$p_{byte} = 1 - (1 - p_{bit})^8 \tag{31}$$

With the average byte error rate, the probability of 'good' period, P_{good}, the probability of 'bad' period, P_{bad}, and the probability of 'terrible' period, $P_{terrible}$ can be expressed as:

$$P_{good} = \sum_{i=0}^{t} \binom{N}{i} \cdot p_{byte}^{i} \cdot (1 - p_{byte})^{N-i} \tag{32}$$

$$P_{bad} = \sum_{i=t+1}^{2t+1} \binom{N}{i} \cdot p_{byte}^{i} \cdot (1 - p_{byte})^{N-i} \tag{33}$$

$$P_{terrible} = \sum_{i=2t+2}^{N} \binom{N}{i} \cdot p_{byte}^{i} \cdot (1 - p_{byte})^{N-i} \tag{34}$$

With a moderately low byte error rate, which means a moderately high SNR, from equation (32) to (34), we can see that the probability of 'bad' period is much higher than that of the 'terrible' period, and with t increasing, the difference increases sharply, as shown in Figure 14, for *RS(208,200)* code over GF(256).

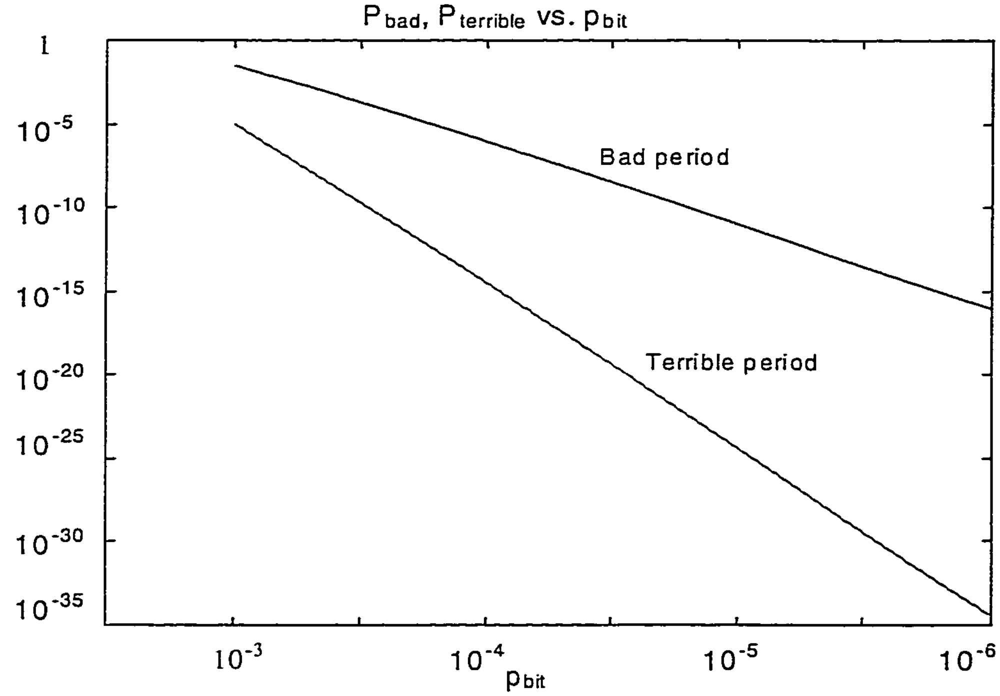

Figure 14 P_{bad} and $P_{terrible}$ vs. p_{bit}

As an example, let's assume a BER of $p_{bit} = 10^{-3}$. With equation (31), we get:

$$p_{byte} = 1-(1-p_{bit})^{8} = 8\times10^{-3} \tag{35}$$

Assume that $N = 208$, $K = 200$ and $t = 4$, we have the 'bad' period and 'terrible' period probabilities are *0.0265* and *8*10⁻⁶*. As this example illustrates, the effect of 'terrible' period can be generally neglected.

From [34], we know that for RS code, the probability of decoding failure is much higher than that of decoding error for the 'bad' period case. This suggests that when there are more than t byte errors, s errors for example, occur in one code word, most probably the decoder will declare a decoding failure rather than try to decode it. Assume that systematic RS code is used and the first K bytes are the information bytes. When a decoding failure is declared, we will just take the first K bytes as the output of the decoder. In the worst case, all of the s error bytes fall into the first K positions, then we have s error bytes in the output word from the decoder. At this point, we can express the bit-error-rate, P_b, at the output of the RS decoder in the following form: [32]

$$P_b \cong \sum_{i=t+1}^{N} \frac{i}{8N}\binom{N}{i} p_{byte}^{i}(1-p_{byte})^{N-i} = \sum_{i=t+1}^{N} \frac{1}{8}\binom{N-1}{i-1} p_{byte}^{i}(1-p_{byte})^{N-i} \tag{36}$$

When the SNR at the receiver end is high enough and with ideal scrambling, for QAM transmission, with good constellation mapping, it is reasonable to say that one error byte in the channel is most likely caused by one channel bit error. Equation (36) is also based on this assumption.

Equation (36) suggests a simplified way to estimate the performance of RS code in a transmission system. The process is described as follows, with the same assumptions about RS code we used before.

- First, because the input bytes to the RS encoder are randomly distributed, the output bytes in any RS code word should also be randomly distributed. Then we can just generate a random byte sequence with length N to stand for the output of the RS encoder directly. In this way, we avoid the time consumed in the encoding process.

- At the receiver end, we just compare the received N byte blocks with the transmitted ones. If the number of error bytes is less than t, then we decide that there will be no error occurring at the output of the decoder. When the number of error bytes is more than t, we assume that a decoding failure is declared, and take the number of error bits in the first K bytes.

  Alternatively, we can take the number of error bits in all of the N bytes in one RS code word as the number of output error bits. In this way, when there is a decoding failure, we will get a BER a little more than the actual one. However, since the number of redundant bytes is always very small relative to the code word length, the BER increase is not significant. This BER increase can also offset the effect of the infrequent decoding error, which often causes more error bits than a decoding failure.

Instead of the simulation process described above, there is an even simpler one, which is also a good approximation. In this scheme, every time we find more than t error bytes in one code word, no matter how many bytes are in error, we just declare that there are $2\times t+1$ error bytes, and still assume that one error bit will occur in one error byte. In this case, the equation (36) will be expressed as:

$$P_b \cong \sum_{i=t+1}^{N} \frac{2\times t+1}{8N} \binom{N}{i} p_{byte}^{i} (1-p_{byte})^{N-i} \tag{37}$$

The number of error bits per error byte can be adjusted to make it somewhat closer to the practical results.

Some previous simulations showed that equation (37) is a very good approximation to equation (36), and the simulation process is simplified.

2. Simulation in burst error environment

In DMT ADSL transmissions, impulse noise is different from AWGN and crosstalk; it is not a stationary process. An impulse will be in the form of a short pulse with high peak amplitude. Clearly, whenever an impulse occurs in a period of one RS code word, that period might be a 'terrible' period. For the 'terrible' period, we know from [34] that the probability of decoding failure is still much higher than that of decoding error, but the difference is not so great as for the 'bad' period. Using the simulation process described above is still not a bad approximation, but the results will not be so close.

4.3 Interleavers

Interleaving/deinterleaving technique is used in combination with coding to improve the burst error correction performance. An interleaver is a device in the transmitter that rearranges the order of a data sequence, and the deinterleaver will recover the original order at the receiver end. When burst errors occur in the channel to the interleaved data sequence, after the deinterleaver, the errors are rearranged and divided into several separated parts. The distance between the separated parts can be controlled easily by setting the interleaver's parameters.

For interleaving used in combination with certain FEC code, an important concept here is the interleave depth, D, which means that a burst must have length of at least $D+1$ in order to strike any code word more than once.

Interleavers can be divided into two catagories as periodic interleavers and pseudorandom interleavers. A periodic interleaver is an interleaver for which the interleaving permutation is a periodic function of time. There are mainly three commonly used periodic interleavers, block interleaver, convolutional interleaver and helical interleaver. They are going to be discussed later in the following sections.

A pseudorandom interleaver is an interleaver which takes a block of L channel symbols after encoding and reorders them into a pseudorandom fashion. This can be implemented by writing the L symbols sequentially into a random access memory (RAM) and then reading them out pseudorandomly. One can store the desired permutation in a read-only memory (ROM) and then use this permutation to address the interleaver memory.

Pseudorandom interleaver provides a high degree of robustness to variability in the burst parameters, but at the cost of more complexity than the periodic interleavers of the same size.

4.3.1 Block Interleavers

Block interleavers accept symbols in blocks and perform identical permutations over each block of symbols.

Assume a block interleaver involves taking the coded symbols and writing them by columns into a matrix with N rows and B columns. The permutation consists of reading these symbols out of the matrix by rows prior to transmission. Such an interleaver is referred to as a *(B,N)* block interleaver.

- Any burst errors of length $b \leq B$ results in single errors at the deinterleaver output each separated by at least N symbols;
- Any burst of length $b = rB(r > 1)$ results in bursts of no more than $[r]$ symbol errors separated by no less than $N - [r]$;
- A periodic sequence of single errors spaced by B symbols results in a single burst errors of length N at the deinterleaver output;
- End-to-end delay is $2NB$ symbols exclusive of the channel delay and the memory requirement is NB symbols in both the interleaver and deinterleaver. The minimum end-to-end delay is $(2MN - 2M + 2)$ symbol times, not including any channel propagation delay.
- Choice of parameter N is dependent on the coding scheme used. In usual applications, the effects of the channel memory should not be observed over any span of N symbols at the deinterleaver output. Thus N should be larger than the decoding span. For block codes N should be larger than the block length, while for convolutional codes N should be larger than the decoding constraint length. Thus, a burst of length $b \leq B$ can cause at most one single error in any block code

word. Similarly with convolutional codes, there will be at most one single error in any decoding constraint length.

4.3.2 Convolutional Interleavers

Convolutional interleavers have no fixed block structure, but they perform a periodic permutation over a semi-infinite sequence of coded symbols.

The structure proposed by Forney is shown in the following Figure 15.

Define the parameter

$$N = MB \tag{38}$$

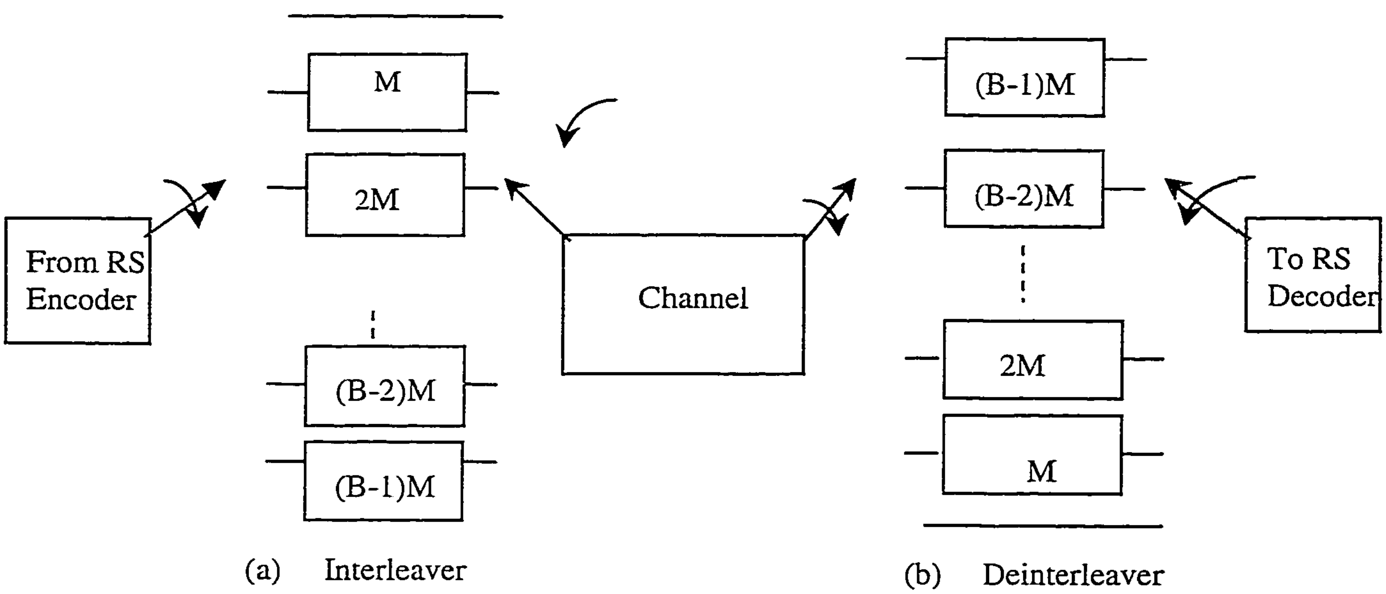

Figure 15 Structure of a convolutional interleaver/deinterleaver

This interleaver is related to a (B, N) block interleaver and has quite similar properties.

- The minimum separation at the interleaver output is B symbols for any two symbols that are separated by less than N symbols at the interleaver input;
- The previous characteristic implies that any burst of $b \leq B$ errors inserted by the channel results in signal errors at the deinterleaver output separated by at least N symbols;

- A periodic pattern of single errors spaced by $N+1$ symbols results in a burst of length B at the de-interleaver output;
- The total end-to-end delay is $N(B-1)$ symbols and the memory requirement is $N(B-1)/2$ in both the interleaver and deinterleaver. Note that this is half the required delay and memory in a block interleaver/deinterleaver.
- B is chosen to be larger than the length of the burst errors. N is chosen to be larger than the block length for block codes or the decoding constraint length for convolutional codes.
- One advantage of the convolutional interleaver is that the synchronization problem is easier than that for a block interleaver. The reason is that the ambiguity is only of degree B for the convolutional interleaver while it is of degree NB in a block interleaver.

4.3.3 Helical Interleaver

In [65,66], a new interleave technique is used, which is called helical interleaving. For helical interleaving, an interleaving block with defined size is given. Then, under some special read-in and read-out regulation, data sequence is written into and read out of the interleaving block. If the interleaving block size and the regulation are properly chosen, helical interleaving can achieve the same performance with convolutional interleaving with the same complexity and same time latency.

Using helical interleaver gives certain advantages over using convolutional interleaver. First, choice of interleaver parameters in helical interleaver is more flexible than that of convolutional interleaver. Second, using helical interleaver gives much loose requirement for interleaver/deinterleaver synchronization. Details about helical interleaving can be found in [65,66].

Chapter 5

Performance of RS code against Random Errors in ADSL DMT Systems

This chapter first gives the detailed simulation structure to evaluate the performance of RS codes against random errors caused by the stationary noises in ADSL DMT systems. Then, the simulation results achieved with this simulation structure are presented and explained. Finally, the performance of RS codes with erasure decoding technique in AWGN channel is analyzed and simulation results are given.

5.1 RS Coding Gain Evaluation Simulation Structure

The structure shown in Figure 16 is used to estimate the coding gain performance of the RS codes used in the ADSL DMT transmission systems. The procedure can be described as follows:

1. With a destination bit error rate, 10^{-7} defined in [2], and the RS code redundancy, r, we can get the required approximate symbol error rate (SER) in each subchannel, under the assumption that all subchannels have the same symbol error rate. Details of this operation are discussed in *section 5.2.*
2. From the symbol error rate obtained in the first step, we calculate the normalized signal-to-noise ratio [19], SNR_{norm}, details will be given in *section 5.3.*
3. With the SNR_{norm} and the total number of bits in one DMT symbol after the RS encoding, b_{DMT}, and the noise condition (including AWGN and crosstalk noise), bit allocation algorithm is carried out to obtain the required minimum transmit power in each subchannel and the total transmit power required. From the power distribution result of the bit-allocation algorithm, the minimum required transmitted PSD could also be obtained. Either the total required transmit-power or the minimum required transmit PSD could be used to estimate the RS coding gain performance.

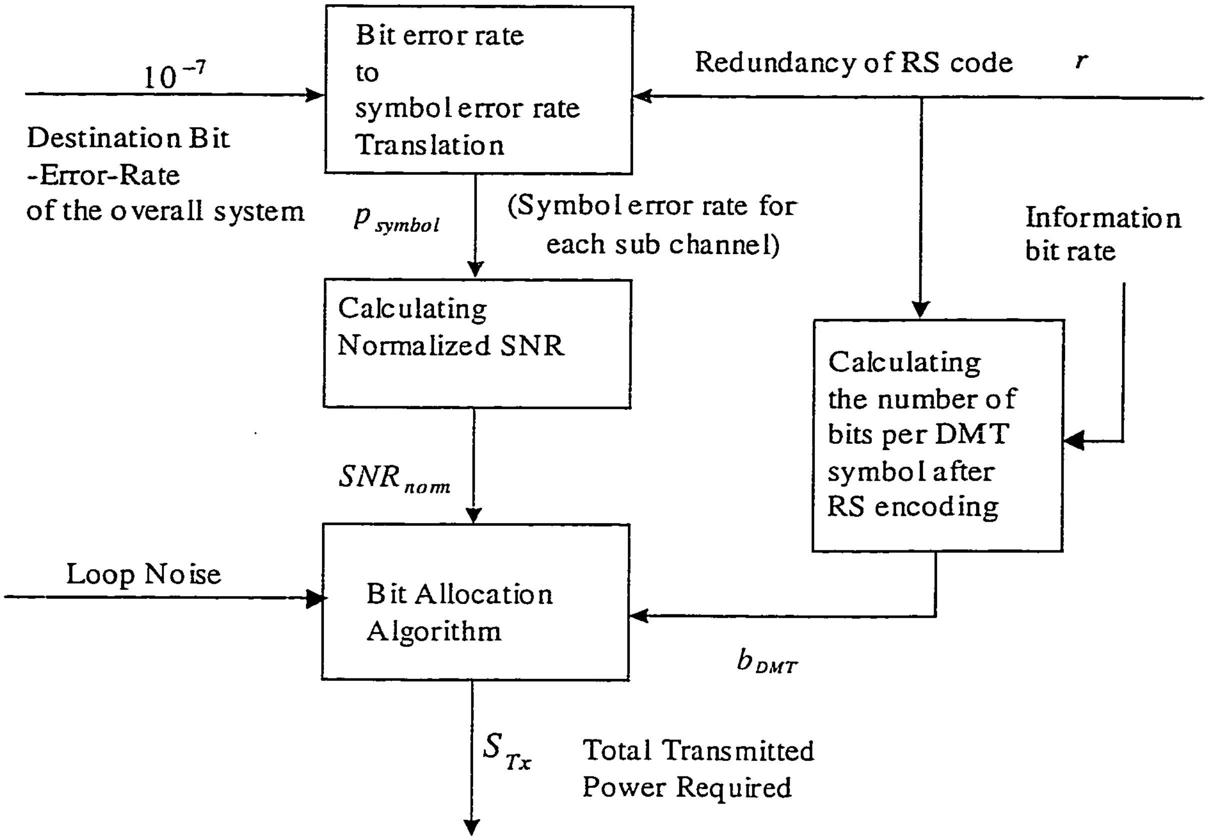

Figure 16 Structure of RS coding gain analysis

4. When the redundancy of the RS code is set to be zero, we can get the total required transmit power without coding, S_0. In the same way, with different redundancy r, we can obtain the required transmit power, S_r, respectively. The ratio of S_0 to S_r, is the coding gain for redundancy r, i.e.,

$$G(r) = -10 \times \log_{10} \frac{S_r}{S_0} \tag{39}$$

5. In practice, the DMT symbols transmitted in the subscriber loops have a constant PSD, *-40 dBm/Hz* [2], which means that each subchannel has a constant transmit power spectral density. The minimum required transmit power spectral density, Λ_c in dBm/Hz, can be achieved through the above bit-allocation algorithm. This is an approximation based on the fact that the power spectral distribution from the bit allocation is almost flat, with less than *+/-2 dB* fluctuations caused by the integer-constraint. Therefore, the performance can also be evaluated by the

relative margins achieved by the RS code with different parameters. The margin is defined as:

$$\Gamma(r) = \Lambda_c(r) - (-40) \quad (dBm/Hz) \tag{40}$$

and the relative margin is defined as:

$$\Gamma_r(r) = \Gamma(r) - \Gamma(0) \tag{41}$$

where r is the number of redundancy bytes of the RS code we used, $\Gamma(r)$ is the PSD margin achieved with a RS code redundancy of r bytes, and $\Gamma(0)$ is the PSD margin when no RS code is used.

Both the total transmit power and the average PSD are used in the simulation to estimate the RS coding gain performance, and the results show very small difference. Results shown later in this chapter are all based on using the total required transmit power.

The following sections discuss the simulation procedure in details.

5.2 BER to SER Translation

With the destination bit error rate (BER), 10^{-7}, and the RS code redundancy, r, we can get the required approximate symbol error rate (SER) in each sub-channel, under the assumption that all subchannels have the same symbol error rate, with equations given in *Chapter 4*.

Reed-Solomon codes $RS(N,K)$ in $GF(256)$ are used. The number of information bytes per codeword K, the codeword length in byte N, and the maximum number of correctable error bytes t, are related such that:

$$t = \left\lfloor \frac{N-K}{2} \right\rfloor \tag{42}$$

where, the redundancy in percentage, v, is expressed as [32]:

$$v = \frac{N-K}{K} \cdot 100\% \tag{43}$$

Assume that the input BER to the RS decoder is p_{bit}, the probability of a byte error can be expressed by:

$$p_{byte} = 1-(1-p_{bit})^8 \tag{44}$$

Then the bit error rate at the output of the RS decoder can be approximated by equation (36), which is rewritten here as:

$$P_{bit} \cong \sum_{i=t+1}^{N} \frac{i}{8N} \binom{N}{i} P_{byte}^{i} (1-P_{byte})^{N-i} = \sum_{i=t+1}^{N} \frac{1}{8} \binom{N-1}{i-1} P_{byte}^{i} (1-P_{byte})^{N-i} \tag{45}$$

Equation (45) is based on the following assumptions:

- The code is employed to correct errors only, not for detecting errors.
- The input bit errors are randomly distributed, which means ideal bit scrambling.
- The factor, $i/(8N)$, is based on the fact that the decoder we use will either decode the codeword correctly in the presence of t or fewer errors or not decode the codeword with a number of errors greater than t. This means that when there are more than t byte errors, the probability of decoding failure is much larger than the probability of decoding error. This was shown in *Chapter 4.*
- A byte error will typically contain only one bit error, explained in *Chapter 4.*

For a $4-QAM$ transmission system, with the decoder output bit error rate fixed at 10^{-7}, using equation (45), we can obtain the relationship between the input symbol error rate and the *RS(N,K)* code redundancy shown in Figure 17, with *K=200.* Note from Figure 17 that when the redundancy is zero, the required channel symbol error is not 10^{-7}, but $2\cdot10^{-7}$. This is because for $L-QAM$ signals we have

$$p_{bit} = \frac{p_{symbol}}{k} \tag{46}$$

where $k = \log_2 L$ is number of bits in one $L-QAM$ symbol. The smallest value of k is 2 for 4-QAM transmission. In our analysis, it is just assumed that for each subchannel, k takes the value of 2. Therefore, the SER we obtained above in Figure 17 is actually an upper bound for those channels with $k \geq 2$. However, it guarantees that with this SER, we should have a BER smaller than 10^{-7} for the overall transmission. This also suggests that the coding gain we obtained here is smaller than the actual coding gain we would have for a real system with an overall BER of 10^{-7}. Apparently, the difference between the real coding gain and the estimated one becomes larger when the constellation size of the QAM signals increases.

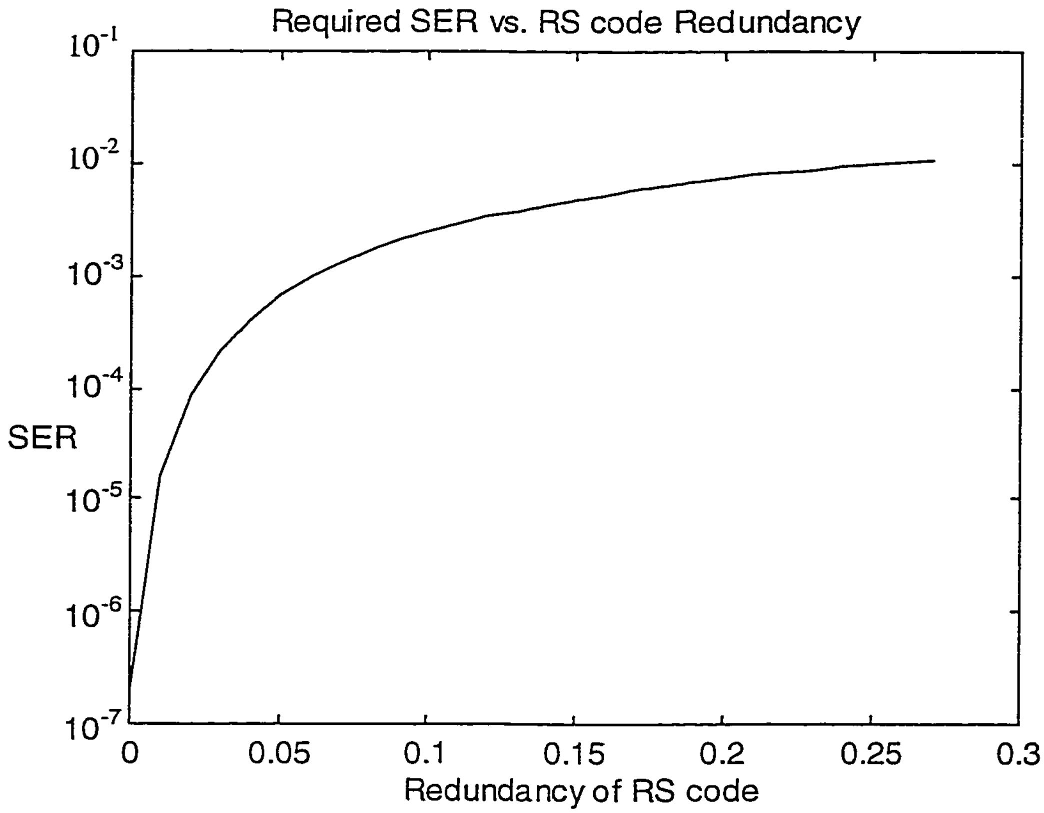

Figure 17 Required SER vs. RS code redundancy for 4-QAM, when the output BER=10^{-7}, $K=200$

5.3 Normalized Signal-to-Noise Ratio (NSNR)

The normalized signal-to-noise ratio (NSNR) of an arbitrary transmission scheme with a data rate of k bits per two dimensional symbol is defined in [19] as,

$$SNR_{norm} \triangleq \frac{SNR_{ZF-DFE}}{2^k - 1} \tag{47}$$

where

$$SNR_{ZF-DFE} = \frac{S_{signal}}{S_n} \tag{48}$$

and S_{signal} is the average received signal power, S_n is the average noise power at the receiver end.

SNR_{ZF-DFE} in (47) and (48) is the signal-to-noise ratio at the receiver of a communication system with ideal zero-forcing-decision-feedback-equalizer (ZF-DFE), which means that the combined effect of the channel and the ZF-DFE can be modeled as a $\delta - function$ with only delay and attenuation, and thus there exists no inter-symbol interference (ISI) caused by the channel.

With an uncoded $L-ary$ QAM signal constellation with minimum distance $d_{\min}$, the normalized average symbol energy is:

$$E_{symbol} = \frac{(L-1) \cdot d_{\min}^2}{6} \tag{49}$$

and the bit rate per symbol can be expressed as,

$$k = \log_2 L \tag{50}$$

Since the noise is assumed to be Gaussian, the symbol error probability can be well approximated at high rates by

$$P_{e\_symbol} \cong 4 \cdot Q\left[\left(\frac{d_{\min}^2}{2 \cdot P_n}\right)^{\frac{1}{2}}\right] = 4 \cdot Q\left[\left(3 \cdot SNR_{norm}\right)^{\frac{1}{2}}\right] \tag{51}$$

where *4* is the number of neighboring signal points to any interior points in the QAM signal constellation. This gives a universal curve, independent of the bit rate k per QAM symbol, for the approximate performance of uncoded $L-ary$ QAM with ZF-DFE with arbitrary high-SNR, over strictly bandlimited Gaussian channels, which is shown in Figure 18.

The NSNR will be used in Cioffi's bit allocation algorithm, which is described in the *section 5.5*.

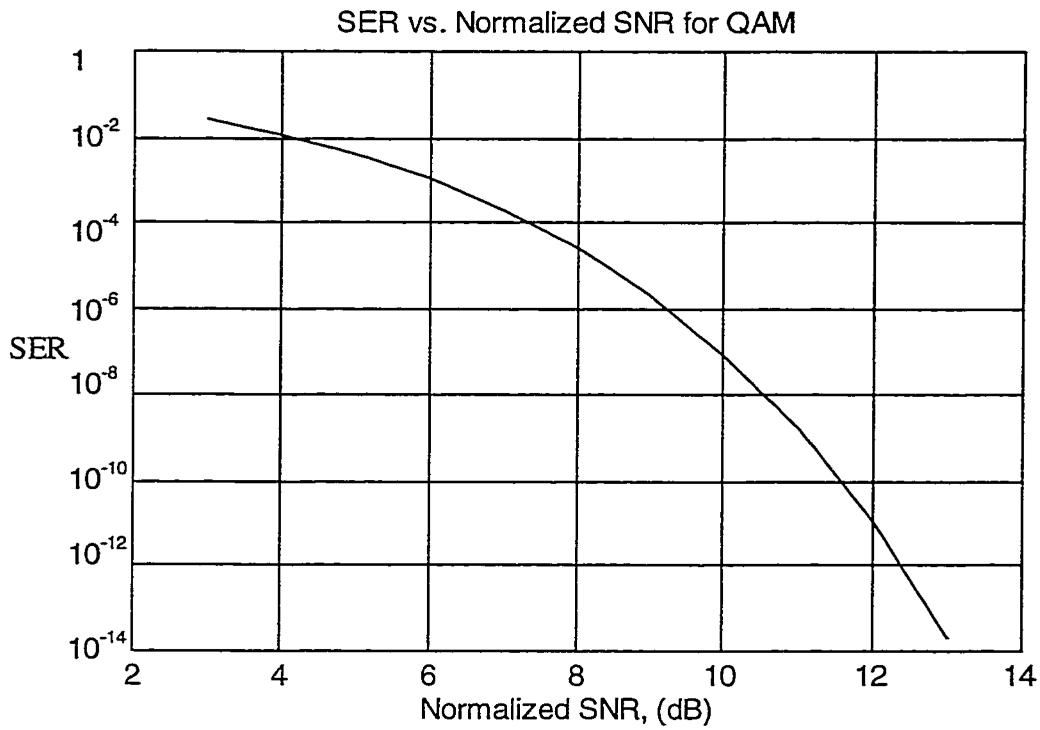

Figure 18 SER vs. normalized SNR for QAM transmission

5.4 FEXT and NEXT Models

The FEXT and NEXT models used in the analysis are taken from [2]. In the simulation, the ADSL FEXT, ADSL NEXT, HDSL NEXT and T1 NEXT are considered.

The following examples are the FEXT and NEXT noise models for ADSL down-stream transmission. For up-stream, the crosstalk models are the same, but have different parameters.

1. Downstream ADSL FEXT noise models

Downstream ADSL FEXT noise comes from downstream transmission signals from other ADSL services, which is called the ADSL downstream disturber. The PSD of the downstream disturber can be expressed as [2]:

$$PSD_{ADSL-down-Disturber} = K_{ADSL} \cdot \frac{2}{f_0} \cdot \frac{\left[\sin\left(\frac{\pi f}{f_0}\right)\right]^2}{\left(\frac{\pi f}{f_0}\right)^2} \cdot \frac{1}{1+\left(\frac{f}{f_{3dB\_low}}\right)^8} \cdot \frac{f^8}{f^8 + f_{3dB\_high}^8} \qquad (52)$$

where

$$f_0 = 2.208 \quad MHz,$$

$$f_{3dB\_low} = 1.104 \quad MHz,$$

$$f_{3dB\_high} = 20 \quad kHz$$

$$K_{ADSL} = 0.1104 \quad Watts,$$

$$0 \le f < \infty \quad Hz$$

K_{ADSL} is the average transmit power of the ADSL system. Equation (52) gives the single-sided PSD; that is, the integral of the PSD, with respect to f, from 0 to infinity, gives the power in Watts.

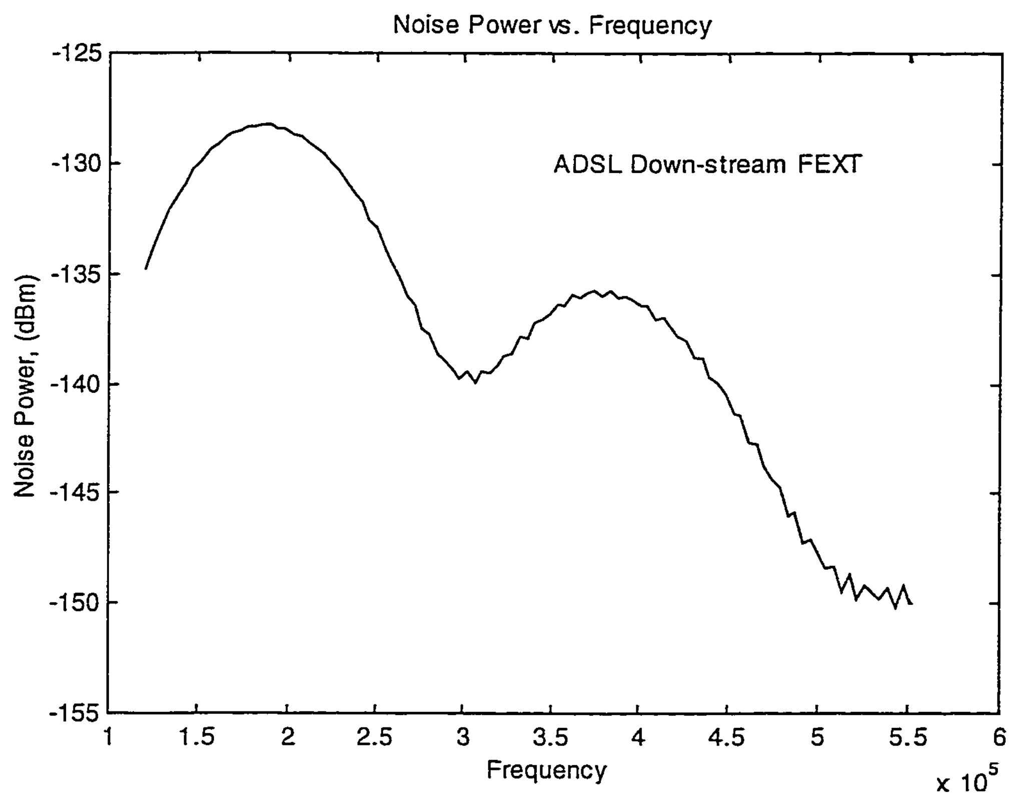

Figure 19 PSD of ADSL downstream FEXT

The FEXT loss filter model is:

$$\left|H_{FEXT}(f)\right|^2 = \left|H_{channel}(f)\right|^2 \cdot k_F \cdot l \cdot f^2 \tag{53}$$

where $H_{channel}(f)$ is the channel transfer function, k_F is the coupling constant and is $3.083*10^{-20}$ for *10, 1%* worst-case disturbers; l is the coupling path length in feet, and f is in Hz.

The PSD of the FEXT noise is therefore expressed as:

$$PSD_{ADSL-down-FEXT} = PSD_{ADSL-down-Disturber} \cdot \left|H_{FEXT}(f)\right|^2 \tag{54}$$

which is shown in Figure 19.

2. Downstream ADSL NEXT model

The NEXT noise for ADSL downstream transmissions comes from the upstream ADSL transmission signals. For frequency duplex ADSL transmission, the upstream ADSL signal nominally occupies the band from *25 kHz* to *138 kHz*, but the upper sidelobes of the upstream signal beyond *138kHz* may still have NEXT contribution into the downstream signal. The effect of this NEXT will depend on the qualities of the front-end filters and the echo cancellors in the transceivers. The PSD of the upstream ADSL NEXT can be expressed as:

$$PSD_{ADSL-us-NEXT} = PSD_{ADSL-us-Disturber}\left(x_n f^{\frac{3}{2}}\right) \quad 0 \le f < \infty \tag{55}$$

where $x_{10} = 3.3982 \times 10^{-14}$ is the coupling constant with 10 disturbers, and the $PSD_{ADSL-us-Disturber}$ is the PSD of the ADSL upstream disturber, which can be expressed as:

$$PSD_{ADSL-us-Disturber} = K_{mask} \cdot \frac{\left[\sin\left(\frac{\pi f}{f_0}\right)\right]^2}{\left(\frac{\pi f}{f_0}\right)^2} \quad 0 \le f < \infty \tag{56}$$

where f_0=*276 kHz* and

$$K_{mask} = \begin{cases} -38 \quad dBm/Hz & 28 \quad kHz \le f \le 138 \quad kHz \\ -38 - 24\left(\dfrac{f - 138000}{43125}\right) \quad dBm/Hz & f > 138 \quad kHz \end{cases} \tag{57}$$

is the NEXT coupling constant, including the effect of the front-end low-pass filter in the transmitter end of the upstream signals, which has a cut-off frequency of *138 kHz*.

Figure 20 shows the PSD of ADSL downstream NEXT given by equation (55).

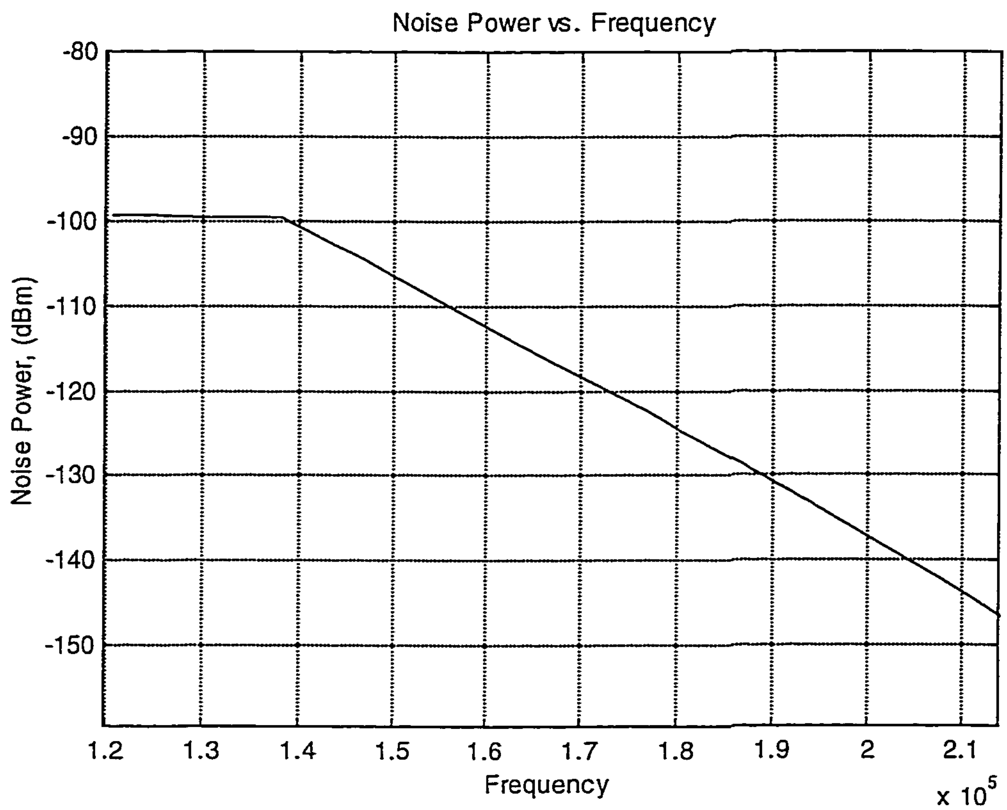

Figure 20 PSD of ADSL downstream NEXT

5.5 A Practical Bit Allocation Algorithm

A practical bit allocation algorithm is given in [33], which is although somewhat sub-optimum relative to the optimum algorithms such as the Hughes-Hartogs algorithm, but has much faster convergence speed. For this reason, it is preferred in current ADSL DMT applications.

This algorithm first finds the (approximately) optimal system performance margin, γ_{margin}, (which is another name of the normalized SNR we discussed in the previous section), then it guarantees convergence with a sub-optimal loop, and at last it adjusts the energy distribution accordingly on a subchannel-by-subchannel basis. A description of the iterative process of this bit-loading algorithm can be found in [33].

In the simulation, the output of the bit allocation algorithm includes the bit allocation, b_k, the power distribution, S_i, and the overall transmit power S_{total}.

5.6 Coding Gain Results using Cioffi's Bit Allocation Algorithm

Using the simulation structure described above, RS coding gain results with different parameters were obtained. Here, it should be noted that the interleave depth is not one of the parameters of interest, because for random error correction, interleaving does not give any performance improvement.

In the simulation, the following assumptions were made:

• FFT length	512
• DMT symbol rate	4.0 kHz
• Lowest carrier	51.75 kHz
• Highest carrier	One below Nyquist
• Bit distribution	[0,2,3,4,5,6,7,8,9,10,11,12,13,14,15]
• TEQ	none
• Bit rate -- full rate	1.6 Mbps for ISDN loops, 6.4 Mbps for CSA loops
• Bit rate – half rate	1.0 Mbps for ISDN loops, 2.0 Mbps for CSA loops
• For all crosstalks	10 disturbers

The assumption of no TEQ is very important for the validity of the coding gain results we obtained. In practice, bit-allocation must be carried out twice in the initialization process. The first bit-allocation is used to decide on which subchannels we can transmit signals. Then after the settings of TEQ have been decided, the second bit-allocation is carried out. At this time, the channel models are no longer the loop models, but the combined transfer function of the channel loops with the TEQ. This, of course, will cause some side-effects on the validity of the results.

	ISDN #9	ISDN #13	CSA #4	CSA #6	CSA #7	CSA #8	mid-CSA
Rate (*Mbps*)	1.6 1.0	1.6 1.0	6.4 2.0	6.4 2.0	6.4 2.0	6.4 2.0	6.4 2.0
Length (*kft*)	10.5	12.0	7.6	9.0	10.7	12.0	6.0

Table 1 The assumed bit rate over the test loops and the length of the test loops

The test loops are given in [2], including ISDN loop #9,13 and CSA loop #4,6,7,8, and mid-CSA loop. The target information transmission rate over these loops and the length of the loops are shown in Table 1.

Figure 21-24 present the coding gain vs. redundancy results for ADSL DMT downstream transmission with AWGN and crosstalk noises. Crosstalk noises are modeled as colored-Gaussian noises whose PSD are given by the formulas in *section 5.4.*

From the figures, we can see that for ADSL DMT systems, we have an optimum value of redundancy with which we can achieve the best coding gain. This is because in a DMT system, the redundancy of RS code is absorbed in the DMT symbols by the bit allocation algorithm, which means that with more redundancy, more bits are required to be transmitted in one DMT symbol. Therefore, with larger coding redundancy, one DMT symbol must contain more bits. Larger coding redundancy gives larger capability of error correction, which results in smaller channel SNR requirement. On the other hand, larger bit load per DMT symbol requires some subchannels to transmit QAM signals in larger constellations, which will require more transmitted power. Thus, a compromise exists and an optimum value of the redundancy must be chosen to achieve near-optimum performance.

Although because every loop has its unique transfer function, which results in a unique RS coding gain performance curve for it, the curves in Figure 21-24 have similar shapes. Furthermore, we can see that for the same transmission rate, the optimal RS coding redundancies are close for transmissions over different test loops, which is about *10%* for *1.6 Mbps* for ISDN loops and *6%* for *6.4 Mbps* for CSA loops.

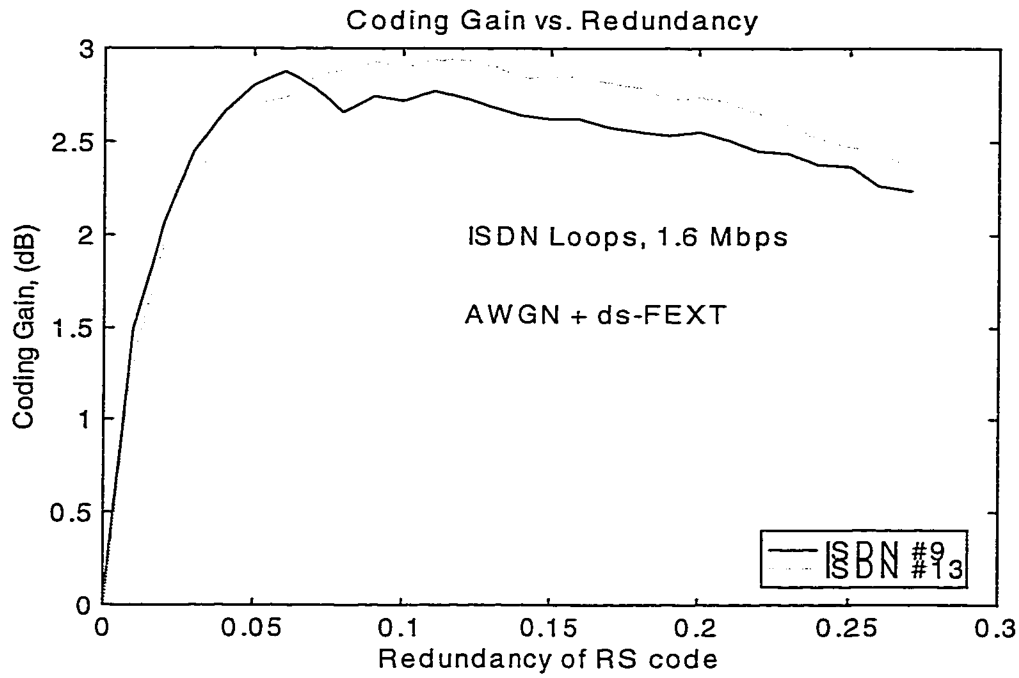

Figure 21 Coding gain performance 1

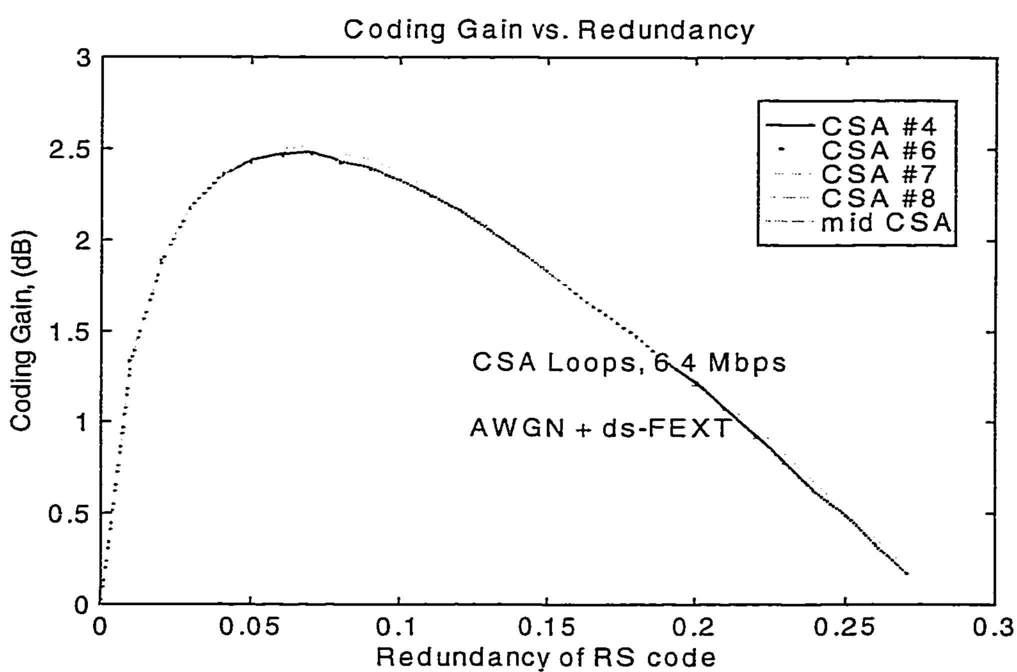

Figure 22 Coding gain performance 2

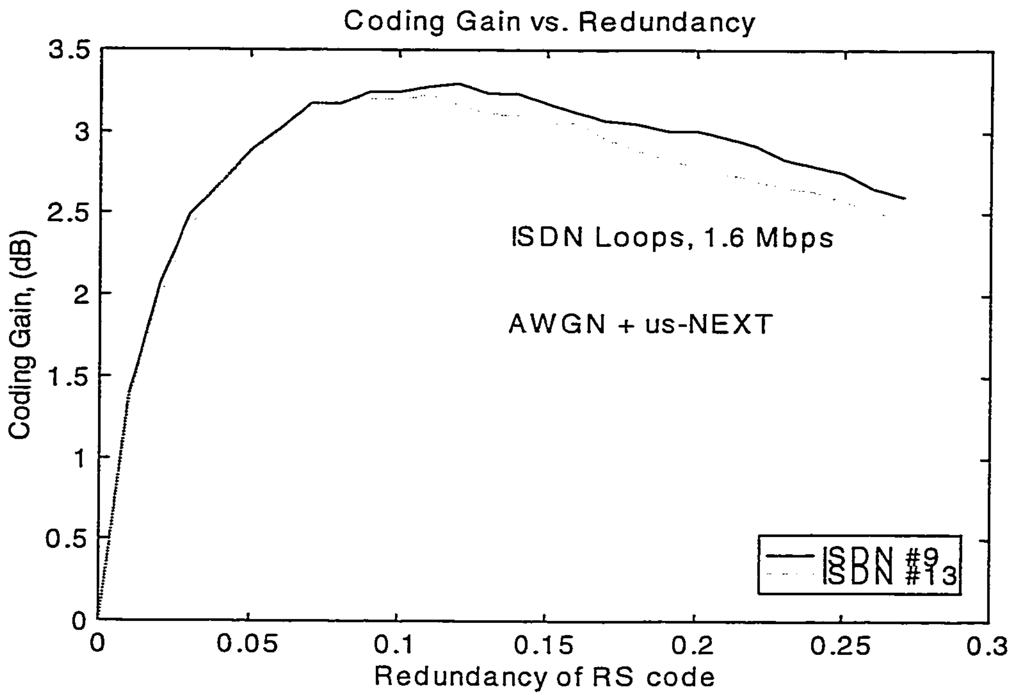

Figure 23 Coding gain performance 3

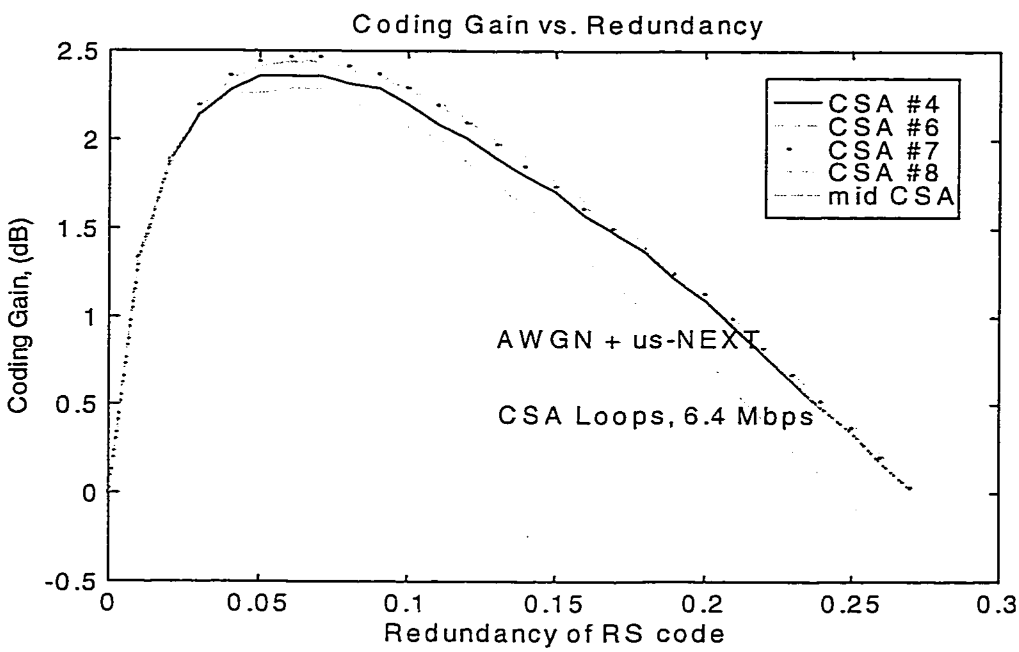

Figure 24 Coding gain performance 4

From the figures, we also found that for lower rate transmission, the optimal redundancy is larger, and the coding gain result decreases slower after the optimal value. While for higher rate transmission, the optimal redundancy is smaller and the coding gain decreases much faster compared to that of lower rate transmission. This is because that higher rate transmission requires more bit in one DMT symbols than a lower rate transmission. Therefore, with the same redundancy rate, more redundant bits must be added to one DMT symbol in higher rate transmission systems. Therefore, increasing the constellation size of some subchannels to absorb the redundancy introduced by the RS code in a high rate transmission ADSL DMT system will cost more power than doing the same operation to a lower rate transmission. Then the redundancy absorbing operation shows earlier and faster offset effect over the RS coding gain in a higher rate transmission ADSL DMT system than it does in a lower rate transmission system.

If we only consider the performance in AWGN plus crosstalk noise environment, what we want is to choose the redundancy as small as possible to increase the system efficiency on condition that certain coding gain can be obtained. However, impulse noise can not be ignored. If there is no restriction on system latency, we could choose our optimal redundancy and then choose the interleave depth according to the requirement of combating impulse noise. However, if our redundancy is chosen as too small, the interleave depth must be very large to meet the requirement, then the latency will become very large. Therefore, there is a comprise in choosing the value of redundancy between the random error correcting ability and the system latency. Within the permissible range of random error correction coding gain, we should choose the redundancy as large as possible to make the interleave depth as small as possible, thus, to make the latency as small as possible. Table 2 gives the optimal values of redundancy we should choose under different noise environments. The entries of the table are in the form "redundancy/least coding gain".

Sometimes, lower transmission rate will be chosen in order to get better transmission quality. Similar coding gain results were obtained for lower transmission rate, *1.0 Mbps* for ISDN loops and *2.0 Mbps* for CSA loops. Optimal values of the redundancy we should choose are listed in Table 3.

	Down-stream FEXT	Up-stream NEXT	ds-FEXT + us-NEXT
ISDN Loops (1.6 Mbps)	5% ~ 20% / 2.5 dB	7% ~ 16% / 3.0 dB, 4% ~ 26% / 2.5 dB	10% ~ 18% / 3.0 dB 4% ~ 27% / 2.5 dB
CSA Loops (6.4 Mbps)	%4 ~ 13% / 2.0 dB	%4 ~ 12% / 2.0 dB	4% ~ 13% / 2.0 dB

Table 2 Optimal redundancy values for ADSL DMT transmissions in different noise environments, *1.6 Mbps* for ISDN loops and *6.4 Mbps* for CSA loops

Results show that with properly chosen redundancy, up to *3 dB* coding gain and at least *2.5 dB* coding gain can be achieved by using RS code only for less than 1.6 Mbps transmission. For higher rate, at least *2.0 dB*, up to *2.5 dB* coding gain can be achieved.

	Down-stream FEXT	Up-stream NEXT	ds-FEXT + us-NEXT
ISDN Loops (1.0 Mbps)	7% ~ 22% / 3.0 dB 4% ~ 25% / 2.5 dB	7% ~ 18% / 3.0 dB 4% ~ 22% / 2.5 dB	10% ~ 20% / 3.5 dB, 7% ~ 27% / 3.0 dB
CSA Loops (2.0 Mbps)	7% ~ 16% / 2.5 dB 4% ~ 21% / 2.0 dB	7% ~ 12% / 2.5 dB 3% ~ 16% /2.0 dB	6% ~ 16% / 2.5 dB 3% ~ 22% / 2.0 dB

Table 3 Optimal redundancy values for ADSL DMT transmissions in different noise environments, *1.0 Mbps* for ISDN loops and *2.0 Mbps* for CSA loops

Results in the tables indicate that for lower transmission rate, we always have a wider range of values to choose from to get satisfactory performance. However, the range is much smaller for higher transmission rates.

The results shown above are all based on the bit-allocation algorithm described in [33]. This algorithm assumes flat power distribution as a pre-assumption, and this is just a sub-optimal solution. Using bit-allocation algorithm described in *section 2.4* will give us optimal solution. Simulations based on the bit-allocation algorithm described in *section 2.4* were also run and corresponding results were obtained. The results are very similar to the results shown above. This demonstrates the fact that the optimal power spectral distribution of a DMT system is an almost flat power distribution.

5.7 ERASURE DECODING PERFORMANCE IN AWGN CHANNEL

5.7.1 Erasure Decoding

In a digital communication system, information is formatted into sequences of symbols and each symbol takes on one value from a finite range of possibilities. These symbols are modulated onto a carrier and the resulting signals are transmitted to one or more receivers. At some point in each receiver, a detection circuit examines the received, processed signal and decides which of the possible transmitted symbols is most likely to have been sent.

In a hard-decision receiver, the detection circuit limits its range of choices to the same group of choices available at the transmitter. Unfortunately hard decisions destroy information that can improve the overall performance of a communication system. In some cases, the received signal may not offer a clear choice as to which of the possible symbols has been transmitted. Rather than forcing a decision that is likely to be incorrect, a soft-decision receiver uses an expanded selection of choices to improve the quality of the received symbol to the error correction decoder. The simplest form of soft-decision receiver uses erasures to indicate the reception of a signal whose corresponding symbol value is in doubt. For example, for a $q-ary$ transmission, the receiver may have $(q+1)$ detection choices; the additional one is called an erasure.

Erasure decoding does not provide significant additional gain for additive white Gaussian noise channels, but it does provide substantial improvement over fading and bursty channels. BCH and Reed-Solomon codes allow for a very efficient means of erasure decoding. Reed-Solomon erasure decoding plays a significant role in the error correction system used in compact audio disc players. From *Chapter 3*, we can see that we can correct twice as many erasures as for errors. This can be explained intuitively by noting that we have more information about the erasures to begin with. We know exactly where the erasures are, but we have no idea as to the locations of the errors.

5.7.2 Erasure Decoding Performance Analysis

Assume that the input to the erasure RS decoder are channel bits, while every 8 bits make up one code word character.

Assume:

Input bit error probability: p_{ee}

Input bit erasure probability: p_{es}

Input bit correct probability: p_c

and we have:

$$p_c + p_{ee} + p_{es} = 1 \tag{58}$$

For a code word character, which contains 8 bits, we have the following probabilities:

The erasure probability is: $$p_{CWS} = \sum_{k=1}^{8} \binom{k}{8} p_{es}^{k} (1 - p_{es})^{8-k} \tag{59}$$

The error probability is: $$p_{CWE} = \sum_{k=1}^{8} \binom{k}{8} p_{ee}^{k} (1 - p_{ee} - p_{es})^{8-k} \tag{60}$$

The correct probability is: $$p_{CWC} = (1 - p_{ee} - p_{es})^{8} \tag{61}$$

Assume that we use $RS(N,K)$ with $r = N - K$, number of errors is e, number of erasure is f, while N, K, r are even numbers.

Then the output bit error probability is approximately:

$$\begin{aligned} p_{out}^{bit} &= \sum_{e=0}^{r/2} \sum_{f=r+1-2e}^{N-e} \frac{e + C \cdot f}{8N} \binom{N}{e} \binom{N-e}{f} p_{CWE}^{e} p_{CWS}^{f} p_{CWC}^{N-e-f} \\ &+ \sum_{e=r/2+1}^{N} \sum_{f=0}^{N-e} \frac{e + C \cdot f}{8N} \binom{N}{e} \binom{N-e}{f} p_{CWE}^{e} p_{CWS}^{f} p_{CWC}^{N-e-f} \end{aligned} \tag{62}$$

A good approximation of equation (62) is:

$$\begin{aligned} p_{out}^{bit} &= \sum_{e=0}^{r/2} \sum_{f=r+1-2e}^{N-e} \frac{(r+1)}{8N} \binom{N}{e} \binom{N-e}{f} p_{CWE}^{e} p_{CWS}^{f} p_{CWC}^{N-e-f} \\ &+ \sum_{e=r/2+1}^{N} \sum_{f=0}^{N-e} \frac{(r+1)}{8N} \binom{N}{e} \binom{N-e}{f} p_{CWE}^{e} p_{CWS}^{f} p_{CWC}^{N-e-f} \end{aligned} \tag{63}$$

Note the constant C in equation (62) is a constant between 1 and 4. For a random error channel with the condition of high SNR, C can be deemed as 1, with the same assumptions made in *Chapter 4*.

5.7.3 Erasure Decoding Performance over AWGN Channel

Here we use a shortened $RS(16,12)$ in GF(256) to test the performance difference between RS coding and Erasure-RS coding. Different performances according to different erasure thresholds are obtained.

Assumptions:

- BPSK
- AWGN channel
- Threshold is normalized by the value in Q-function: δ, while when $threshold = 0.2$ means that the real threshold is $\pm 0.2 \times \delta$.
- Threshold takes the values: *0, 0.1, 0.2, 0.3, 0.4, 0.5.*

The results obtained from equation (62) are shown in Figure 25. From this figure, we can see that when the threshold is 0.1, the performance of Erasure-RS coding is better than that of pure RS coding. But when we increase the threshold, the performance seems to degrade. When the relative threshold is more than 0.3, its performance is worse than that of pure RS coding. Also we can find that the advantage of Erasure-RS coding is getting better with the SNR at the receiver.

Figure 26 is the results obtained where equation (63) is used. When we compare Figure 25 and Figure 26, we find that the difference is very small. Thus we know that, the same thing as for simulating RS coding process, for Erasure-RS coding, we can also have a relative simple simulation method. When compare the received code word with the correct one, if $(2e + f) > 2t$, where $N - K = 2t$, we declare that there are $e + 2 * f$ error bits.

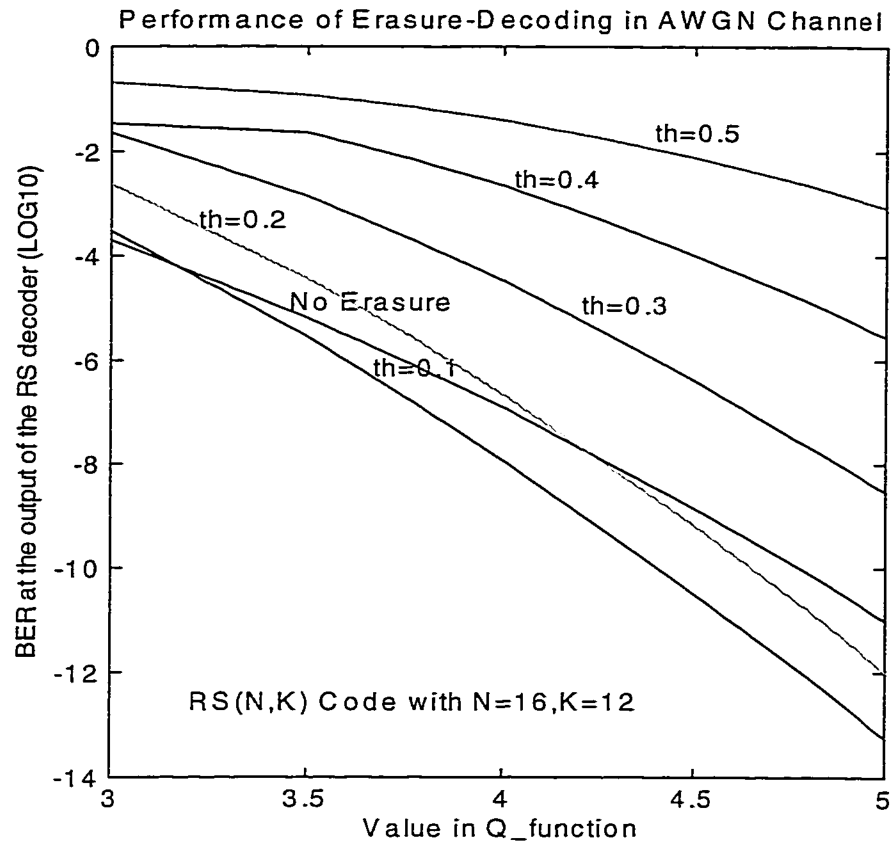

Figure 25 Performance of RS code with erasure decoding technique in AWGN channel, using equation (62)

Simulations with RS codes of different code word lengths were run and similar results were obtained. Also, simulations using different QAM signals were also tested. It is found that the larger the QAM constellation, the less gain we can achieve. When the number of signal points in the constellation is larger than *256*, almost no gain can be achieved. However, with 4-QAM, more than *0.5 dB* coding gain improvement can be achieved with carefully chosen threshold.

However, from the simulation, the coding gain improvement is not significant compared to the additional complexity for AWGN channels. This is in agreement with the previous results of erasure decoding, which stated that erasure decoding technique is more important for error correction in burst error environment.

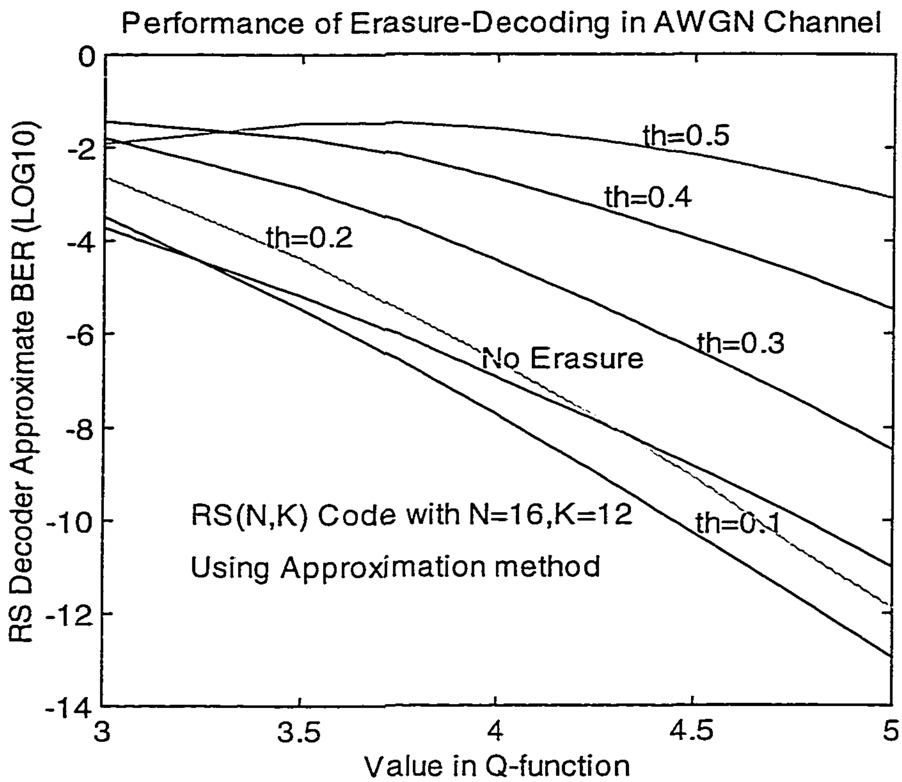

Figure 26 Performance of RS code with erasure decoding technique in AWGN channel, using equation (63)

Indeed, erasure decoding is proposed here mainly because of its performance improvement over burst errors caused by impulse noise in ADSL DMT systems, which is a topic of next chapter.

Chapter 6

Evaluating ADSL DMT System Performance in Impulse Noise Environment

Impulse noise is a major performance limiting impairment in ADSL DMT transmissions. While the RS code used in the ADSL DMT systems must provide certain coding gain against stationary noise (mainly crosstalk noises), it must also guarantee a satisfactory system performance in the presence of impulse noise. In *Section 6.1*, an overview of impulse noise in subscriber loops is first introduced. Then, in *Section 6.2*, an approach to estimate the performance of RS codes in ADSL DMT systems against impulse noise is presented. The simulation results that employ this approach are given in *section 6.3*. Two other performance evaluation approaches that could have been used are presented in *Appendix A* and *B*.

6.1 Overview of Impulse Noise

6.1.1 Introduction

Non-stationary impulse noise is characterized as infrequent, short-duration pulses with relatively high amplitude; it is one of the major impairments in the subscriber-line transmissions. The sources of impulse noise in the subscriber lines can be divided into two categories, internal sources and external sources. External sources include high-voltage devices, power plants and distribution, transportation means (railways, underground,...), fluorescent tubes, lightning surges and electrostatic discharges. Internal sources include signaling in forms of dialing pulses, busy signals, ringing and mechanical switch noise [39]. All these very different sources give impulse noise extremely complex statistical properties.

The voltage, inter-arrival time and the duration are the three most important statistical characteristics of impulse noise. Since there are so many varied factors in the occurrence of the impulse noise, it is impossible to give a theoretical expression of their probability density functions (PDF). This makes it necessary to rely on extensive experimental data to derive analytical models for the statistics of the impulse noise.

A lot of work has been done in the literature trying to get a proper impulse noise model, with which the performance of different transmission systems in the presence of impulse noise can be properly evaluated. Ever increasing digital transmission rate over telephone lines requires more and more exact analysis of the impulse noise. The introduction of high-speed transmission over subscriber lines such as HDSL and ADSL initiated new impulse noise studies. Especially in the case of ADSL, impulse noise could be the major disturbance, because for pure ADSL transmission, near-end crosstalk from other ADSL lines can be completely avoided by frequency duplex transmission.

6.1.2 Impulse Noise Model

For evaluating the performance of subscriber-line transmission systems, a close impulse noise model must be used. There are several impulse noise models raised in the literature. Here, we will only go through the models suitable for subscriber-line transmissions.

For high rate subscriber-line transmission, a common impulse may last over several transmit symbols. Therefore, a good impulse noise model should represent the randomness of the waveform and its finite duration properly. In [40], Melbourne Barton introduced a method where impulse noise is modeled as an ensemble of random waveforms of finite duration. In this model, the peak impulse voltage distribution is modeled as Gaussian, Laplacian or hyperbolic. The inter-arrival time is modeled as a Poisson process, which is not favored by the results from various surveys. The impulse event durations and impulse waveforms are fixed. This is a simplified model of impulse noise in the practical subscriber lines. However, some of its statistics must be validated before it can be employed.

Instead of basing the model on some assumptions, massive number of measurements was taken and statistical analysis was performed by several different research groups. Based on the results of the statistical analysis, by curve fitting, the relevant parameters were obtained in Germany [35], Britain [41] and North America [42,43,45]. Based on the parameters obtained, impulse voltage, inter-arrival time and duration can all be generated.

Furthermore, typical waveforms can be obtained from a fixed mean energy spectral density (ESD, refere to the definition in next section) and a fixed mean phase.

6.1.3 Statistical Characteristics

To built an impulse noise model, we must know the statistical characteristics of the impulse noise. Important statistical characteristics of impulse noise include:

- PDF of the Voltages
- PDF of the Inter-Arrival Times
- PDF of Impulse Lengths
- Energy spectral density (EDS)

  Impulse noise is not a stationary random process, so it does not have a power spectral density (PSD). However, its energy spectral density (ESD) exists.

  The time-sampled impulse noise record is denoted as $g(t)$. The spectrum of each record with N_s samples

$$G(f) = \sum_{k=1}^{N_s} g(k\tau)\exp(-i2\pi fk\tau) \tag{64}$$

  was found with a FFT. The energy spectra of the records from each location were averaged to estimate the energy spectral density (ESD) of the impulse noise:

$$ESD(f) = \sum_{j=1}^{NIMP} \frac{|G(f)|^2}{NIMP \cdot \Delta f \cdot R} \tag{65}$$

  here τ is the sample interval, Δf is the frequency interval of the FFT and R is the receiver resistance, $NIMP$ is the number of totally detected impulses.

- Phase Properties and 'Representative' Impulse

6.1.4 Influence of Impulse Noise in ADSL DMT Systems [46,47]

In [47], the received signal level in ADSL systems is analyzed and the effect of impulse noise on the system performance with assumed signal level and loop attenuation is given.

In this section, the same analysis will be performed on the ADSL DMT systems. Also, the effect of impulse noise on the transmitted symbols will be presented.

The transmission system is as shown in Figure 27. $X(k)$ is the complex QAM signal transmitted in the k^{th} subchannel. After IFFT operation, time domain discrete signal $x(n)$ is generated and converted into an analog signal $x(t)$, which is transmitted in the channel. $y(t)$ is the received analog signal, which is converted into a discrete form, $y(n)$. Then, $Y(k)$ is obtained by FFT operation on $y(n)$.

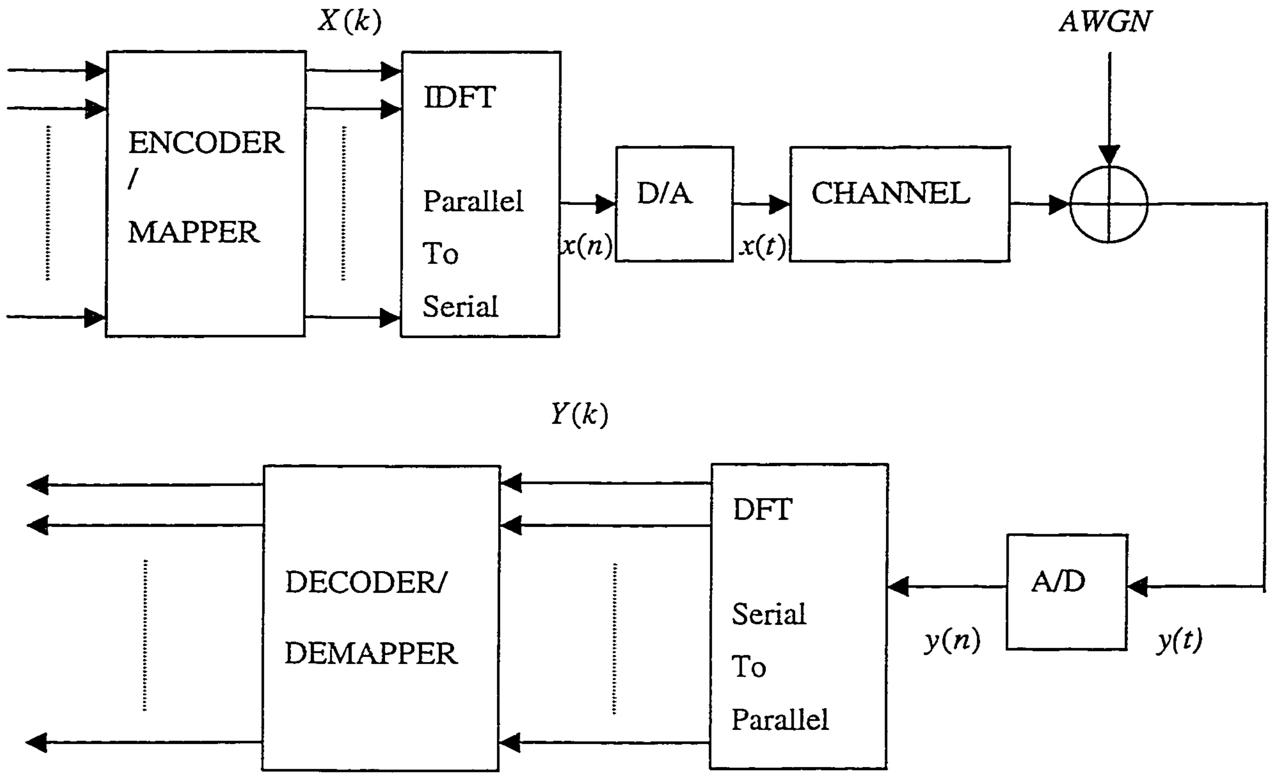

Figure 27 System configuration

Assume an ADSL DMT transmission system with:

- $N=128$ subchannels
- $2N=256$ point IFFT/FFT operation
- Each tone has a bandwidth of $w = 4.3125$ kHz

- The totally used bandwidth is $W = 552 \quad kHz$
- The sampling rate is $f_s = 1.104 \quad MHz$
- The transmitted DMT signal in the loops has a PSD of *PSD=-40 dBm/Hz*, as defined in ADSL DMT Standard T1E1.4/97-007R6
- A termination of $R = 100 \quad \Omega$ is used.

The input signal to IFFT $X(k)$ can be expressed as:

$$X(k) = a_k + jb_k \tag{66}$$

where a_k, b_k are the coordinates of the QAM signal transmitted in the k^{th} tone.

Then, $x(n)$ is:

$$x(n) = \frac{1}{2N} \cdot \left\{ \sum_{k=0}^{2N-1} (a_k + jb_k) \cdot \left[\cos\left(\frac{2\pi nk}{2N}\right) + j\sin\left(\frac{2\pi nk}{2N}\right)\right]\right\} \cdot \Pi\left(\frac{n-N}{2N}\right) \tag{67}$$

where

$$\Pi\left(\frac{n-N}{2N}\right) = \begin{cases} 1 & 0 \le n \le 2N-1 \\ 0 & otherwise \end{cases}$$

The analog transmitted signal $x(t)$ is thus expressed as:

$$x(t) = \frac{1}{2N} \cdot \sum_{k=0}^{2N-1} X(k) \cdot e^{\frac{2\pi kt}{2N \cdot T}} \Pi\left(\frac{t-NT}{2NT}\right) \qquad (0 \le t \le 2NT-1) \tag{68}$$

where T is the sampling interval $1/f_s$, $X(k) = a_k + jb_k$ is the complex expression of the QAM signal.

For all uncorrelated *X(k)* with zero mean and variance σ_k^2, the PSD of *x(t)* is given in [15] as

$$S_x(f) = \frac{T}{2N \cdot R} \cdot \left(\sum_{k=0}^{2N-1} \sigma_k^2 \cdot Sinc^2\left[2NT \cdot \left(f - \frac{k}{2NT} \right) \right] \right) \tag{69}$$

where R is the load resistance at the receiver end.

If σ_k^2 is a constant σ^2 for all k, (69) can be rewritten into

$$S_x(f) = \frac{T \cdot \sigma^2}{2N \cdot R} \cdot \left(\sum_{k=0}^{2N-1} Sinc^2\left[\frac{f}{w} - k \right] \right) \tag{70}$$

The summation item on the right hand side of equation (70) actually gives an approximately square-wave with unit amplitude. Therefore, we can see that the PSD is approximately flat in the range $[0, f_s]$, with an amplitude of

$$PSD = \frac{T \cdot \sigma^2}{2N \cdot R} \tag{71}$$

For a $L-QAM$ transmission system, the variance σ^2 of the transmitted QAM signals can be expressed as:

$$\sigma^2 = \frac{1}{6} \cdot (L-1) \cdot d_{\min}^2 \tag{72}$$

where $d_{\min}$ is the minimum distance in the L- QAM constellation between adjacent signal points.

Then, we have

$$\sigma^2 = \frac{PSD \cdot 2N \cdot R}{T} = \frac{10^{-7} \cdot 256 \cdot 100}{1/(1.104 \cdot 10^6)} = 2826 \tag{73}$$

with a 100 Ω termination, this corresponds to a minimum distance of:

$$d_{\min} = \sqrt{\frac{6 \cdot \sigma^2}{L-1}} = \sqrt{\frac{16956}{L-1}} \tag{74}$$

For ADSL DMT transmission system, data transmitted in different subchannels go through different attenuation. Bit allocation algorithm is used to adjust the numbers of bits transmitted in the subchannels to get the maximum system throughput, which can be achieved, under certain power constraint. Without power scaling operation after the bit allocation, which is used to set the DMT signal's PSD to be *-40 dBm/Hz*, the resulting PSD from the bit allocation is already approximately a flat one with less than *±2 dB* fluctuations. Now, we assume that the scaling operation is just multiplying the signals in all the subchannels by a constant, which is not exactly the case in a practical system.

Since the bit-allocation algorithm aims at achieving a fixed symbol error rate of 2×10^{-7} in each subchannel, and also because of the well known approximation, equation (55), which is repeated here as:

$$P_{symbol} = 4\times Q\left[(3\times SNR_{norm})^{1/2}\right] \tag{75}$$

we conclude that with the resulting PSD from the bit allocation algorithm, the normalized signal-to-noise ratio (SNR_{norm}) in different tones at the receiver end of the transmission system is also a constant. While SNR_{norm} is defined by (52) as:

$$SNR_{norm} \stackrel{\Delta}{=} \frac{SNR_{ZF-DFE}}{2^k - 1} = \frac{d_{\min}^2}{6\cdot\sigma_n^2} \tag{76}$$

where $L=2^k$ is the constellation size of the used QAM symbols, SNR_{ZF-DFE} is the average signal-to-noise ratio at the receiver end with ideal zero-forcing decision-feedback equalizer, which means an ideal channel model with just attenuation is assumed, and d_{min} is the minimum distance between adjacent signal points in the QAM constellation at the receiver end, σ_n^2 is the noise variance at the receiver end.

What really matters is the minimum distance d_{min} at the receiver end, not the average power received. Assume only AWGN is considered, the noise variance σ_n^2 in equation (76) is thus a constant for all subchannels. Under the above assumptions, the minimum distance d_{min} is thus also a constant for all subchannels at the receiver end, though different QAM constellations are used.

The above analysis leads to the conclusion that it makes sense to analyze the received DMT signal only from one tone instead of from all of the tones with only AWGN in the channel, because they have the same d_{min} at the receiver.

Assume *1.6 Mbps* DMT signals are transmitted on an ISDN loop #9, then each DMT symbol contains *400 bits*. The subchannel with carrier $\hat{f} = 258.75kHz$ is chosen to be analyzed. Through simple calculation, the channel attenuation at this carrier *is* $H = 0.0016 = -56\ dB$. The number of bits allocated to this sub-channel is *4*, which means that *16-QAM* signals are transmitted in this subchannel.

For this subchannel, the minimum distance d_{min} can be calculated using equation (74), with the result of $d_{min\text{-}tx}=33.62$ at the transmitter end. Because of the attenuation, the minimum distance at the receiver end $d_{\min-rx} = H \cdot d_{\min-tx} = 0.0538$.

For ADSL DMT transmission system, the impulse noise will go through FFT operation at the receiver end before it is clear whether or not it will cause any error in any of the subchannels. Therefore, we can not judge the effect of the impulse noise to the DMT symbols by their peak voltages directly. However, for a specific impulse noise, we can calculate the disturbance in each sub-channel by the FFT operation, for those sub-channels with impulse noise contribution of more than $d_{min\text{-}rx}/2$, which is *0.02519* in the above example, error will certainly occur.

The above analysis can give an approximate estimation of how impulse noise will cause errors and in which subchannels to the ADSL DMT systems. It doesn't consider the effect of FEXT/NEXT, which will cause QAM constellations with different $d_{\min-rx}$ in the subchannels. From the analysis above, we can see that the larger the $d_{\min-rx}$, the harder for the impulse noise to cause any error in that tone.

6.1.5 Coding Strategies for Impulse Noise in Multicarrier Modulation Systems

One advantage of multicarrier transmission system over single carrier one is its robustness against impulse noise. Besides the smearing effect, the effect of distributing impulse noise power into a lot of sub-channels, of multi-carrier system, tone-shuffling, variable tone margins, time-domain clipping and MSE monitoring can all be used in advance of any error correction to substantially reduce the effect of impulse noise in multi-carrier systems [48,49].

Several error-correction-coding methods were proposed to mitigate the effect of impulse noise in the literature. We will discuss them here.

1. Weakness of trellis codes against impulse noise

Trellis codes can be used with either multicarrier or single carrier modulation methods to increase the effective signal-to-noise ratio for a given subscriber loop, when the noise is stationary random process. However, burst errors render these codes ineffective, unless some form of interleaving can be used to ensure that large noise samples are distributed so that their occurrence is more "random".

Another trellis coding approach would be to use a trellis code designed for fading channels. In this case, the code has diversity and can cope with burst errors. However, the AWGN coding gain associated with these codes is rather low.

2. Interleaved RS code in concatenation with Trellis code

Reed-Solomon code with convolutional interleaving has been proposed in several papers as a means of effectively mitigating the effects of impulse noise in ADSL transmissions. Using Reed-Solomon code with long code word, we can combat long impulse noise while keeping the redundancy at a reasonable level. For even longer impulse noise, interleaving is used to improve the performance.

Trellis code is still recommended because of its error-correction capability for random errors. However, just as discussed above, its performance in impulse noise environment is much worse. Therefore a concatenated coding scheme, in which RS code with convolutional interleaving acts as outer code and trellis code acts as the inner code, is proposed.

Performance of RS code and the concatenated coding scheme in AWGN channel are shown in [32]. With RS code only, we can achieve *2* to *3 dB* coding gain in different loops, while with concatenated coding, an additional *2 dB* more coding gain can be achieved.

There is no reference available on the performance of the concatenated coding scheme in an impulse noise environment yet. It is expected that with the properly selected parameters for RS code and the interleaving, more coding gain might be achieved than that is possible with only using RS codes.

3. Interleaved Trellis Codes [51]

In [51], Interleaved Trellis (ITCM) scheme was proposed to improve the performance of communication systems against impulse noise. ITCM uses a bank of identical trellis encoders in a time-multiplexed fashion. This will provide symbol-interleaving capability, which can disperse the effect of impulse noise in the decoding process at the receiver. The number of encoder/decoder pairs used indicates the depth of symbol interleaving. Apparently, the more encoder/decoder pairs are used, the more improvement we have against the impulse noise.

However, the system complexity increases with the increasing capability of combating impulse noise. This method could only find its usage in some kind of mild impulse noise environment. For impulses with long duration over tens of symbol period, the complexity of this system will be prohibitive.

6.2 Impulse Noise Survey Results and Performance Evaluation Methods Based on Different Surveys

6.2.1 Performance Evaluation Simulation Approach

This performance evaluation approach is based on using the two typical impulses, impulse C-1 and C-2, given in the ANSI ADSL DMT Standard T1.413 [2]. A structure for estimating the performance of ADSL DMT transmissions is introduced in Clause 11 in the standard. The interference in the test system is caused by AWGN, crosstalk coupling from other subscriber line services, POTS signaling and impulse noise.

The two impulse waveforms are reconstructed from actual recorded impulses observed in field tests. They represent the most likely waveforms at specific measurement sites, respectively. The samples of these two impulses with *160 ns* sampling-interval are given in [2].

With the two given impulses, a simple performance evaluation procedure can be used, provided we make close assumption of the mean inter-arrival time.

6.2.1.1 Evaluation Method described in the STANDARD [2]

Performance testing procedure described in the Standard consists of injecting the selected impulse waveforms with varying amplitude levels and random phases. The amplitude (u_e mV) at which half the impulses cause errors is determined for each waveform. This value will be used as the smallest amplitude during the testing.

With the amplitude u_e for each impulse waveform, the estimated probability that there will be any error in a second is calculated with equation (77).

$$E = 0.0037 \cdot p(u > u_e^{(1)}) + 0.0208 \cdot p(u > u_e^{(2)}) \qquad (77)$$

where:

$$p(u > u_e) = \frac{25}{u_e^2} \qquad for \quad u_e \le 40mV \qquad (78)$$

$$p(u > u_e) = \frac{0.625}{u_e} \qquad for \quad u_e > 40mV \qquad (79)$$

and $u_e^{(k)}$ refers to the amplitude corresponding to impulse k, $k = 1,2$.

Equation (78) and (79) and the parameters can be found in [44]. Using (78,79) suggests that a *5 mV* threshold is used [44]. There is a problem of using this *5 mV* threshold: while the length of the impulse noise C-1 is shorter than that of C-2, its occurrence frequency is smaller than that of C-2. This is in contradiction with results from most of the previous surveys.

However, some other statistics obtained from some other surveys can also be used. Such an occurrence frequency $R\_1 = 0.0037$ can be found in [43], which gives that with a threshold voltage of $u_{sh-c1} = 7mV$, the average impulse interval rate in the test location of Mountain View *is 0.0037 impulses/s*. In [40], the author gives a likely value of occurrence frequency $R\_2 = 0.02589$ for the average impulse event rate with a threshold $u_{sh-c2} = 3mV$, with hyperbolic probability density function of the peak voltage. However, from the inter-arrival vs. peak voltage relationship given in [44], as an extrapolation result, the impulse event occurrence rates, R_1, R_2 and the thresholds u_{ch-c1}, u_{ch-c2}, should satisfy the following equation:

$$R\_2 = \left({u_{sh-c1}}/{u_{sh-c2}} \right)^{2.5} \cdot R\_1 \tag{80}$$

With $R\_1 = 0.0037$, $R\_2 = 0.0208$, $u_{ch-c1} = 7mV$, u_{sh-c2} should be approximately $3.5mV$.

6.2.1.2 Impulse Noise Statistics from the data result of the survey performed by Deutsche [44]

The statistics introduced here are used by the ADSL DMT Standard [2] to evaluate the ADSL DMT system performance.

1. Cumulative Amplitude Distribution

Based on all 150,000 registered impulse noise events, the amplitude distribution is quite well expressed by the equations

$$\begin{aligned} &P_R(V_R) = \left(\frac{V_R}{V_2} \right)^{-2} \quad if \quad V_R \le 40mV \\ &where \quad V_2 = 5mV \\ &P_R(V_R) = \left(\frac{V_R}{V_1} \right)^{-1} \quad if \quad V_R \ge 40mV \\ &where \quad V_1 = 0.625mV \end{aligned} \tag{81}$$

The probability $P_R(V_R) = P_R(V_R; V_{th})$ means that the random variable V_R exceeds the threshold, V_{th}, while here, V_{th} is $5mV$.

$P_R(V_R)$ is found to be independent of the observation period and the bandwidth of the receiver.

2. Pulse-inter-arrival Distribution

An impulse event is claimed to occur whenever the amplitude threshold, V_{th}, is exceeded. In [44], this process is assumed to be a Poisson process having exponential distribution with the following density:

$$W(t/V_R > V_{th}) = \frac{1}{T} \cdot e^{-t/T} \tag{82}$$

where T is the mean interval.

However, this can only be a rough approximation, because it is found in other surveys [35, 41], that Poisson distribution can not approximate the inter-arrival time distribution satisfactorily.

The mean inter-arrival time as a function of impulse event threshold V_{th} is also given in [44]. From the plot given, we can have an approximate relationship as:

$$\overline{T} \propto V_{th}^{2.5} \tag{83}$$

This relationship is somewhat in agreement with those results shown in [41].

6.2.1.3 Performance Evaluation Procedure

We use both impulses C-1 and C-2 to estimate the performance of the ADSL DMT transmission systems with different "weight". However, it shows that only impulse C-2 has effect on the transmission quality. Impulse noise C-1 will not give much trouble to the transmission. Therefore, only impulse noise C-2 will be used in further simulations. The procedure of evaluation is presented below.

1. Fix the threshold voltage to be $3\ mV$ (or $5\ mV$) for impulse noise C-2.
2. Calculate the occurrence frequency of the impulse events.

   This is equivalent to calculating the mean inter-arrival time with the event threshold in step 1. With the mean inter-arrival time, calculate the probability of impulse noise occurring and not occurring, p_{occur} and p_{no_occur}, where $p_{occur} + p_{no\_occur} = 1$.

3. Calculate the probabilities of the occurrence of the impulses with different amplitudes, A_k, $p(A_k)$, when it is time for an impulse noise to occur, where $\sum_k p(A_k) = 1$.

4. For those DMT symbols without any impulse noise, the bit error probability with AWGN, crosstalk noises, $p_{e-random}$, with the effect of FEC, is assumed known.

5. For those DMT symbols with impulse noise inside, we run simulations to test the error performance. When there is an impulse noise in a DMT symbol, the bit error probability is always very large, so we do not need to run very long simulation to find the average error probability. In this way, we can find the average BER, p_{e_k} with respect to the impulse with amplitude A_k, at the output of decoder of FEC with certain coding and interleaving parameters.

Two problems will occur here. The first one is how many DMT symbols one impulse noise contaminates. One DMT symbol interval is about $1/4312.5 = 2.3188 * 10^{-4} s$, the shorter impulse C_1 has length of $140 \times 160 \times 10^{-9} = 2.24 \times 10^{-5} s$, which is 8.96% of one DMT symbol interval, while the longer one has length of $480 \times 160 \times 10^{-9} = 7.68 \times 10^{-5} s$, which is 30.7% of one DMT symbol interval. Since each of the two impulses has length much shorter than one DMT symbol, we can make the simplification that each time an impulse occurs, all of the impulse samples are included in one DMT symbol.

However, there is possibility that an impulse falls in two DMT symbols. In this case, one impulse will contaminate two DMT symbols, while at the same time, the effect of the impulse on each of the two DMT symbols will usually be less. Furthermore, if RS code is used, the two DMT symbols will probably fall into two code words, which will improve the BER performance at the output of the decoder.

Through simulations, it was also found that if an impulse noise contaminates two DMT symbols, most probably that one DMT symbol will be destroyed badly and it just has little effect on the other one. This is because of the fact that the main part (high-voltage part) is very short for both impulses C-1 and C-2.

The second problem is that the receiver front-end filters must be considered here. Apparently, these two impulses are from surveys with very wide bandwidth, with sampling frequency of *6.25 MHz*. In our application, the frond-end filters have bandwidth much lower than the impulses' bandwidth. The impulse noise will go through a bandpass filter before it gives any effect to our transmitted information data.

6. The overall bit error probability is then calculated as follows:

$$p_e = p_{no\_occur} \cdot p_{e\_random} + p_{occur} \cdot \sum_k \left(p(A_k) \cdot p_{e\_k}\right) \tag{84}$$

6.2.2 Other Performance Evaluation Simulation Approaches

There are two other performance evaluation simulation approaches proposed in the literature. Details of these two approaches are presented in *Appendix A* and *B*.

6.3 Performance of RS and Erasure RS codes against Impulse Noise in ADSL DMT Transmission

Two impulses are given in [2]. One of them is chosen to be the test impulse noise in our simulation, because the other one proves to have little effect on the ADSL DMT transmissions. In [2], the voltage samples of the chosen impulse are listed in a table called Table C-2. Thus, here we call it C-2 impulse.

The characteristics of the C-2 impulse are shown in Figures 28-31.

It is very interesting to find that this impulse noise shows some kind of bandpass property; in frequency band from zero to *2 MHz*, it exhibites high PSD. This result disagrees with the previous survey results which said that most of the impulse noise power concentrates in the frequency band lower than *500 kHz*. This impulse noise is a "terrible" impulse for our DMT system, because it has very high PSD in the frequency range of our interest.

From *Chapter 3*, we know that for RS or erasure RS code perforamnce-evaluation, we do not necessarily need to encode and decode the information sequence. We just need to get the statistics of channel error bytes before the decoder. From the statistics of the channel error bytes, the BER of the recovered information output from the decoder can be precisely estimated.

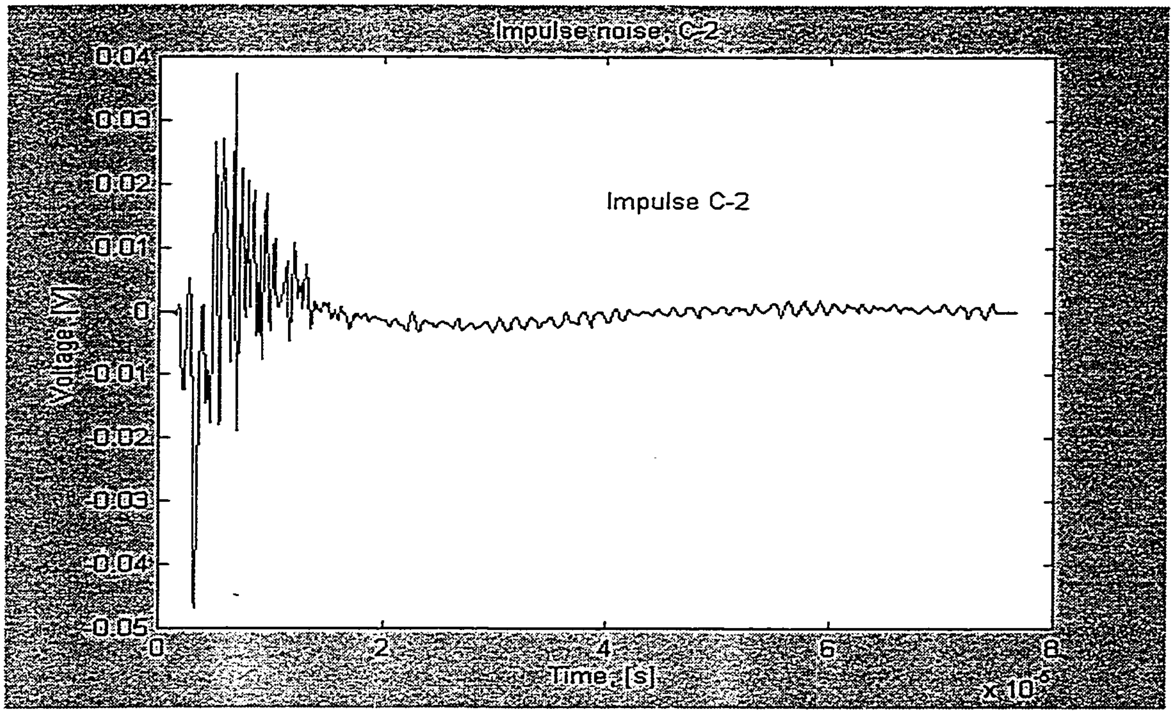

Figure 28 Time domain impulse C-2

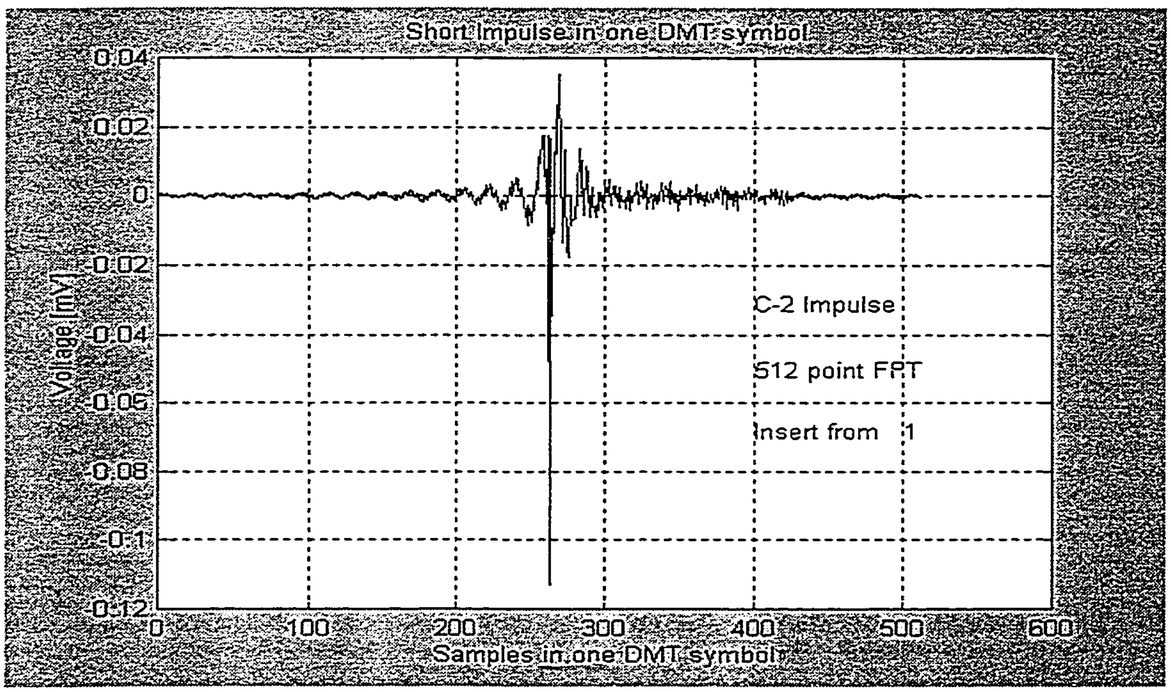

Figure 29 Bandpass filtered impulse noise C-2 in one DMT symbol

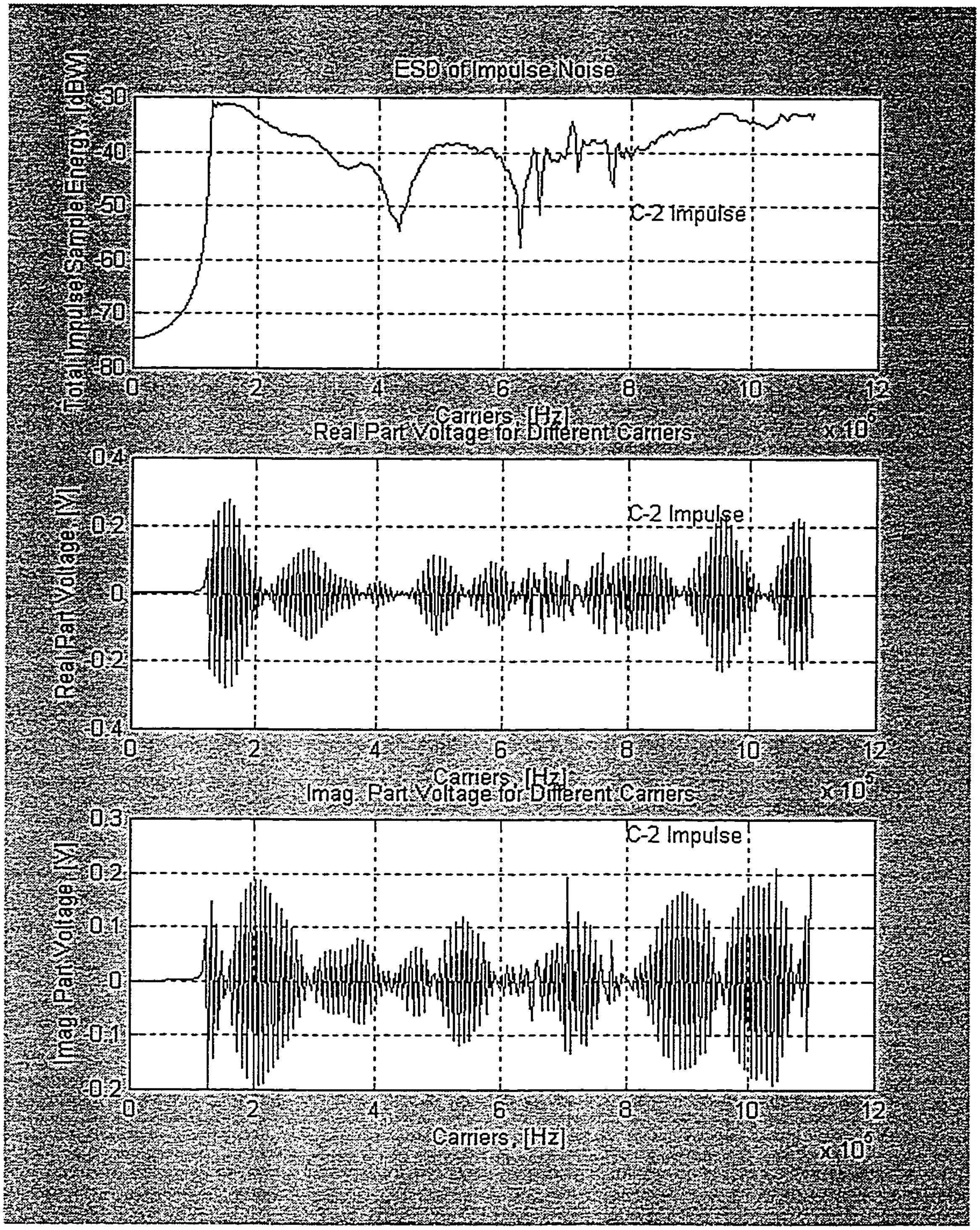

Figure 30 Output power and in-phase & quadrature component in each tone

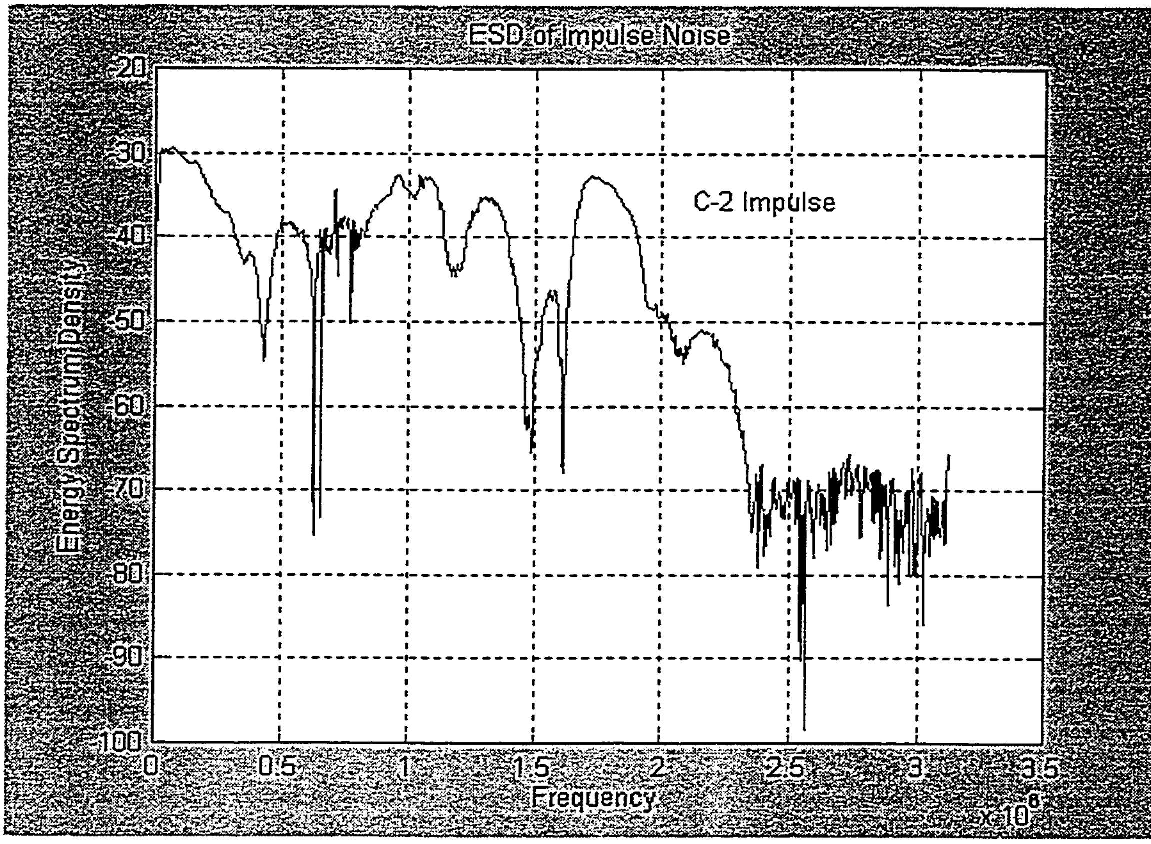

Figure 31 Energy spectral density of impulse C-2

In the simulation, the following assumptions are made:

- AWGN channel without crosstalk
- Minimum number of bits per tone is *2*
- Maximal number of bits per tone is *15*
- Highest carrier is *552 kHz*
- Lowest carrier is *120.75 kHz*
- ISDN Loop #9
- *400* information bits per DMT symbol
- $RS(N,K)$, $K = 200$

- Using approximation: $P_{bit} = \dfrac{P_{sym}}{2}$
- One impulse / *50 seconds*, even distribution
- Channel bit rate is *1.728Mbps*, which indicates a redundancy of *16 bytes*.

The reason why we made the last assumption is that, with more redundancy, some subchannels will use larger QAM constellations. While with the same PSD, using larger constellation will induce more errors caused by the same impulse noise. Here, we chose a typical value of redundancy, *16* redundant bytes, which corresponds to *8%* redundancy.

Table 4 gives the probabilities of the impulse noises with different peak amplitudes and the corresponding BER and number of error bytes.

Table 4 can be explained in the following way:

- The "Vpeak (Range)" indicates the peak amplitude range of the impulse noises.
- The "Vpeak" values are taken as the average value of the "Vpeak-range" values; we assume that impulse noises with peak amplitude within the "Vpeak (Range)" have a unique peak amplitude of "Vpeak".
- The occurrence frequency of the impulse C-2 with amplitude larger than $3mV$ is set to be *0.02/second.*
- "Probability of occurrence" gives the probability that an impulse noise with peak amplitude in the corresponding range occurs when an impulse show up, calculated by equation (81).
- "Number of error bytes" gives the average number of error bytes in the DMT symbol contaminated by the impulse noise with corresponding peak amplitude.
- "BER/DMT" gives the ratio of the error bits in the DMT symbols containing impulse noises.
- "BER" gives the system BER caused by the impulse with this peak amplitude, if every time an impulse occurs, it has a peak amplitude of "Vpeak".

- "BER_Contri" gives the contribution of BER given by impulses with peak amplitude in the corresponding range. This is the product of the BER and the occurrence probability.

Vpeak (mV) (Range)	[4,6]	[6,8]	[8,10]	[10,15]	[15,20]	[20,30]	[30,40]	>40
Vpeak (mV) (Average)	5	7	9	12.5	17.5	25	35	60
Probability of occurrence	31%	11%	5%	5%	1.75%	1.25%	0.438%	0.562%
No. of error bytes	22	30	35	43	48	52	53	54
BER/DMT	0.0726	0.1063	0.1454	0.2180	0.2967	0.3610	0.4231	0.4833
BER ($*10^{-7}$)	3.63	5.315	7.27	10.9	14.835	18.05	21.155	24.165
BER_Contri. ($*10^{-8}$)	11.235	5.85	3.635	5.45	2.6	2.26	0.93	1.36
Residual BER ($*10^{-8}$)	33.32	22.085	16.235	12.6	7.15	4.55	2.29	1.36
# of Needed Parity Bytes	44	60	70	87	96	104	106	108

Table 4 Error performance of impulse noise in coded ADSL DMT systems

- "Residual BER" gives the BER caused by the impulse noise if the RS code used in the system can not correct errors caused by impulse in the corresponding peak amplitude range and higher ones.

- "# of needed parity bytes" gives the number of minimum required parity bytes in one RS code word which guarantee correction of all the errors caused by impulses with peak amplitude in the corresponding range.

Note in Table 4, the peak voltage range [0,4] is not considered because simulation results showed that no error occur when the impulse has a peak amplitude less than $4\ mV$.

We can see from Table 4 that once the impulse begins to cause errors, it will cause burst errors. This is because in time domain, impulse noise has high peak and short duration, which in turn suggests a flat frequency spectrum. Therefore, when the impulse contribution in one tone causes errors, most likely, it will cause error to other tones as well.

6.3.1 RS Coding Performance with Interleaving

In Table 4, it is seen that if we want a BER caused by impulse noise to be less than 10^{-7}, the RS code we used must be able to correct errors caused by impulses with height up to $15\ mV$, where the residual BER caused by impulse noise is $7.15*10^{-8}$. Check Table 4, we found at this time, our RS code must be able to correct *43* byte errors in D RS code words, where D is the interleave depth. For smaller residual BER, if the system requires impulses with height up to $20\ mV$ can be combated, with a residual BER of about only $4.55*10^{-8}$, check from Table 4, now *48* byte errors must be corrected in the D RS code words. In the following, we assume that a residual BER of $7.15*10^{-8}$ is good enough.

Assume that $RS(N,K)$ code with interleaver of interleave depth D is used in the system, and the redundancy of the RS code is $r = N - K$. In this case, to guarantee satisfactory performance with the above case, the following equation must hold:

$$r \cdot D \geq 86 \quad bytes \tag{85}$$

We know that the optimal value of r is about *12* to *24* bytes to combat stationary noise, which in turn corresponds to a redundancy percentage from *6%* to *12%*. We can have a table of minimal interleave depth with the corresponding optimal redundancy percentage as shown in Table 5.

We can see that without interleaving, it is impossible to get satisfactory performance in the presence of this impulse noise. Interleave depth about *8* is suggested in Table 5. From Figure 21 and 23, it is easy to see that for *1.6 Mbps* transmission, we can set the redundancy relatively large without much coding gain loss against AWGN and crosstalk noise. From *11%* to *20%* redundancy, we only suffer less than *0.5 dB* coding gain loss.

Therefore, in this case, we can choose the redundancy to be relatively large to decrease the required interleave depth, thus decrease the latency of the message transmission. In the above example, we can choose the redundancy to be *20%*, then the interleave depth can take the value of only *3*.

	4%, 8 bytes	5%, 10 bytes	6%, 12 bytes	7%, 14 bytes	8%, 16 bytes
Minimum D	11	9	8	7	6
	10%, 20 bytes	12%, 24 bytes	16%, 32 bytes	20%, 40 bytes	
Minimum D	5	4	3	3	

Table 5 Required minimum interleave depth with the corresponding optimal redundancy percentage, hard-decision decoding technique

Again, we see that we must sacrifice some coding gain against crosstalk to get satisfactory performance over impulse noise. With larger interleave depth, the loss of this gain can be made very small.

However, for those services that require latency as small as possible, small interleave depth must be chosen. Then, the gain loss is apparent. For *6.4 Mbps* transmission, the loss is expected to be more severe than the above example, because in Figure 22 and 24, we can see that the coding gain curves decreases much faster with the redundancy after the optimum redundancy point.

Impulse noise is a kind of non-stationary process. The measurements in different sites show very different characteristics. In the NYNEX study, it was found that impulses with amplitude in the *10* to *40 mV* range occurred as often as *10* times per minute [42]. For such sites with more frequent impulses, we must be prepared to correct burst errors caused by a whole DMT symbol. High interleave depth is required.

6.3.2 Erasure RS Coding Performance with Interleaving

Erasure decoding technique for QAM signal has two parameters that hard-decision decoding technique doesn't have. The outer threshold, TH, and inner threshold th, normalized by half the minimum distance in the received signal constellation. The outer threshold is the area outside the QAM constellation; received signal points that fall into this area will be erased, and the *TH* is the distance from the outer signal points to this area. In the same way, part of the space inside the QAM constellation is also erasure area, which can be shown in Figure 32.

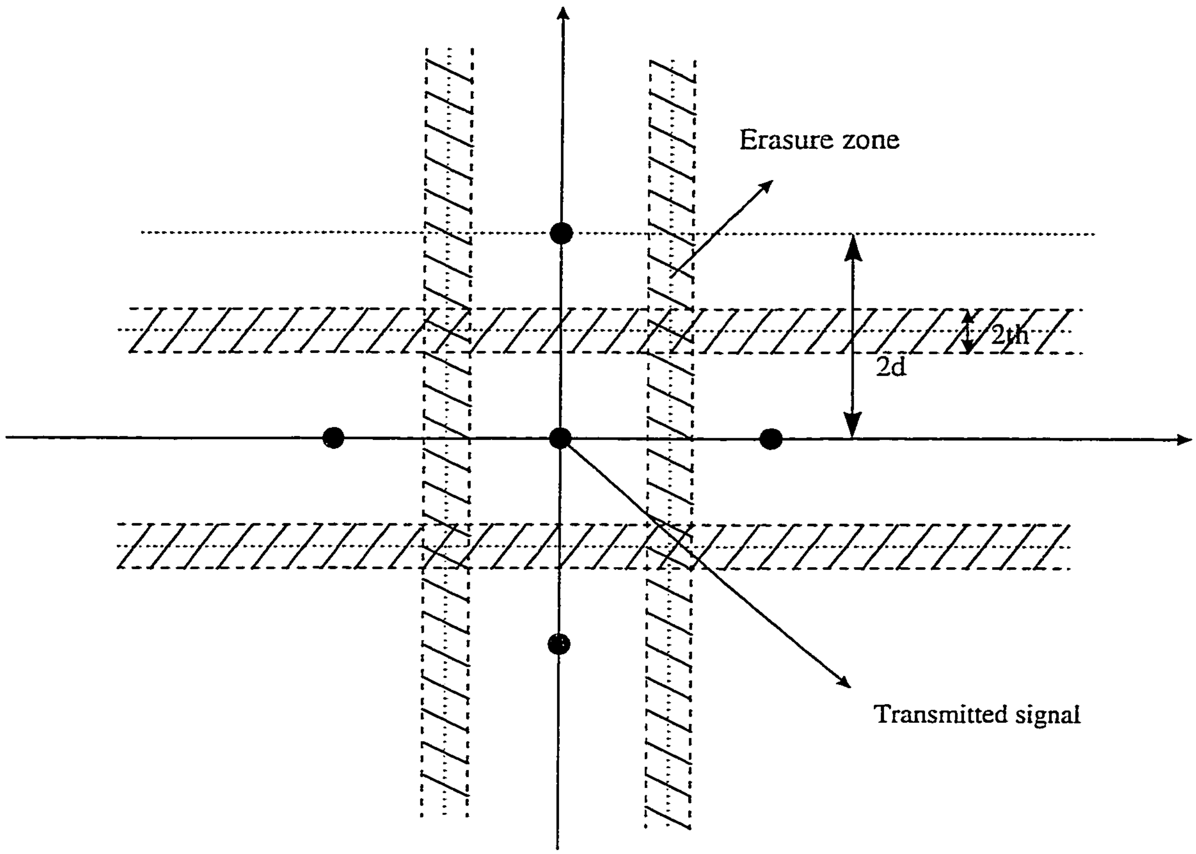

Figure 32 Erasure area

With the same system parameter assumptions, similar results are obtained for erasure RS coding performance. In the simulations, one additional assumption is made here:

- $TH = 1$; Value of th is changed to find the best one.

The required redundancy in D RS code words, where D is the interleave depth, is listed below in Table 6.

The following conclusions can be made from Table 6:

1. Using erasure-decoding technique gives better performance than using hard-decoding technique. Still, we require that the RS code we use must be able to combat impulse

noise of height less than *15mV*. For erasure decoding, we see that we only need minimum *56* parity bytes in D code words to keep satisfactory performance. It *is 30 bytes* less than that required in hard-decision case in *section 6.3.1*.

Vpeak (mV) (Range)	[4,6]	[6,8]	[8,10]	[10,15]	[15,20]	[20,30]	[30,40]	<40
Vpeak (mV)	5	7	9	12.5	17.5	25	35	60
$th = 0$	44	60	70	87	96	104	106	108
$th = 0.1$	37	52	56	67	72	71	70	60
$th = 0.2$	40	51	57	61	67	65	67	57
$th = 0.3$	41	49	58	55	65	59	59	57
$th = 0.4$	40	51	57	53	60	59	57	56
$th = 0.5$	42	54	55	56	58	57	56	55

Table 6 Required number of parity bytes when $TH = 1$ with different th

As a consequence, we could have smaller interleave depth to decrease the system latency. We have Table 7 for interleave depth requirements in this case.

We can see that the required interleave depth is decreased significantly. This is very useful for services that can not stand long latency.

	4%, 8 bytes	5%, 10 bytes	6%, 12 bytes	7%, 14 bytes	8%, 16 bytes
Minimum D	7	6	5	4	4
	10%, 20 bytes	12%, 24 bytes	16%, 32 bytes	20%, 40 bytes	
Minimum D	3	3	2	2	

Table 7 Required minimum interleave depth with the corresponding optimal redundancy, using erasure decoding technique

On the other hand, if the interleave depth is fixed, for example $D = 2$, the coding gain loss against stationary noises caused by erasure decoding technique will be better than that caused by hard-decision decoding technique. For our case, if we choose

$th = 0.5$, the redundancy required per code word is about *28* bytes, which is *14%*. For hard-decision example in the previous section, it is *44* bytes, which is *22%*. Almost *0.5 dB* coding gain improvement can be found in Figure 16,18. For higher rate transmission like shown in Figures 17, 19, more coding gain improvement should be expected, because the curve declines with redundancy much faster.

2. For both hard-decision RS code and erasure decoding RS code, there is a saturation point, at which most of the bytes in one DMT symbols are in error or erased. We say that there is an error saturation in a DMT symbol if error bytes and erased bytes make up more than *90%* of all the bytes contained in this DMT symbol.

   After the saturation point, the required number of parity bytes will be twice of the total number of bytes in one DMT symbol using hard-decision RS codes, however, it is only slightly more than the number of bytes in one DMT symbol when an erasure scheme is used. The difference is very apparent.

   In Table 4, we can see that to keep the residual BER caused by impulse noise less than 10^{-7}, at least *86* parity bytes are needed in D RS code words. However, in Table 6, we can see that when the inner threshold is chosen to be 0.5 normalized by half of the minimal distance of the QAM constellation at the receiver end, *58* parity bytes in D RS code words are need to correct all the errors cause by impulses with almost any height. This means with *58* parity bytes in D RS code words, using erasure-decoding technique can achieve somewhat error-free performance for impulse noise.

   However, this result is mostly based on the fact that the impulse we used in our simulation can only contaminate one DMT symbol at a time, because the high peak voltage only occur in very short duration. For longer impulses that can affect several DMT symbols, this result is not necessarily right. However, this kind of impulses rarely occur, so their impact can be ignored in most of the cases.

3. For sites with more often impulse event, erasure-decoding technique will be further beneficial, because in this case, it is very easily to arrive at an error saturation state.

It is shown in *Chapter 5* that erasure-decoding technique does not improve the system performance much over AWGN channels. Therefore, it should not be used for all the

DMT symbols transmitted in the system. Just for those DMT symbols containing impulses, using erasure decoding will achieve some coding gain improvement. Then we need some kind of watch signal to indicate whether there is an impulse in the current DMT symbol or not.

This problem can be solved by setting some unusable tones to be our “watch tones”. Impulse noise always has high peak and short duration, which makes its frequency spectrum tend to be flat. Therefore, we can set one (always, lower tones will be better indicator tones) or more than one tones to be “watch tones”. When the detector finds power stronger than certain power threshold in the watch tones, then erasure decoding will be used instead of hard-decision decoding for this DMT symbol. Hard-decision decoding is a special case of erasure decoding in some sense, so it is very easy to switch between these two decoding techniques.

Chapter 7

Conclusions and Suggestions for Future Work

7.1 Conclusions

In this thesis, the performance of RS codes in ADSL DMT systems has been studied through both simulation and theoretical analysis.

A simulation structure for evaluating the performance of RS code against AWGN and crosstalk noises in ADSL DMT systems has been proposed. With this simulation structure, it has been found out that an optimal RS code redundancy exists in RS coded ADSL DMT systems. Further increasing the RS code redundancy beyond the optimal value will degrade the system performance. Although every subscriber loop has its unique transfer function, which results in different optimal values of redundancy and the corresponding maximum coding gains for different loops, the RS coding gain vs. RS code redundancy curves for all test loops with the same transmission rate are of the similar shape. It has been found that up to *3 dB* coding gain for *1.6 Mbps* transmission and up to *2.5 dB* coding gain for *6.4 Mbps* transmission can be achieved with properly chosen redundancy of the RS codes. Also, higher rate transmission systems were found to be more sensitive to the optimal value of the redundancy than lower rate transmission systems; their performance improves faster with increasing redundancy before the optimal value and degrades faster after the optimal value.

Since impulse noise is a performance limiting impairment in ADSL DMT systems, RS code performance in the presence of impulse noise was considered next. A performance evaluation approach was designed and employed in *Chapter 6*. Using this approach, it has been determined that without interleaving, using only RS code could not achieve satisfactory performance for an ADSL DMT system with a transmission rate above *1 Mbps*. For ADSL services with small latency requirement, some RS coding gain against AWGN and crosstalk noise must be sacrificed to achieve satisfactory performance in the presence of impulse noise.

Erasure decoding is proposed to replace hard-decision decoding to improve the coding performance against burst errors caused by impulse noise. It has been determined through simulation that erasure decoding would not give much coding gain improvement over hard-decision decoding technique in AWGN channels. However, for combating impulse noise, it has been shown in *Chapter 6* that erasure decoding does give some coding gain improvement. More importantly, erasure decoding can reduce the required parity bytes significantly, which in turn decreases the latency.

7.2 Suggestions for Future Work

1. In this work, the RS code performance against stationary noise is evaluated and analyzed. However, adding a multi-dimensional trellis code as the inner code is expected to further improve the system performance. In future work, this part hopefully can be simulated.
2. In evaluating the performance of RS code against impulse noise, a very simple way is used and only one waveform is applied. Although the waveform is the most typical waveform in one site of measurement in North America, it can not stand for all the cases. Further simulations should be conducted using proposals given in the *Appendix A* and *B* in this thesis, which will give a much more random waveform of the impulse noise, although a typical energy spectral density of impulse noise is still needed in constructing the impulse noise model. Another way is to choose the impulse waveform from a finite set of impulse waveforms, or use their combinations. This will also give more random waveforms of impulse noises.
3. Performance of concatenated code with multi-dimensional trellis code as inner code should be evaluated in an impulse noise environment.
4. Performance of erasure decoding technique should be further studied.

Appendix A

A Second ADSL DMT Transmission System Performance Evaluation Approach in the Presence of Impulse Noise: Henkel's Model

An extensive measurement campaign was carried out in the network of Deutsche Bundespost Telekom. These measurements were conducted at seven locations within Germany. The results consist of the recordings of impulses, inter-arrival times and the determination of voltage histograms. The data was used to derive analytical models for the statistics of impulsive noise including the probability density functions of the voltages, the impulse lengths, and the inter-arrival times and the mean energy-spectral density together with the phase properties. Such a noise model and corresponding impulse noise generator is presented by Werner Henkel in [35,36]. This noise model represents the practical measured impulse noise in loop plant much better than previous ones from other surveys [41,43,44,45], especially in modeling the statistics of voltage, inter-arrival time and impulse length. This model may be further improved by including a typical phase of the impulse noise.

I. Impulse Noise Statistics

The analytical results of the statistical characteristics of the impulse are presented in this section.

1. **Probability Density Function (PDF) of the Voltages**

The PDF of the impulse-noise voltage can be well modeled by:

$$f_i(u) = \frac{1}{240u_0} e^{-\left|\frac{u}{u_0}\right|^{1/5}} \qquad (u_0 > 0) \tag{86}$$

This distribution is a double exponential distribution with a power of $1/5$ in the exponent and with the parameter $u_0 > 0\ \ V$.

For the probability distribution of the voltage, only the parameter u_0 need to be determined. Good fitting values for the parameter u_0 for impulses from different test locations are shown in [35]. The values change with locations, and in some cases, they change dramatically.

2. **Probability Density Function of the Inter-Arrival Times**

For daytime measurements, a generalization of the Poisson law (exponential PDF) proved to be a good approximation of the inter-arrival time distribution, whereas in some cases with strongly varying telephone traffic (day and nighttime measurements), an average over the Poisson law according to Fano [37] yielded closer results.

It is more useful to use its distribution for daytime, because the daytime statistics are more severe and of more interest. A generalized exponential density is obtained and can be expressed as

$$f_d(x) = \frac{10^{a_1}}{\ln(10)} x^{a_4 - 1} 10^{-\frac{a_4}{\ln(a_2)} a_2^{(\log_{10}(x) - a_3)}} \tag{87}$$

where $x = t/100\ ns$.

For the probability of the inter-arrival time, there are three independent parameters to be determined, a_2, a_3, a_4. Value of parameter a_1 must guarantee that the $f_d(x)$ is closed.

Estimated values of a_2, a_3, a_4 change with different locations. Some reference values can be found in [35].

3. **PDF of Impulse Lengths**

A typical measured length-frequency distribution $f(t)$ can be approximated by the sum of two log-normal densities

$$f_l(t) = B \frac{1}{\sqrt{2\pi} s_1 t} e^{-[\ln^2(t/t_1)]/(2s_1^2)} + (1-B) \frac{1}{\sqrt{2\pi} s_2 t} e^{-[\ln^2(t/t_2)]/(2s_2^2)} \tag{88}$$

where t_1, t_2 are the median values and s_1, s_2 are the shape parameters of the log-normal densities.

Here, values of five parameters, t_1, t_2, s_1, s_2, B, are to be determined. Typical values for the parameters in (88) are listed in [35].

4. **Properties of the Energy Spectral Density (ESD)**

Although the mean ESD at different locations are not similar, they can roughly be approximated by one or two straight lines in double logarithmic representation:

$$\overline{L(f)} / dB(pW / kHz) = \begin{cases} -15\log_{10}(f / Hz) + \gamma_1, & 5kHz \le f \le f_x \\ -20\log_{10}(f / Hz) + \gamma_2, & f_x \le f \le 4MHz \end{cases} \tag{89}$$

where γ_1, γ_2 are constants and f_x denotes the point of intersection.

For this distribution, values of three parameters γ_1, γ_2 and f_x are to be determined.

5. **Phase Properties and 'Representative' Impulse**

Simple solutions to model the phase properties of the impulses are to set the phase to zero or to use a discrete Hilbert transform [38] based on the square root of the mean ESD.

The first approach is used to define the tap coefficients of a filter that will be used for the impulsive noise simulation scheme, but both alternatives can not be used to obtain an impulse shape similar to the real measured impulses.

It is shown that a quantity similar to the group delay $-(1/(2\pi))d\phi(f)/df$ always follows a simple analytic formula. It was observed that the phase difference

$$\Delta\phi(k\Delta f) = \phi(k\Delta f) - \phi((k-1)\Delta f), \qquad k \ge 1 \tag{90}$$

between neighboring spectral lines of the FFT spectrum can be approximated by

$$\Delta\phi(k\Delta f) = \phi_0 + \phi_1(1 - e^{-k/\phi_2}) - \phi_3 k, \quad k \ge 1, \quad \Delta f = 5 \ kHz \tag{91}$$

with the approximation parameters $\phi_v, v = 0,1,2,3$. The phase $\phi(k\Delta f)$ is determined from the approximation of $\Delta\phi(k\Delta f)$ with the initial condition $\phi_0 = 0$. From this phase together with the square root of the mean ESD, one can achieve a 'representative' impulse.

Values of parameters $\phi_v,\ for\ \ v = 0,1,2,3$ must be known before we use phase setting.

II. Impulse Noise Generator

The impulse noise generator is shown in Figure 33. Three specially developed random-number generators for the probability density functions of the voltage, the inter-arrival time, and the length of the impulse are used. Additionally, the impulse noise is filtered and, optionally, the impulse phase is corrected.

A trigger signal is generated with time interval duration generated by the inter-arrival time generator. This signal is used to trigger the length generator. The length generator produces length values each time it is triggered. Then, a sequence of samples for an FFT block is constructed out of *200* preceding samples, and trailing zeros until the end of the block. The number of voltage samples equals to the length.

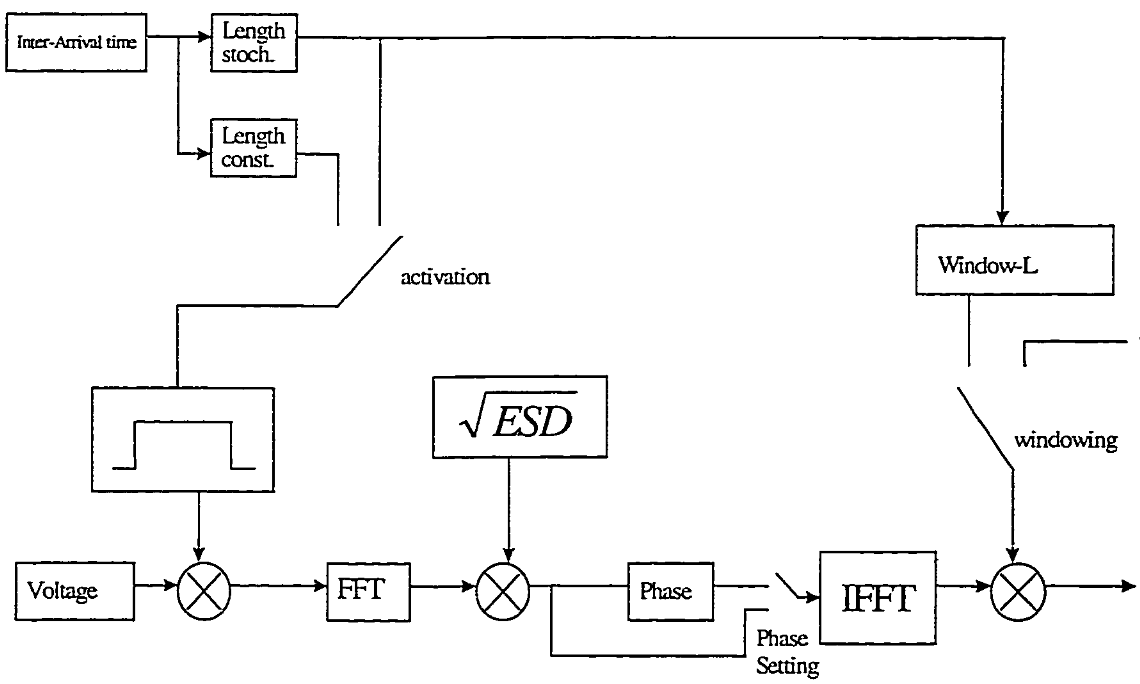

Figure 33 Block diagram of the impulse noise generator

Note, in this structure, the phase part is optional. It is shown in [36] that adding phase can make the generated impulse more like a real one. However, not setting the phase gives us advantages in some of the statistical properties, such as the length distribution and the length-energy relationship, which are very important for system evaluation process.

In [39], Melinand Robin built a simplified impulse noise generator according to the structure we talked above. The structure of this generator is shown in Figure 34.

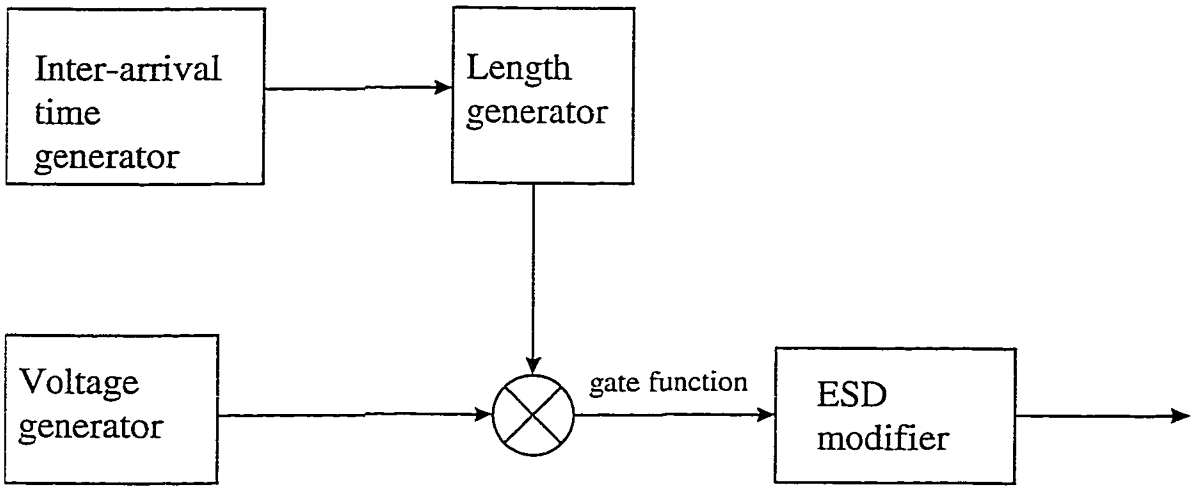

Figure 34 Block Diagram of a Simplified Generator

The principle of this generator is the same as the one shown in Figure 33, just without any phase adjusting and windowing, while for us, they are the minor factors.

With this generator proposed by Robin, we can generate certain number of impulse noises according to the statistical characteristics of the inter-arrival time, length and voltage. The ESD modifier uses a typical ESD from certain measurement place.

III. Performance Evaluation

For evaluating the performance of our ADSL DMT transmission systems with impulse noise, we must be able to generate the impulse noises like those in practice. In this proposal, we can use the impulse noise generated by the impulse noise generator in Figure 34. This model is based on an extremely extensive survey, and the analytical models of the statistical characteristics are well defined. The impulse noises generated by the generator above are shown to express the real impulse noise much better than other impulse noise model proposed in the literature. Now we describe the simulation process as follows:

1. Find good values for the parameters used in the impulse noise model.

   There are a couple of parameters whose values must be determined before we can generate the impulses we want. In [35], suitable values of all the parameters in the noise models for impulses from different measurement locations are given. Unfortunately, we can see from [35] that for some parameters, their values change from location to location dramatically, so it is impossible to get typical values for those parameters suited for all locations.

   Therefore, if we want to generate impulse noises, which can simulate the impulse noise measured in the subscriber-loops in North America, we should use the data results from the surveys [42,43,45] conducted in North America, choose the proper values for those parameters, also use the corresponding typical impulse ESD.

2. Generating Impulse noise by the noise generator with the parameters determined in step 1

   With Robin's impulse noise generator, we can generate a sample sequence of certain length with a prescribed number of impulses contained in it. This sequence starts from all zero values; impulse noises are inserted into the sequence at certain locations decided from random outputs of the inter-arrival times and impulse lengths generated during the course of simulation. This sequence can be added directly to a practical transmitted data sample sequence.

   As to the typical ESD used in the impulse noise generator, we have a couple of choices. The best choice may be using the two typical impulse noises given in the ANSI ADSL DMT Standard T1.413 [2].

3. Estimating the bit-error-rate of the system in the presence of impulse noise

   A very inefficient way is to generate a very long impulse noise sample sequence (zeros on the locations where there are no impulse), and add this sequence to a long data sample sequence, run this simulation to get the result. It is not practical to do so because it is too time consuming with a destination BER of 10^{-7}.

The simulation can be done in a simple way. We can just generate one impulse noise sample sequence with enough impulse noises inside. Then the whole sequence is divided into blocks, while each block has a length equal to one DMT symbol length. From the knowledge of all the impulse noises contained in the sequence, which blocks contain samples from impulse noises are known to us. For those blocks that have no samples belonging to impulse noises, we know exactly what their performance will be with certain RS code. Therefore, we only need to run simulation on those blocks with impulse noise samples inside. The time of the simulation can be reduced dramatically.

For example, assume that an average number of *10* impulses occur in *1 second*, with a prescribed trigger voltage. The average length of impulse is assumed to be *0.2 ms*, which is about twice of the measured average length from the survey. Let's consider the *1.6 Mbps* transmission over ISDN loops with sub-channel bandwidth of *4.0 kHz*. Each DMT symbol lasts *0.25 ms* and contains *400* bits inside. There are totally *4000* DMT symbols transmitted per second. With the assumed average parameters of the impulse noise, they can contaminate, in the worst case, *20* DMT symbols. In this case, we just need to care about *1/200* of all the transmitted DMT symbols. The simulation time is shortened by about *200* times.

Appendix B

A third ADSL DMT Transmission System Performance Evaluation Approach in the Presence of Impulse Noise: "Cook" Pulse Model

An extensive survey of impulsive noise in the UK access network was carried out with equipment based on a filter bank for spectral decomposition. In this survey, wide bandwidth digital recording was used with simultaneous recording of both the differential and common-mode components. These features combined with analysis techniques, which yield pertinent statistics, prove to be very useful for the purposes of evaluating and designing the subscriber-line transmission systems.

In the survey, instead of trying to extract features from the ESD, John Cook processed the pulses through a range of bandpass filters and measured the peak voltages at the output of each of these filters. The filters chosen are reasonable approximations of those that would be used in real baseband transmission systems and, although there will be differences, the trends in the peak voltages obtained should still be meaningful.

I. Impulse Noise Statistics

1. Peak differential voltage

The method used in the survey was to find a boundary voltage, V_b, which is exceeded once in a defined interval, τ, on average over the collection period for each line at the output of each system filter.

In [41], the boundary voltages are given for a number of different subscriber lines as a function of filter equivalent signaling rate, *f*, for averaging times of 15 minutes and 2 hours. Despite the variation of the voltages for different lines, one trend is very clear: V_b is an increasing function of the system signaling rate, *f*, and approximately proportional to $f^{3/4}$.

The difference between the mean boundary voltages for the 15 minutes and 2 hours ($1:2^3$ occurrence frequency ratio) duration cases is nearly 6 dB (1:2 peak voltage ratio), which suggests that V_b varies as $\tau^{1/3}$. This relationship given in [41] is not very reliable based on only two time interval points, but there are some other references which support a power value between $1/2$ and $1/3$ [44,53]. In [44], some statistical results of the inter-arrival times show a power of about $1/2.33$.

Using the two relationships allows V_b to be expressed as a function of f and τ:

$$V_b\,(differential) = \lambda \cdot f^{\frac{3}{4}} \cdot \tau^{\frac{1}{3}} \tag{92}$$

where V_b is in mV, f in Hz and τ in hours.

The constant of proportionality, λ, allows various degrees of confidence to be expressed.

2. Inter-arrival time

The inter-arrival can be well approximated by: [41]

$$P(T > t) = 1 - \exp(-T_e/t) \tag{93}$$

where T_e is the time constant associated with an inverse exponential distribution.

II. A Symbolic Pulse for Impulsive Noise Testing

Analysis of BT's impulsive noise survey in [41] has shown that the observed peak differential voltage entering a baseband receiver (with a signaling rate f) varies as $f^{3/4}$. This suggests that the voltage varies as $t^{-3/4}$ (where t is time). Such a characteristic is exhibited by a pulse of the form shown in Figure 35, and can be described mathematically by: [41]

$$\begin{aligned} V(t) &= Vp \times |t|^{-3/4} & t &> 0 \\ V(t) &= 0 & t &= 0 \\ V(t) &= -Vp \times |t|^{-3/4} & t &< 0 \end{aligned} \tag{94}$$

This pulse has been shown to mimic the peak voltage versus signaling rate characteristics of the ensemble of collected impulse noise data. It produces a received peak voltage, which increases with signaling rate, and an energy spectral density, which is dominated by lower frequency [54]. This latter characteristic is in accordance with the observations of other impulsive noise surveys [53,55,56].

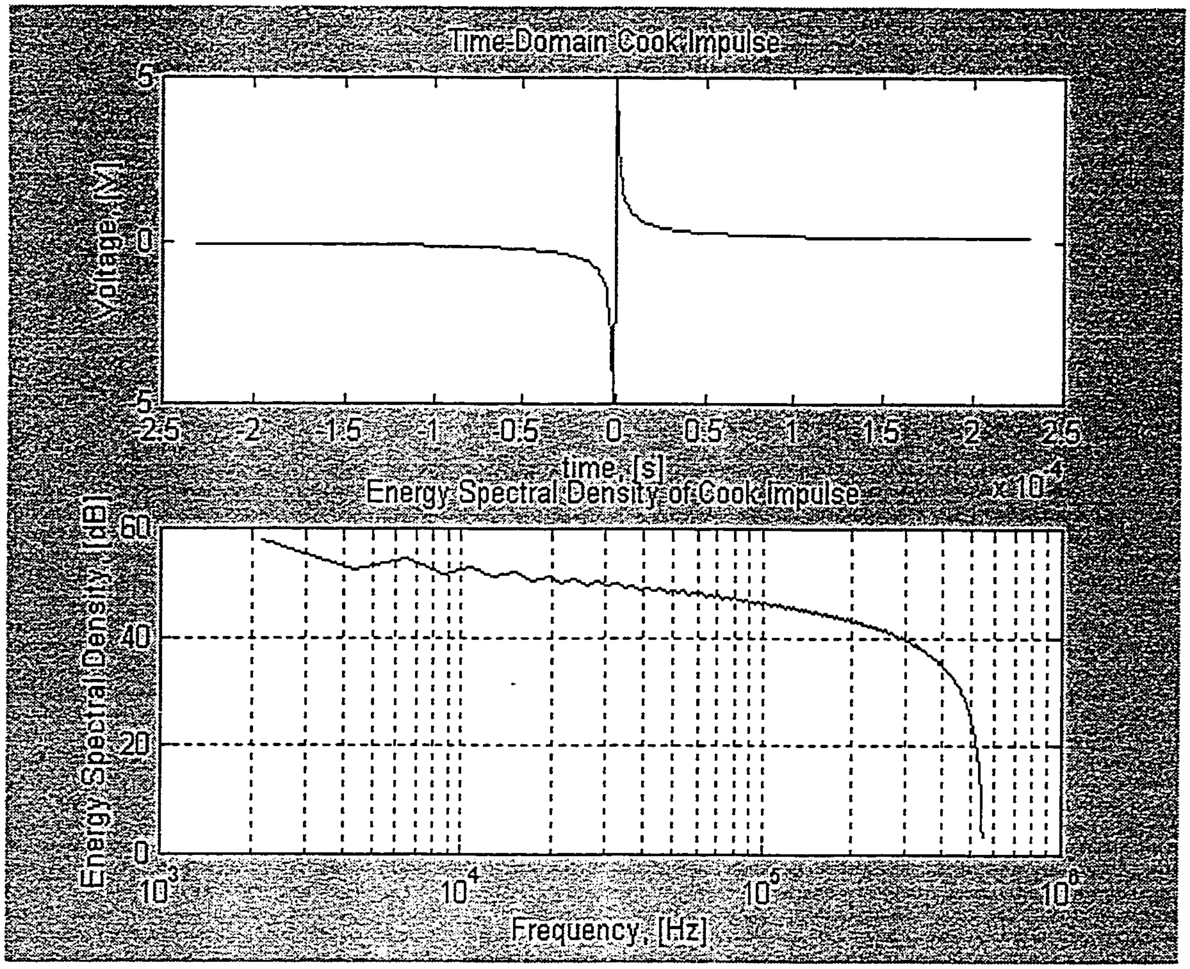

Figure 35 Time-domain "Cook" pulse and its ESD

The pulse described above is named "Cook" pulse. It has a spectrum that is relatively wide band rolling off at 5 dB per decade (see Figure 35). The pulse may be approximated by a sampled representation. This pulse may then be applied to the transceiver under test in a similar manner as that used for simulated NEXT [57] or via the use of combination with the noise injection technique [58]. It has been used to estimate HDSL performance in [59].

III. Performance Evaluation Procedure Using Cook Pulse

The peak voltage level of the "Cook" pulse, which we will use in our simulation, is determined from the statistical analysis of impulse noise event [41]. Impulses with large peak amplitudes are seen less frequently than impulses with smaller peak amplitudes. Therefore with a given frequency of occurrence, we will be able to determine the peak-to-peak amplitude of the "Cook" pulse to be generated (and not the repetition rate at which this pulse is applied). Then, we can estimate the long term BER due to impulsive noise by collecting the error extension data caused by "Cook" pulses with different peak amplitudes. The weighted average error extension together with the likely frequency of occurrence of the impulse will yield an estimate of the long term BER. Thus BER estimates can be made for various levels of impulsive noise interference.

The amplitude versus inter-arrival time relationship can be approximated for the average impulsive noise characteristics found in the BT survey [41,47]. However, care must be taken in interpreting these results as they represent an extrapolation of the measured data. Some values are listed in a table in [47], and we refer to these values here in Table 8.

The values in Table 8 show a very good relationship between the peak amplitudes and mean inter-arrival times in accordance with equation (92), for differential equipment.

Therefore, the following process is proposed to evaluate the performance of ADSL DMT transmission system using "Cook" pulses.

1. Using the values for peak amplitudes and inter-arrival times to calculate the weights of the impulses with different peak amplitude.

   We can either use the values in the Table 8, or we can give some more values by extrapolation. Now, assume we decide to use those values in this table.

Peak Amplitude (mV)	Mean Inter-arrival Time (s)	Mean Occurrence Freq. (/s)
10	499	0.0020
8	256	0.0039
5	62	0.0161
2	4	0.25

Table 8 Impulse noise peak amplitude versus inter-arrival time

Assume that there is an impulse event every 4 seconds, which corresponds to the time interval τ with a boundary voltage of $V_b = 2\ mV$. The cases that the peak amplitudes are more than *5, 8, 10 mV* are all included in these impulse events. Therefore, the mean occurrence frequencies listed in Table 4 can be seen as a cumulative distribution.

Let's assume that the total time interval is *1000 s*, on the average case, we have the following values in Table 9.

Peak Amplitude (mV)	Average number of Impulses in 1000 s	Peak Amplitude Range (mV)	Average number of Impulses
>10	2	>10	2
>8	4	>8 & <10	2
>5	16	>5 & <8	12
>2	250	>2 & <5	234

Table 9 Distribution of impulse noise with peak amplitude in different ranges

In the testing simulation, if we fix that an impulse event comes every 4 seconds, then there is a discrete distribution of impulse with certain peak amplitude coming at any interval. From Table 9, assuming that impulse noises with amplitudes between V_1 and V_2 are averaged to $\frac{V_1+V_2}{2}$, we can get the distribution of the impulse noises we will use.

Peak Amplitude Range (mV)	Average Peak Amplitude (mV)	Number in totally 250 detected Impulses	Occurrence Probabilities (%)
>10	15	2	0.8
>8 & <10	9	2	0.8
>5 & <8	6.5	12	4.8
>2 & <5	3.5	234	93.6

Table 10 Occurrence probabilities of impulse noises with peak voltages in different ranges

The number of impulses in each voltage range in the totally detected *250* impulses, as a subsequence of the assumptions above, with peak amplitudes over *2* mV are listed in Table 10, the corresponding occurrence probabilities are also listed.

The output of this step is the probabilities $\{P_i\}$ corresponding to different impulse noise peak voltages $\{V_{b\_i}\}$, where $i \in \{1,2,3,4\}$.

2. Run small simulations to get the error performance of those DMT symbols with "Cook" pulses inside. This procedure is repeated for four 'cook' pulses with four different peak amplitudes listed in Table 10.

   The length of the "Cook" pulse can be decided as follows. The *128*th point in either positive direction or negative direction in a "Cook" pulse has amplitude 2.63% of the maximal amplitude. In the case of peak *10* mV cook impulse, the *128*th point has amplitude of $0.263mV$. This is quite small compared to the peak amplitude. Therefore, for simplicity, we can omit the influence of those points out of the range $[-127,128]$. Thus, our "Cook" pulse should have a length of *256* sample points.

   A *95%* total power principle can also be used here to get the length of the impulse. This will require *512* samples length "Cook" pulse instead of *256* sample length "Cook" pulse described above, which has *95%* of the total power inside.

   There is a problem as to from what point in the sample vector of one DMT symbol we should insert the "Cook" pulses. Two cases are considered. A "Cook" pulse is contained only in one DMT symbol, or a "Cook" pulse is divided from the middle points into two parts. It is difficult to say directly which case will give the worse performance.

   The output of this step should be the error probabilities $\{p_{bit-error-i}\}$ and erasure probabilities $\{p_{bit-era-i}\}$ corresponding to "Cook" pulse with different peak voltages, where $i \in \{1,2,3,4\}$, for those DMT symbols with "Cook" pulses inside.

3. Calculate the average bit error probability and bit erasure probability for those DMT symbols with "Cook" pulses inside.

$$p_{bit\_error} = \sum_i P_i \cdot p_{bit-error-i} \tag{95}$$

$$p_{bit\_erasure} = \sum_i P_i \cdot p_{bit-eras-i} \tag{96}$$

4. Time to calculate the long term bit error rate.

Now, we assume that one impulse noise occurs every *4 s*. Also, we have the average bit error rate of those DMT symbols, and the number of DMT symbols, which are contaminated by the impulse noise. From these, we can calculate on average how many bits are decoded erroneously or erased, assume the numbers are N_{error} and $N_{erasure}$.

From the approximation of the output bit error rate vs. the input bit error rate of the RS decoder, the output bit error rate p_{bit_error} can be estimated.

Since the system transmission rate is known, the totally transmitted bits in these *4* seconds can be calculated, suppose to be N_{total}. The over all bit error rate caused only by the impulse noise is calculated by:

$$p_{bit\_error} = \frac{N_{bit\_error}}{N_{total}} \tag{97}$$

BIBLIOGRAPHY

[1] ADSL Forum, "**ADSL Tutorial – Twisted Pair Access to the Information Highway**", WWW site materials at http://www.adsl.com/adsl_forum.html.

[2] John Bingham Frank, Van Der Putten, "**ADSL DMT STANDARD, T1.413, Issue 2**", Sept. 26, 1997.

[3] O. Edfors, M. Sandell, J.-J. van de Beek, D. Landström, and F. Sjöberg, "**An Introduction to Orthogonal Frequency-Division Multiplexing**", Research Report TULEA 1996:16, Div. of Signal Processing, Luleå University of Technology, Luleå, Sept. 1996.

[4] John M. Cioffi, "**A Tutorial Review of DMT ADSL Issue 2 [96-016]**", ANSI T1E1 Contribution, T1E1.4/96-016, Jan. 22, 1996.

[5] John A. C. Bingham, "**Multicarrier Modulation for Data Transmission: An Idea Whose Time Has Come**", IEEE Commun. Magazine, pp. 5-14, May 1990.

[6] Jean-Jacques Werner, "**The HDSL Environment**", IEEE Journal on Selected Areas in Communications, Vol. 9, No. 6, pp. 785-800, Aug. 1991.

[7] David L. Waring, "**The Asymmetrical Digital Subscriber Line (ADSL): A New Transport Technology for Delivering Wideband Capabilities to the Residence**", pp. 1979-1986, Globecom'91.

[8] Peter S. Chow, Jerry C. Tu, John M. Cioffi, "**Performance Evaluation of a Multichannel Transceiver System for ADSL and VHDSL Services**", IEEE Journal on Selected Areas in Commun., Vl 9, No. 6, pp. 909-919, Aug. 1991.

[9] S. B. Weinstein and Paul M. Ebert, "**Data Transmission by Frequency-Division Multiplexing Using the Discrete Fourier Transform**", IEEE Trans. on Commun. Tech., Vol. Com-19, No. 5, pp. 628-634, 1971.

[10] T. Nicholas Zogakis, James T. Aslanis Jr., John M. Cioffi, "**A Coded and Shaped Discrete Multitone System**", IEEE Trans. on Commun., Vol. 43, No. 12, pp. 2942-2949, Dec. 1995.

[11] Irving Kalet, "**The Multitone Channel**", IEEE Trans. on Commun., Vol. 37, No. 2, pp. 119-124, Feb. 1989.

[12] Melbourne Barton, Michael L. Honig, "**Optimization of Discrete Multitone to Maintain Spectrum Compatibility with Other Transmission Systems on Twisted Copper Pairs**", IEEE Journal on Selected Areas in Commun., Vol. 13, No. 9, pp. 1558-1563, Dec. 1995.

[13] Abraham Peled, Antonio Ruiz, "**Frequency Domain Data Transmission Using Reduced Computational Complexity Algorithms**", Proc. IEEE ICASSP, pp. 964-967, 1980.

[14] Jorge Luis Seoane, Sarah Kate Wilson and Saul Gelfand, "**Analysis of Intertone and Interblock Interference in OFDM When the Length of the Cyclic Prefix is Shorter Than the Length of the Impulse Response of the Channel**", Globecom 92.

[15] Antonio Riuz, John M. Cioffi, Sanjay Kasturia, "**Discrete Multiple Tone Modulation with Coset Coding for the Spectrally Shaped Channel**", IEEE Trans. on Commun., Vol. 40, No. 6, pp. 1012-1029, June. 1992.

[16] Lee-Fang Wei, "**Trellis-Coded Modulation with Multidimensional Constellations**", IEEE Trans. on Information Theory, Vol. IT-33, No. 4, pp. 483-501, July 1987.

[17] M. Ghosh, "**Analysis of the Effect of Impulse Noise on Multicarrier and Single-Carrier QAM Systems**", IEEE Trans. on Commun., 44(2): 145-147, Feb. 1996.

[18] J. T. Aslanis and J. M. Cioffi, "**Achievable Information Rates on Digital Subscriber Loops: Limiting Information Rates with Crosstalk Noise**", IEEE Transactions on Communications, Vol. 40, No. 2, pp. 361-372, Feb. 1992.

[19] G. David Forney, Jr., M. Vedat Eyuboglu, "**Combined Equalization and Coding Using Precoding**", IEEE Communications Magazine, pp. 25-34, Dec. 1991.

[20] Naofal Al-Dhahir, John Cioffi, "**A Low-Complexity Pole-Zero MMSE Equalizer for ML Receivers**", in Proc. Allerton conf. Commun., Control, Comput., pp. 623-632, Sept. 1994.

[21] Naofal Al-Dhahir, John M. Cioffi, "**Optimum Finite-Length Equalization for Multicarrier Transceivers**", IEEE Trans. Commun., Vol. 44, No. 1, Jan. 1996.

[22] Naofal Al-Dhahir, John M. Cioffi, "**A Bandwidth-Optimized Reduced-Complexity Equalized Multicarrier Transceiver**", IEEE Trans. Commun., Vol. 45, No. 8, Aug. 1997.

[23] D. Falconer and F. Magee, "**Adaptive Channel Memory Truncation for Maximum Likelihood Sequence Estimation**", Bell System Technical Journal, 52(9): 1541-1562, Nov. 1973.

[24] Inkyu Lee, John M. Cioffi, "**A Fast Computation Algorithm for the Decision Feedback Equalizer**", IEEE Trans. Commun., Vol. 43, No. 11, Nov. 1995.

[25] Inkyu Lee, Jacky S. Chow, John M. Cioffi, "**Performance Evaluation of a Fast Computation Algorithm for the DMT in High-Speed Subscriber Loop**", IEEE Journal on Selected Areas in Commun., Vol. 13, No. 9, Dec. 1995.

[26] Walter Y. Chen, James L. Dixon, and David L. Waring, "**High Bit Rate Digital Subscriber Line Echo Cancellation**", IEEE J. Selected Areas Commun., Vl. 9, No. 6, pp. 848-860, Aug 1991.

[27] Minnie Ho, John M. Cioffi, and John A. C. Bingham, "**High-Speed Full-Duplex Echo Cancellation for Discrete Multitone Modulation**", pp.772-776, ICC 93.

[28] Minnie Ho, John M. Cioffi, John A. C. Bingham, "**Discrete Multitone Echo Cancellation**", IEEE Trans. Commun., Vol. 44, No. 7, pp.817-825, July 1996.

[29] J. Yang, S. Roy, and N. H. Lewis, "**Data-Driven Echo Cancellation for a Multitone Modulation System**", IEEE Trans. Commun., Vol. 42, No. 5, May 1994.

[30] John M. Cioffi, John A. C. Bingham, "**A Data-Driven Multitone Echo Canceller**", IEEE Trans. Commun., Vol. 42, No. 10, pp.2853-2869, Oct. 1994.

[31] Younce, R.C., Melsa, P.J.W., and Kapoor, S., "**Echo Cancellation for ADSL**", Proceedings 1994 IEE, pp. 301-305, May 1994, New Orleans.

[32] T. N. Zogakis, P. T. Tong, and J. Cioffi, "**Performance Comparison of FEC/Interleave Choices with DMT for ADSL**", ANSI T1E1.4 Committee Contribution, T1E1.4/93-091.

[33] Peter S. Chow, John M. Cioffi, and John A. C. Bingham, "**A Practical Discrete Multitone Transceiver Loading Algorithm for Data Transmission over Spectrally Shaped Channels**", IEEE Trans. on Commun., Vol. 43, No. 2/3/4, FEB./MARCH/APRIL, 1995.

[34] Elwyn R. Berlekamp, "**The Technology of Error-Correcting Codes**", Proceedings of the IEEE, 68(5): 564-593, May 1980.

[35] W. Henkel, T. Kebler, "**A Wide-band Impulsive Noise Survey in the German Telephone Network: Statistical Description and Modeling**", AEU, Vol. 48, No. 6, pp. 277-288, May 1994.

[36] W. Henkel, T. Kebler, Hong Y. Chung, "**Coded 64-CAP ADSL in an Impulse Noise Environment - Modeling of Impulse Noise and First Simulation Results**", IEEE Selected Areas in Comm., Vol. 13, No. 9, pp. 1611-1621, Dec. 1995.

[37] R. M. Fano, "**A Theory of Impulse Noise in Telephone Networks,**" IEEE Trans. Commun., vol. COM-25, pp. 577-588, 1977.

[38] Oppenheim, A. V.; Schafer, R. W., "**Digital Signal Processing**", London, Prentice-Hall, 1975.

[39] Melinand Robin, "**Impulse Noise Modeling and Simulation in the Loop Plant**", Internship Report, University of Ottawa, 1996.

[40] Melbourne Barton, "**Impulse Noise Performance of an Asymmetric Digital Subscriber Lines Passband Transmission System**", IEEE Trans. On Commun., Vol. 43, No. 2/3/4, Feb./Mar./Apr., 1995.

[41] J. W. Cook, "**Wideband Impulsive Noise Survey of the Access Network**", BT Tech. J, vol. 11, No. 3, July 1993.

[42] J. J. Werner, "**Impulse Noise in the Loop Plant**", ICC'90, Session 348.1.

[43] C. F. Valenti and K. Kerpez, "**Analysis of Wideband Noise Measurements and Implications for Signal Processing in ADSL Systems**", International Conference on Communications, Vol. 2, pp. 826-832, 1994.

[44] K. Szechenyi, "**On the NEXT and Impulse Noise Properties of Subscriber Loops,**" Conference Record GLOBECOM'89, pp. 1569-1573, Dallas, Nov. 27-30, 1989.

[45] NYNEX Corp., "**Characteristics of Impulse Noise on Selected NYNEX Metropolitan Loops,**" ECSA Contribution T1D1.3/86-144.

[46] Robert W. Lawrence, "**Impulse Noise Test Results for Three Line Code Technologies Proposed for ADSL - Final Report**", STANDARDS PROJECT: Asymmetric Digital Subscriber Line (ADSL), (NYNEX Science and Technology, Inc.), May 10, 1993.

[47] Gavin Young, "**Contribution T1E1.4/92-214 - Impulsive Noise in ADSL Systems**", T1E1.4 Contribution, T1E1.4/92-214, 2nd Dec. 1992 (Anaheim, L.A., Cailfornia).

[48] T. N. Zogakis, P.S. Chow, J. T. Aslanis, and J. M. Cioffi, "**Impulse Noise Mitigation Strategies for Multicarrier Modulation**", pp. 784-788, ICC-93.

[49] P. S. Chow, J. M. Cioffi, R. K. Maxwell, "**Performance of Multicarrier with DSL Impulse Noise**", T1E1.4/91-195, Nov. 11, 1991.

[50] J. W. Lechleider, "**Impulse Noise Cancellation for ADSL**", ANSI T1E1.4 Committee Contribution, No. 92-154, Portland, OR, August 1992.

[51] Hong Y. Chung, "**Performance of Interleaved Trellis Codes in the Presence of Impulse Noise**", ICC Proc., pp. 1809-1813, 1993.

[52] Mario Blaum, Patrick G. Farrell, Henk C. A. Van Tilborg, "**A Class of Burst Error-Correcting Array Codes**", IEEE Trans. On Inform. Theory, Vol. IT-32, No. 6, Nov. 1986.

[53] Szechenyi K and Bohm K: "**Impulsive Noise Limited Transmission Performance of ISDN Subscriber Loops**", ISSLS '88 (1988).

[54] Kevin T. Foster & John W. Cook, "**Contribution T1E1.4/92-143 - A Symbolic Pulse for Impulse Noise Testing**", T1E1.4/92-143.

[55] Ungar S.G., "**Testing Basic Access Loops for Service-Affecting Impulse Noise**", Globecom 89.

[56] Tol S.J.M. & Vim Van der Bilj, "**Measured Performance of ISDN Transmission in Dutch Local Telephone Network**", ISSLS 86.

[57] "**Generic Requirements for High-Bit-Rate Digital Subscriber Lines**", Technical Advisory TA-NWT-00120, Issue 1 October 1991.

[58] Foster K.T. & Cook J.W., "**A Method of NEXT Injection Offering Much Improved Calibration Accuracy**", T1E1.4/90-025, 12 March 1990 (San Antonio meeting).

[59] Jacky S. Chow, Ronald R. Hunt, "**Impulse Noise Measurements for DMT System**", Contribution to T1E1.4, T1E1.4/92-211, Dec. 1, 1992.

[60] P.S. Chow, J. M. Cioffi, R. K. Maxwell, "**Performance of Multi-carrier with DSL Impulse Noise**", T1E1.4/91-159, Nov. 11, 1991.

[61] G. David Forney, Jr., "**Burst-Correcting Codes for the Classic Bursty Channel**", IEEE Trans. Commun., Vol. COM-19, No. 5, pp.772-781, Oct. 1971.

[62] James W. Modestino, David H. Sargrad, and Robert E. Bollen, "**Use of Coding to Combat Impulse Noise on Digital Subscriber Loops**", IEEE Trans. Commun., Vol. 36, No. 5, pp.529-537, May 1988.

[63] David H. Sargrad, James W. Modestino, "**Errors-and-Erasure Coding to Combat Impulse Noise on Digital Subscriber Loops**", IEEE Trans. Commun., Vol. 38, No. 8, pp.1145-1155, Aug. 1990.

[64] John L. Ramsey, "**Realization of Optimum Interleavers**", IEEE Trans. Inform. Theory, Vol. IT-16, No. 3, 1970.

[65] Danny T. Chi, "**A New Block Helical Interleaver**", MICCOM 92, pp.799-805.

[66] William W. Wu, David Haccoun, Robert Peile, and Yasuo Hirata, "**Coding for Satellite Communication**", IEEE J. Selected Areas Commun., Vol. SAC-5, No. 4, pp.724-748, May 1987.

[67] Bernard Sklar, "**Digital Communications Fundamentals and Applications**", Prentice Hall, 1988, Englewood Cliffs, New Jersey.

[68] George C. Clark, Jr., and J. Bibb Cain, "**Error-Correction Coding for Digital Communications**", Plenum Press, 1981, New York.

[69] Arnold M. Michelson, Allen H. Levesque, "**Error-Control Techniques for Digital Communications**", GTE Government Systems Corporation, Needham Heights, Massachusetts.

[70] Stuart D. Sandberg, Michael A. Tzannes, "**Overlapped Discrete Multitone Modulation for High Speed Copper Wire Communications**", IEEE J. Selected Areas Commun., Vol. 13, No. 9, Dec. 1995.

[71] A. D. Rizos, J. G. Proakis, and T. Q. Nguyen, "**Comparison of DFT and Cosine Modulated Filter Banks in Multicarrier Modulation**", IEEE Global Telecommunications Conference. Vol. 2, 1994, Pp.687-691.

[72] Jacky S. Chow, Jerry C. Tu, and John M. Cioffi, "**A Discrete Multitone Transceiver System for HDSL Application**", IEEE J. Selected. Areas Commun., Vol. 9, No. 6, Aug. 1991.

[73] J. G. Proakis, "**Digital Communications**", New York: McGraw-Hill, 1983.

[74] G. D. Forney, Jr., et. Al., "**Efficient Modulation for Band-limited Channels,**" EEE J. Select. Areas Commun., Vol. SAC-2, pp. 632-647, Sept. 1984.

[75] Richard Gross, Dale Veeneman, "**SNR and Spectral Properties for a Clipped DMT ADSL Signal**", 0-7803-1825-0/94, Vol. 2, pp. 843-847, 1994.

[76] Denis J. G. Mestdagh, Paul Spruyt and Bernard Biran, "**Analysis of Clipping Effect in DMT-based ADSL Systems**", Contribution, T1E1.4/93-129.

[77] Alan Gatherer and Michael Polley, "**Clip Mitigation Techniques for T1.413 Issue3**", T1E1.4: ADSL Issue3, December 8-12, 1997.

[78] Jacky S. Chow, John A. C. Bingham, Mark S. Flowers, "**Mitigating Clipping Noise in Multi-carrier Systems**", ICC'97.

[79] A. E. Jones, T. A. Wilkinson and S. K. Barton, "**Block Coding Scheme for Reduction of Peak to Mean Envelope Power Ratio of Multicarrier Transmission Schemes**", Electronics Letters, pp. 2098-2099, 1994.

[80] S. J. Shephert, P. W. J. Van Eetvelt, C. W. Wyatt-Millington, S. K. Barton, "**Simple Coding Scheme to Reduce Peak Factor in QPSK Multicarrier Modulation**", Electronics Letters, Vol. 31, No. 14, pp. 1131-1132, 6th July 1995.

[81] R. Bauml, R. Fischer, and J. Huber, "**Reducing the Peak-to-Average Power Ratio of Multicarrier Modulation by Selected Mapping**", ElectronicLetters, Vol. 32, No. 22: pp2056-2057, October 1996.

[82] S. Muller and J. Huber, "**A Novel Peak Power Reduction Scheme for OFDM**", Accepted for presentation at IEEE PIMRC'97, Helsinki, Finland, September 1997.

[83] S. Muller and J. Huber, "**OFDM with Reduced Peak-to-Average Power Ratio by Optimum Combination of Partial Transmit Sequences**", Electronics Letters, Vol. 33, No. 5: pp.368-369, February 1997.

[84] Stefan H. Muller and Johannes B. Huber, "**A Comparison of Peak Power Reduction Schemes for OFDM**", Globecom 1997.

[85] M.V. Eyuboglu and G. D. Forney, Jr., "**Trellis Precoding: Combined Coding, Precoding and Shaping for Inter-symbol Interference Channels**", IEEE Trans. Inform. Theory, pp.301-314, Mar 1992.

[86] M Eyuboglu, G. D. Forney, P. Dong, G. Long, "**Advanced Modulation Techniques for V. Fast**", Eur. Trans. on Telecom., pp.243-256, May 1993.

IMAGE EVALUATION TEST TARGET (QA-3)

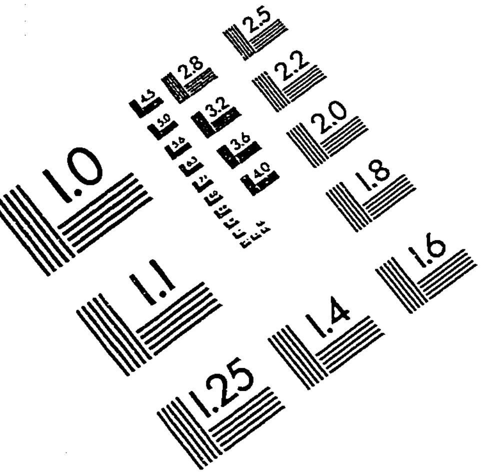
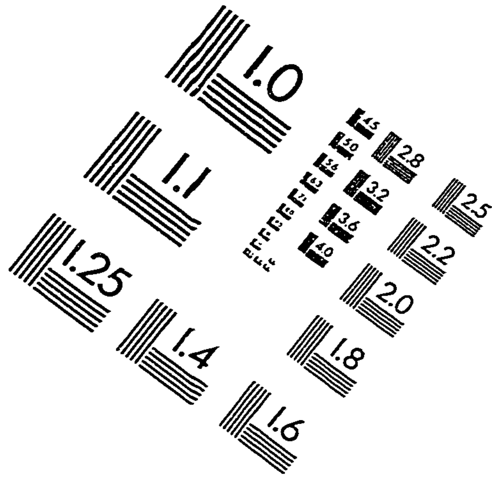
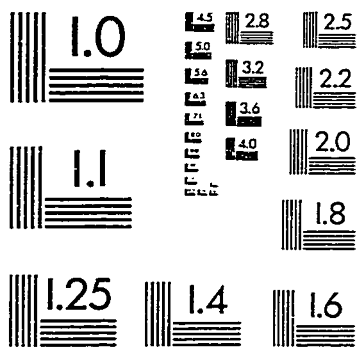

150mm

6″

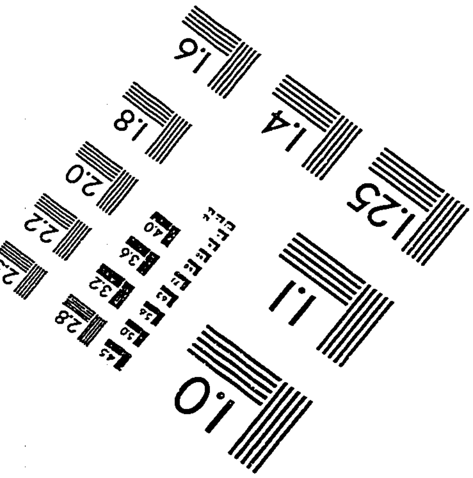
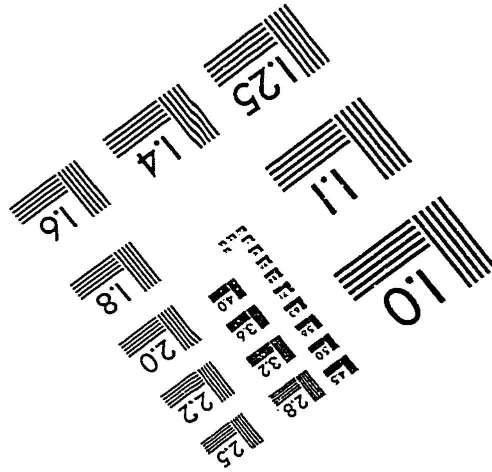

APPLIED IMAGE . Inc
1653 East Main Street
Rochester, NY 14609 USA
Phone: 716/482-0300
Fax: 716/288-5989

© 1993, Applied Image, Inc., All Rights Reserved